

**MULTIMODAL ASSESSMENT OF PARKINSON'S
DISEASE USING ELECTROPHYSIOLOGY AND
AUTOMATED MOTOR SCORING**

A Dissertation
Presented to
The Academic Faculty

by

Teresa H. Sanders

In Partial Fulfillment
of the Requirements for the Degree
Doctor of Philosophy in
Bioengineering

School of Electrical and Computer Engineering
Georgia Institute of Technology
May 2014

Copyright © 2014 by Teresa H. Sanders

MULTIMODAL ASSESSMENT OF PARKINSON'S
DISEASE USING ELECTROPHYSIOLOGY AND
AUTOMATED MOTOR SCORING

Approved by:

Professor Mark A. Clements, Advisor
School of Electrical and Computer
Engineering
Georgia Institute of Technology

Professor Thomas Wichmann, M.D.
Department of Neurology
Emory University

Associate Professor Garrett Stanley
School of Biomedical Engineering
*Georgia Institute of Technology and
Emory University*

Associate Professor Beth Buffalo
Department of Physiology and
Biophysics
University of Washington

Associate Professor Chris Rozell
School of Electrical and Computer
Engineering
Georgia Institute of Technology

Date Approved: 31 March 2014

Dedicated to God and my family

ACKNOWLEDGMENTS

The findings described in this dissertation are based on data obtained in monkeys rendered parkinsonian with the dopaminergic neurotoxin precursor MPTP. I am grateful for the use of these primate data, collected and initially analyzed by personnel in Thomas Wichmann's laboratory (Annaelle Devergnas and Jesus Soares). I am also grateful to the human volunteers who gave their time to help us test the multi-modal monitoring system.

Throughout my five and a half years at Georgia Tech and Emory, I have been inspired and helped by many. I will try to express my thanks here, although I am sure I will forget some names: I appreciate the support of the Bioengineering program office, who always answered my questions with patience and trustworthy information, and helped me navigate through some difficult times. In particular, I would like to thank Andres Garcia for leading the BioE program with fairness and good humor, and Chris Ruffin, for providing excellent program advisement and support. Chris passed away last year and I greatly miss his calm, consistent advice, and informative e-mails.

I am grateful to Yomi Oyelere who taught me Biochemistry and to Hanjoong Jo who taught and moderated the Systems Physiology course. Their classes opened my eyes to the wonders of the molecular mechanisms inside the human body, and changed my view of the world. I am also very thankful to Yoland Smith, Dieter Jaeger, Justin Romberg, Chris Rozell, and Pam Bhatti for allowing me to audit their classes to gain additional knowledge in Neuroscience, Signal Processing, and Electrophysiology. I hope this dissertation and future work will be a worthy reflection of the knowledge they shared with me.

I appreciate the opportunities extended to me by Phil Santangelo and Dr. Wichmann to rotate through their labs and learn cell culture, microscopy, optogenetic, and electrophysiology skills. I am thankful to the members of their labs who graciously allowed me to work alongside them and helped me on many occasions. I am very grateful to Beth Buffalo for suggesting that a rotation at Yerkes might be possible, and I express my heartfelt thanks to Adriana Galvan, who spent a lot of time teaching me how to work with non-human primates and perform electrophysiologic mapping.

Special thanks to Mark Clements for advisement and for partially funding the Parkinson's disease monitoring system, and to Dr. Wichmann for helping me understand the important issues in Parkinson's disease, and for trying to help me learn the art of scientific writing.

Many thanks to the NSF Teaching Fellowship and the Texas Instruments Leadership University (TILU) for funding my research, and, of course, to my committee for their time and participation.

TABLE OF CONTENTS

ACKNOWLEDGMENTS	iv
LIST OF TABLES	x
LIST OF FIGURES	xi
SUMMARY	xvi
I INTRODUCTION	1
1.1 Electrophysiologic analysis of parkinsonism	3
1.2 Connections between motor signs and electrophysiology	4
1.3 Multimodal monitoring	4
1.4 Organization	5
II BACKGROUND	7
2.1 Parkinson's disease	7
2.1.1 Motor and Non-motor Symptoms	7
2.1.2 Diagnosis	7
2.1.3 Affected Brain Regions	8
2.1.4 Treatments	10
2.1.5 1-methyl-4-phenyl-1,2,3,6-tetrahydropyridine (MPTP) Monkey Model	12
2.2 Analysis Methods and Models	12
2.2.1 Electrophysiology	12
2.2.2 Rate characterization	13
2.2.3 Oscillation characterization	14
2.2.4 Classification	15
2.2.5 Neural feature selection	16
2.2.6 Cross-frequency-coupling	17

III	PARKINSONISM-RELATED FEATURES OF NEURONAL DISCHARGE IN PRIMATES	19
3.1	Motivation	20
3.2	Methods	21
3.2.1	Animals	22
3.2.2	Surgical procedures	22
3.2.3	Electrophysiology	23
3.2.4	Administration of MPTP	24
3.2.5	Histology	25
3.2.6	Data analysis	25
3.3	Results	32
3.3.1	Discrimination achieved using results of different feature ranking algorithms	33
3.3.2	Comparison of features selected by the different methods	34
3.3.3	Top features for each nucleus	35
3.3.4	Reproducibility of results	38
3.4	Discussion	41
3.4.1	Best feature sets for discriminating between normal and parkinsonian states in different basal ganglia nuclei	41
3.4.2	Discrimination between nuclei	44
3.5	Conclusion	47
3.6	Contributions to work	47
IV	PARKINSONISM-RELATED FEATURES FROM SUBTHALAMIC NUCLEUS LOCAL FIELD POTENTIALS AND CORTICAL ELECTROENCEPHALOGRAMS	48
4.1	Discrimination between normal conditions and parkinsonism based on wavelet packet transform analysis of electroencephalographic (EEG) and subthalamic local field potential recordings	50
4.2	Classification of four stages of parkinsonism based on complex continuous wavelet transform phase-amplitude coupling features	52
4.2.1	Introduction	53

4.2.2	Methods	53
4.2.3	Results	56
4.2.4	Discussion	60
4.2.5	Conclusion	62
4.2.6	Contributions to work	63
V	CORRELATION BETWEEN MOTOR SCORES AND PHASE-AMPLITUDE COUPLING FEATURES IN PARKINSONISM PROGRESSION	64
5.1	Canonical correlation to estimate the degree of parkinsonism from local field potential and electroencephalographic signals	64
5.1.1	Motivation	64
5.1.2	Methods	66
5.1.3	Results	70
5.1.4	Discussion and conclusions	75
5.1.5	Contributions to work	76
5.2	Comparison between phase-amplitude coupling features and standard statistical measures for estimating the degree of parkinsonism	77
5.2.1	Methods	77
5.2.2	Correlation between Modulation Indices and Motor Scores	78
5.2.3	Discussion	82
5.2.4	Conclusion	86
VI	MULTIMODAL MONITORING SYSTEM FOR NEUROLOGICAL DISORDERS	87
6.1	Motivation	87
6.2	Background	88
6.3	Methods	90
6.3.1	Overview	90
6.3.2	Data Collection	91
6.3.3	EEG Analysis	92
6.3.4	Complex Continuous Wavelet Transform	92

6.3.5	Motor Data Analysis	92
6.3.6	Conclusion	93
6.4	Multi-sensor mobile monitoring human subject study	94
6.4.1	Introduction	95
6.4.2	Methods	96
6.4.3	Results	101
6.4.4	Discussion	104
6.4.5	Discussion and Conclusions	106
6.5	EEG assessment of PD in humans	107
VII	CONCLUSION	110
7.1	Importance of multiple, optimally-selected, non-redundant features. .	110
7.2	Correlation between motor signs and electrophysiology	111
7.3	Multimodal monitoring technology.	112
	REFERENCES	113
	VITA	126

LIST OF TABLES

1	Neuronal Discharge Features	23
2	Data Segments.	26
3	Table of Best Features	44
4	Accuracy of Motor Scores Estimated using Weighted Modulation Indices.	75
5	Statistical significance for Monkey 1 Canonical Correlation	81
6	Statistical significance for Monkey 2 Canonical Correlation	81
7	Statistical significance for Monkey 3 Canonical Correlation	82

LIST OF FIGURES

1	Impact of Parkinson’s disease on neural circuits [39]. Gray lines indicate connections that are predominantly excitatory; black lines indicate inhibitory connections. Thicker lines indicate increased effects; dashed lines indicate degenerating connections. M1 - Motor Cortex, PMC - Premotor Cortex, SMA - Supplementary Motor Area, CMA - Cingulate Motor Area, CM - Centromedian nucleus of the thalamus, VA/VL - Ventral Anterior/Ventral Lateral nuclei of the thalamus, SNc - Substantia nigra pars compacta, GPe - globus pallidus externa, STN - subthalamic nucleus, GPi/SNr - globus pallidus interna/Substantia nigra pars reticulata, PPN - pedunculopontine nucleus. Reprinted from Clinical Neurophysiology , vol. 119, no. 7, Adriana Galvan and Thomas Wichmann, “Pathophysiology of parkinsonism”, pp1459-1474, Copyright © 2008, with permission from Elsevier.	9
2	Neurons have characteristic patterns of firing in normal versus parkinsonian conditions that can be seen in the above signals captured at a high sampling rate (40 kHz) with microelectrodes placed in close proximity to individual neurons [39]. Reprinted from Clinical Neurophysiology , vol. 119, no. 7, Adriana Galvan and Thomas Wichmann, “Pathophysiology of parkinsonism”, pp1459-1474, Copyright © 2008, with permission from Elsevier.	13
3	It can be difficult to determine the presence and degree of parkinsonism when electrodes are not close to parkinsonian single cells, as shown in these Local Field Potential (LFP) examples. Top row shows z-scored LFPs in the pre-parkinsonian condition, then in mild, and moderate parkinsonism (left to right) for Monkey 1. Bottom row shows the same categories of z-scored LFP examples for Monkey 2. Each sample shows 10 seconds of activity. The y-axis for each sample ranges from -8 to +8.	14
4	Phase-amplitude coupling	18
5	Pearson Cross Correlations	31
6	Discrimination results for four different feature ranking methods	34
7	Summary Results. A: Single feature discrimination. B: Discrimination using optimal feature selection approaches.	36
8	Top two features providing the best discrimination for A. globus pallidus externa (GPe), B. globus pallidus interna (GPi), and C. Subthalamic nucleus (STN).	39

9	Data and trend lines for STN fractional spectral powers versus median intraburst firing rate; A. High frequency (30-100 Hz), and B. Low frequency (3-8 Hz) spectral power	40
10	Fraction correct discrimination between the baseline condition and three stages of parkinsonism using Wavelet Packet Transform (WPT) features. Shown for features extracted from both STN LFP and motor cortex electroencephalogram (EEG) data for Monkey 1 (left set of bars) and Monkey 2 (right set of bars). Error bars indicate the standard deviation for the 5-fold cross-validation.	52
11	Example Modulation Index (MI) feature images for a single parkinsonism score. Red corresponds to a high degree of cross-frequency-coupling, while dark blue corresponds to an absence of cross-frequency-coupling. The 36 MI features can be displayed in a 6x6 array (left) or in a column vector (right). This analysis used the column vector configuration in order to show changes in the features with increasing parkinsonism.	55
12	Phase-Amplitude Coupling features versus degree of parkinsonism for Monkey 1, Monkey 2, and Monkey 3. Vertical lines indicate columns of data belonging to each of the four stages of parkinsonism: Baseline (beginning to bold line), Stage 1, Stage 2, and Stage 3. Horizontal lines group the features by modulating phase. Within each phase group, the amplitude band increases from top to bottom.	57
13	Left: mean beta phase-amplitude cross-frequency-coupling (CFC) MIs; Right: Mean delta phase-amplitude CFC MIs; Monkey 1 (red), Monkey 2 (green), and Monkey 3 (blue).	58
14	Summed beta phase-amplitude CFC features (left) and beta powers (right) for Monkey 1 (top), Monkey 2 (middle), and Monkey 3 (bottom). The beta CFC features (left column) show low values under baseline conditions (0) and at maximum parkinsonism (12-12.5), with elevated beta values in between, while the beta powers (right column) do not show a consistent trend across the three monkeys.	59
15	Raw modulation index (MI) values per 10 second epoch for 1 of the 36 features (low beta phase modulation of the alpha amplitude) for Monkey 1 (top), Monkey 2 (middle), and Monkey 3 (bottom). Horizontal lines indicate the average baseline value for each monkey. The length of the baseline data segment is indicated underneath each graph. . .	61
16	Comparison between measured composite motor scores (dashed line) and motor scores estimated from the sum of the optimally weighted LFP MIs (solid line) for Monkey 1.	71

17	Distributions of the sum of the optimally weighted LFP MIs (composite modulation index) for each of the measured balance motor scores (x-axis) for Monkey 2. For each box, the central mark is the median, while the edges of the box are the 25th and 75th percentile. “Plus” symbol is an outlier.	72
18	Comparison between weighted EEG MIs (solid line) and composite motor scores (dashed line) for Monkey 1.	73
19	Distributions of the weighted EEG MIs corresponding to the freezing motor scores for Monkey 1.	73
20	Comparison between 2 STN LFP MIs and their reconstruction with EEG MIs for Monkey 1.	74
21	Correlation of parkinsonism rating with CFC MIs and standard statistical features extracted from band-filtered STN-LFP and M1-EEG data. As shown in the legend, the 3 standard statistical measures used were: magnitude of signal in all 6 bands, variance of signal in all 6 bands, and variance of signal in the beta band.	79
22	Parkinsonism estimates using CFC MI features (black), magnitude within frequency bands (magenta), and variance within frequency bands (blue). The visually rated parkinsonism scores are shown in red. (Monkey 1 left cortex data)	80
23	Parkinsonism estimates using CFC MI features (black), magnitude within frequency bands (magenta), and variance within frequency bands (blue). The visually rated parkinsonism scores are shown in red. (Monkey 3 STN data)	80
24	Parkinsonism estimates using CFC MI features (black), magnitude within frequency bands (magenta), and variance within frequency bands (blue). The visually rated parkinsonism scores are shown in red. (Monkey 2 right cortex data)	83
25	Z-scored variances in the 6 frequency bands for increasing parkinsonism (left to right). The x-axis denotes the data file number. Top row shows cortical variances. Bottom row shows STN variances. Left to right images show Monkey 1, Monkey 2, and Monkey 3, respectively.	83
26	Low beta STN (left) and cortical (right) variance (top row) and MI features (bottom row) for Monkey 1 (red), Monkey 2 (green), and Monkey 3 (blue) for increasing stages of parkinsonism. Note that the Monkey 2 cortical beta phase CFC MI plot (green trace in lower right figure) does not follow the same trend as Monkeys 1 and 3. This is consistent with the less accurate estimate of parkinsonism obtained using the Monkey 2 cortical MIs.	84

27	Mean raw (non-z-scored) cortical low beta variances (top row) and MIs (bottom row) for Monkey 1 (red), Monkey 2 (green), and Monkey 3 (blue) for increasing stages of parkinsonism. The variance features are dissimilar for the three monkeys, while the MI baseline features are similar for all monkeys. As previously shown in Figure 26, the Monkey 2 cortical MI features do not follow the same trend as the cortical MI features for the other two monkeys.	85
28	Target system: smartphone with accelerometer and gyroscope, wrist watch with accelerometer, and EEG headset	90
29	International 10-20 electrode configuration. Note the locations of A1, A2, C3, and C4.	91
30	Obtaining the PD score from the motor signals	95
31	Smartphone accelerometer output. Red, green, and blue lines indicate the x-, y-, and z- accelerations. Top plot shows normal movement. Bottom plot shows simulated parkinsonism.	97
32	Smartphone gyroscope output. Red, green, and blue lines indicate the angular velocities around the x-, y-, and z-axes. Top plot shows normal movement. Bottom plot shows simulated parkinsonism.	98
33	Smartphone accelerometer and gyroscope features with statistically significant discriminative power ($*p < 0.05$, $**p < 0.01$, $***p < 0.001$, $****p < 0.0001$)	99
34	Classification of normal and parkinsonian state based on trunk sensors. The leftmost set of bars shows the discrimination performance when the underlying activity type is unknown. The following 3 sets of bars show the discrimination performance conditioned on the activity type.	102
35	Classification of activity types. Note that a hierarchical classification of rest vs. movement (2nd set of bars) followed by STS vs. WWT (3rd set of bars) gave better results than the 3-way classification of movement (1st set of bars).	103
36	Watch accelerometer output. Note that the sit-to-stand (middle of top plot) and walking-with-turns (right of top plot) activities are visible in the normal (top) accelerometer trace.	104
37	Spectra from the watch accelerometer for two individuals (left and right). For each graph, the upper signal was captured during simulated tremors while the lower signal was captured during the normal movement sequences.	105

38 EEG CFC features for a single individual talking, then walking, and finally sitting quietly. Each column represents a 30 second epoch of data. 109

39 EEG CFC features for three different individuals. The first segment of talking is from individual one, immediately followed by the segments for individual two and three. The data is concatenated the same way for the walking and sitting activities. Each column represents a 30 second epoch of data. The data is z-scored to common μ and σ values for all three individuals. 109

SUMMARY

This research presents signal processing applications for extracting information from brain electrophysiology and movement signals. The approach taken does not assume any particular stimulus, underlying activity, or synchronizing event, nor does it assume any particular encoding scheme. Instead, novel signal processing applications of complex continuous wavelet transforms, cross-frequency-coupling, feature selection, and canonical correlation were developed to discover the most significant electrophysiologic changes in the basal ganglia and cortex of parkinsonian rhesus monkeys and how these changes are related to the motor signs of parkinsonism. The resulting algorithms effectively characterize the severity of parkinsonism and, when combined with motor signal decoding algorithms, allow technology-assisted multi-modal grading of the primary pathological signs. Based on these results, parallel data collection algorithms were implemented in real-time embedded software and off-the-shelf hardware to develop a new system to facilitate monitoring of the severity of Parkinson's disease signs and symptoms in human patients. Off-line analysis of data collected with the system was subsequently shown to allow discrimination between normal and parkinsonian conditions.

A suite of signal processing algorithms designed for decoding neural disease states, along with new insights gained by applying these tools to understanding parkinsonism, are presented in the following chapters. The main contributions of this work are in three areas: 1) Evidence of the importance of optimally selecting multiple, non-redundant features for understanding neural information, 2) Discovery of significant correlations between certain pathological motor signs and brain electrophysiology in

different brain regions, and 3) Implementation and human subject testing of multi-modal monitoring technology.

CHAPTER I

INTRODUCTION

Parkinson's disease (PD) is a degenerative disorder strongly linked to the death of dopaminergic neurons in the midbrain. The motor symptoms associated with the death of these neurons are known collectively as "parkinsonism". The cardinal motor symptoms of PD are: tremor at rest, bradykinesia (slowness of movement), akinesia (inability to move), stiffness or rigidity of the limbs and trunk, and postural instability. Carefully adjusted medication protocols can typically control symptoms for many years. However, controlling Parkinson's disease (PD) symptoms without generating side effects is difficult, particularly in patients 5-10 years or more post diagnosis [99]. The augmentation of standard medication protocols with deep brain stimulation (DBS) often reduces required medication dosages and associated side effects [100]. However, incorporating DBS, which also needs to be adjusted periodically, adds another level of complexity to an already difficult regulation problem. Current monitoring methods do not allow timely regulation of medication and DBS parameters.

In the research described in this document, both standard and novel electrophysiologic features that correlate with the motor signs of parkinsonism were identified. The electrophysiologic features allowed estimation of the degree of parkinsonism, outperformed current approaches, and behaved consistently across individuals. The electrophysiologic features and associated signal processing algorithms were used to design an approach for PD monitoring that allows long-term assessment of symptoms in an environment that is convenient and accessible for the patient. Based on the design specifications, parallel data collection algorithms were implemented in

real-time embedded software and off-the-shelf hardware to develop a new system to facilitate monitoring of the severity of Parkinson’s disease signs and symptoms in human patients. The resulting long-term multi-modal PD monitoring capability has the potential to provide physicians with valuable information needed to optimize patient treatment protocols and thereby improve PD patient quality of life.

Results from this research may not only improve PD treatments through more comprehensive monitoring, but may also add to our knowledge about how electrophysiologic changes in the brain relate to the severity of parkinsonism. Knowledge of how these biological descriptors behave may give insight into how the signaling pathways change in the brain as the disease progresses. Also, since these electrophysiologic changes are not measured relative to a particular stimulus or event, it is likely the measures contain a representation of the current state of the brain region from which they are recorded. Since the normal baseline state can be differentiated from the pathological PD state, it may be similarly possible to differentiate PD from other diseases, and other diseases from the normal baseline state using the approaches presented here. Further, monitoring such brain changes may allow development of closed-loop treatments that administer medication or deep brain stimulation until more normal brain states are achieved.

The algorithms and technologies developed in this dissertation have broad application, since the ability to decode brain signals associated with physical motor states and pathologies has the potential to impact many areas such as detecting, monitoring, and treating a wide variety of neurological disorders including dystonia, ALS, and Huntington’s disease, developing brain-machine-interfaces, and improving prosthetic devices through motor monitoring.

The methods for brain state detection in the absence of stimulus discussed in this dissertation have particularly wide application since most human activities vary depending on an individual’s current brain state. For example, human behavior is

impacted strongly by sleep state, emotional state, intoxication level, developmental state, and attention level, in addition to pathological brain states caused by disease or injury.

The main contributions of this work are in three areas: 1) Evidence for the importance of optimally selecting multiple, non-redundant features for understanding electrophysiological information, 2) Discovery of significant correlations between certain pathological motor signs and electrophysiology in different brain regions, and 3) Implementation and human subject testing of multi-modal monitoring technology.

1.1 Electrophysiologic analysis of parkinsonism

Analysis methods for neural decoding have historically been categorized as either rate, pattern, or oscillation approaches [25, 96]. However, the behavior of neurons cannot always be strictly characterized by any of these single categories. A better characterization may be possible with multiple descriptive features, particularly in the basal ganglia nuclei and other regions of the brain where neural behavior may vary broadly depending on underlying brain states. In Part 1, Chapter 3 (published in [106]), optimal feature selection approaches are used to identify the features most relevant for distinguishing between cells recorded in the parkinsonian versus non-parkinsonian state.

Similarly, historical analyses of electroencephalograms (EEGs) and local field potentials (LFPs) have focused on analysis of power within frequency bands [98, 35, 49]. In particular, the most commonly reported marker for Parkinson's disease has been increased power in the beta band [53, 77]. The coefficient of variation (CV) of beta magnitude has also been recently proposed as a potential marker for PD [77].

1.2 Connections between motor signs and electrophysiology

Correlation between electrophysiologic features and movement in PD has been explored in a few publications [69], however, relationships between electrophysiology and particular motor signs have not been clearly defined for PD motor signs other than resting tremor [50, 52]. In Chapter 5, canonical correlation was used to show statistically significant correlations between different weighted sets of electrophysiologic features and the bradykinesia, balance, and freezing motor signs.

1.3 Multimodal monitoring

Recently, there has been tremendous growth in the “quantified self” phenomenon, whereby consumers monitor their own activities using wearable devices and software. The growth in these devices and apps combined with the Twitter and blog buzz surrounding them makes it clear that consumers find self-help health tools useful, and are willing to wear unobtrusive mobile health devices regularly. Additionally, research indicates that such devices are promoting positive long-term lifestyle changes for many consumers [22]. These and other factors have prompted research and development efforts aimed at creating mobile methods for testing glucose levels, heart health, and cellular and molecular pathologies. For individuals with chronic medical conditions, such monitoring technologies are helpful for health status tracking and safety, and perhaps even more importantly, for assessing response to treatments. The latter is also important for drug and treatment developers. In the future, clinical trials will likely take advantage of monitoring technologies to quantify patient response to treatment. Chapter 6 presents a multi-modal monitoring system for assessing movement disorders. It is currently specifically targeted to parkinsonism and uses the electrophysiologic features described in Chapter 5 along with motor features from wearable accelerometers and a gyroscope.

1.4 *Organization*

In the work described in Chapter 3, classical signal processing approaches were applied to a set of single cell data from three basal ganglia nuclei in rhesus monkeys: subthalamic nucleus (STN), globus palladis interna (GPi), and globus palladis externa (GPe), to provide a set of optimal measures for discriminating between normal and parkinsonian recordings. The results showed that the three nuclei behave differently in the parkinsonism state as compared to the normal state, and gave insight into the most changed aspects of neural discharge, suggesting critical features for models of cellular behavior in parkinsonism and providing knowledge that may be useful for surgical treatment approaches using single cell measures to locate optimal regions for lesioning or placing neuromodulation implants.

The most changed aspects of single unit neural discharge in the parkinsonian state were measures of individual cell bursting and oscillation activity, particularly in the STN, suggesting that other measures of STN oscillation activity, such as STN local field potential (LFP) frequency measures, might also be useful for characterizing and discriminating between parkinsonian and normal conditions. This work has been published in [106].

Further work, described in Chapter 4, showed that wavelet packet transform (WPT) measures of STN LFP oscillations allowed discrimination between the two conditions in rhesus monkeys, and found that WPT measures of primary motor cortex (M1) EEGs also allowed discrimination. Evidence of discriminable population activity in both STN and M1 in the parkinsonian state provided a set of related measures that can be used to analyze correlation and changes in correlation between STN and M1 in parkinsonian and normal conditions.

The work presented in Section 4.2 identified common discriminable parkinsonian patterns occurring in three monkeys for four stages of parkinsonism.

In work described in Section 5.1 and published in [105], correlations between STN

and M1 cross-frequency-coupling (CFC) features were identified and a set of M1 CFC features were used to estimate two STN CFC features important for discriminating between data recorded in normal and parkinsonian states.

In the same work, significant correlations between composite and individual parkinsonism motor scores and the STN and M1 CFC features were found. The presence of these significant correlations suggest that STN and M1 CFC features can be used either alone or in conjunction with parkinsonism motor scores to assess degrees of parkinsonism.

A comparison of the methods used in Section 5.1 with current standard statistical measures is presented in Section 5.2. It is shown that, while commonly used statistical markers are somewhat correlated to the increase in motor scores, the wavelet features and cross-frequency-coupling measures described in Section 5.1 are more correlated and better discriminate between baseline neural conditions and severity of parkinsonism. Based on the analysis, the optimal set of markers introduced in this work may be useful biomarkers for grading parkinsonism in humans, and possibly also for providing feedback for adaptive treatment approaches such as deep brain stimulation (DBS).

Chapter 6 describes the prototype PD monitoring system and presents the data analysis results for a preliminary study with human subjects. The initial prototype design has been published in [104].

CHAPTER II

BACKGROUND

2.1 Parkinson's disease

Parkinson's disease (PD) is a degenerative nervous system disorder. The motor symptoms associated with PD are known collectively as "parkinsonism". The average age for PD onset is 60 years, but patients younger than 19 years of age have been diagnosed [2]. Due to the expected increase in the 60+ age group in the US population, the number of diagnosed cases is likely to rise significantly in the next decades [28]. PD is chronic and progressive and most cases are idiopathic (of unknown cause). There is no cure, although treatments are available to manage symptoms [91, 126].

2.1.1 Motor and Non-motor Symptoms

The cardinal motor symptoms of PD are: tremor at rest, bradykinesia (slowness of movement), akinesia (inability to initiate movement), stiffness or rigidity of the limbs and trunk, and postural instability (impaired balance and coordination). However, symptoms vary among individuals and may include stooped posture, shuffling gait, decreased arm swing when walking, difficulty rising from a chair, micrographia (small, cramped handwriting), and lack of facial expression. Non-motor symptoms such as a diminished sense of smell (now indicated as one of the earliest symptoms), difficulty speaking and low voice volume, sleep disturbances, depression, cognitive impairment, and drooling may also occur [88].

2.1.2 Diagnosis

Many of the motor symptoms of PD are caused by the death of dopaminergic neurons in the substantia nigra pars compacta (SNc). Confirmed death of these neurons,

along with the presence of Lewy bodies (eosinophilic cytoplasmic inclusions, primarily composed of alpha-synuclein) in the brain, is the primary observation leading to post-mortem diagnosis of PD [111, 44]. The mechanisms behind the loss of these dopaminergic neurons are not fully understood, and difficult to observe. However, the reduction in dopamine (DA) caused by the loss of these cells leads to a well-known group of symptoms, upon which PD is typically diagnosed [39]. The Unified Parkinson's Disease Rating Scale (UPDRS) is the most commonly used scale for rating PD signs and symptoms. Scores from part III of the UPDRS, the motor examination, indicate the clinician's assessment of 18 items related to individual motor signs and the overall severity of parkinsonism.

Since 2011, reduction in dopamine transporter (DAT) in the putamen observed using single photon emission computed tomography (SPECT) imaging with the ioflupane (^{123}I) ligand known as DaTscan, has been approved in the United States as a useful aid for confirming diagnosis of PD. The results of a DaTscan are useful for differentiating between essential tremor and PD. However, it cannot differentiate between PD and multiple system atrophy (MSA) or progressive supranuclear palsy (PSP), which can also produce a loss of dopamine in the brain.

2.1.3 Affected Brain Regions

The mechanisms underlying the development and manifestation of parkinsonisms are not fully known [49, 30]. It is known that the nigrostriatal dopaminergic pathway that connects the SNc with the portion of the striatum implicated in the control of movement is particularly involved in parkinsonism [109, 94]. A classical diagram showing regions of the thalamus, brainstem and motor cortex that may also contribute to parkinsonism is shown in Figure 1 [41, 73, 42, 24]. More recently, other interactions relevant to PD pathology have also been identified [117].

Parkinsonism results in firing abnormalities of basal ganglia neurons in the subthalamic nucleus (STN) and the internal and external pallidal segments (GPi and GPe, respectively) [88, 30, 42, 121]. It is very likely that such abnormalities are linked to the generation of the motor signs of Parkinson's disease, given the remarkable antiparkinsonian effects of pallidotomies and other surgical interventions aimed at the basal ganglia [5, 70, 76, 81, 119].

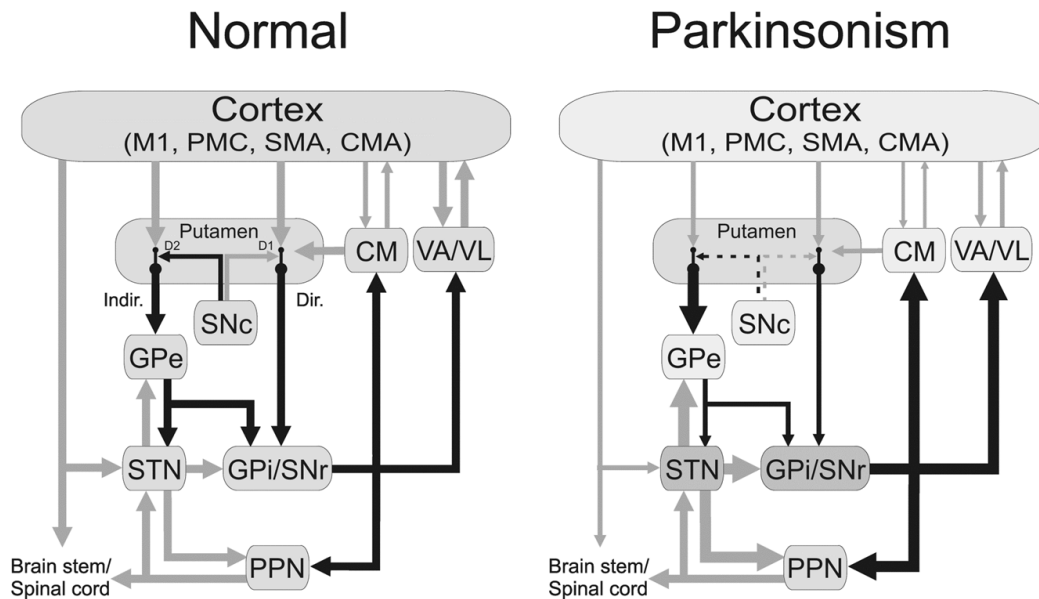


*Figure 1: Impact of Parkinson's disease on neural circuits [39]. Gray lines indicate connections that are predominantly excitatory; black lines indicate inhibitory connections. Thicker lines indicate increased effects; dashed lines indicate degenerating connections. M1 - Motor Cortex, PMC - Premotor Cortex, SMA - Supplementary Motor Area, CMA - Cingulate Motor Area, CM - Centromedian nucleus of the thalamus, VA/VL - Ventral Anterior/Ventral Lateral nuclei of the thalamus, SNc - Substantia nigra pars compacta, GPe - globus pallidus externa, STN - subthalamic nucleus, GPi/SNr - globus pallidus interna/Substantia nigra pars reticulata, PPN - pedunculopontine nucleus. Reprinted from *Clinical Neurophysiology*, vol. 119, no. 7, Adriana Galvan and Thomas Wichmann, "Pathophysiology of parkinsonism", pp1459-1474, Copyright © 2008, with permission from Elsevier.*

2.1.4 Treatments

2.1.4.1 Medication

PD is currently treated primarily with medications that seek to re-instate the effects of dopamine in parkinsonian patients. Levodopa, combined with a decarboxylase inhibitor such as carbidopa, is the most effective medication for PD, although treatments with dopamine agonists such as pramipexole or ropinirole have been shown to be beneficial for many patients [28].

2.1.4.2 Deep Brain Simulation

If medication does not adequately control symptoms due to the disease progression, surgical interventions can be used [67]. In particular, surgical installation of electrodes in the basal ganglia region for the purpose of deep brain stimulation (DBS) has proven helpful for regulating symptoms in medically refractory PD [12]. DBS treatments consist of electrical stimulation of portions of the brain with high frequency pulses (usually 130 Hz) through implanted macroelectrodes. The biological effects of DBS are poorly understood. DBS electrodes are surgically implanted in deep brain regions such as the STN or GPi, while the pulse generator (pacemaker) is implanted in the subclavicular region. An insulated electrical extension connects the pacemaker with the electrodes [65]. At present, DBS treatments run continuously. However, there is interest in developing closed-loop DBS that can trigger or adjust stimulation as needed [78, 101, 36]. The advantages of such a technique include a reduced potential for DBS-induced side effects, such as difficulty with speech or balance, due to less time on, and improved longevity of the device and its batteries (important since replacement requires repeated costly surgeries) [36].

2.1.4.3 *Monitoring*

PD patients often require frequent medication dosage adjustments, especially in advanced stages of the disease when they develop “wearing off” effects (reduced symptom relief in between medication doses) or dyskinesias (involuntary muscle movements) which are common side effects of long-term levodopa therapy [28]. Likewise, DBS parameters have to be frequently adjusted to retain sufficient DBS benefit while limiting side effects. This is logistically difficult, as patients typically see their physicians very intermittently, and because physician assessments on observations during such clinic visits may not capture the full breadth of patient symptoms and signs [12].

Since the degeneration of the dopaminergic system in PD is associated with changes in brain signaling and pathological synchronizaton, analysis of brain activity through LFPs and EEGs in the affected brain regions may be useful for detection and objective monitoring of the symptoms and signs of PD. LFP measurements for this pupose can be collected using implanted DBS electrodes as recording electrodes. However, this procedure is complicated by the fact that monitoring activity from chronically implanted DBS electrodes requires careful signal conditioning to avoid artifact effects, and can be variable over time due to impedance and frequency response changes [1]. EEG signals, on the other hand, are attractive for monitoring because they can be used in patients without implanted DBS electrodes, are comparatively inexpensive, and can be recorded with minimally invasive electrodes. However, in the past, high electrode noise levels and inconsistent findings in EEGs have impeded progress in their use. Recent successful efforts to reduce electrode noise [80, 127] and advanced signal processing approaches [112, 66] have led to renewed interest in the technology. Similarly, ECoG has recently become of interest for long-term monitoring due to newer, less invasive implantation techniques [102].

2.1.5 1-methyl-4-phenyl-1,2,3,6-tetrahydropyridine (MPTP) Monkey Model

Several animal models have been developed to aid in studying PD. The current gold standard is the non-human primate 1-methyl-4-phenyl-1,2,3,6-tetrahydropyridine (MPTP) model [16, 123, 29]. Administration of the neurotoxin precursor MPTP to monkeys damages neurons in the SNc and produces parkinsonism [8]. The effect of common treatments for PD are also faithfully replicated in the MPTP model of primate parkinsonism [23, 26]. Because of the similarities in motor signs, affected brain structures, and response to treatments, MPTP-induced parkinsonism is useful for studying potential therapies for parkinsonism.

2.2 *Analysis Methods and Models*

2.2.1 Electrophysiology

Electrical activity from neurons can be captured with a variety of different electrodes. The recorded signals are filtered differently depending on the characteristics of interest. Firing times of individual action potentials (spike times) are obtained by isolating individual action potentials in band-pass filtered signals from extracellular microelectrodes placed within close proximity ($< 0.3 \text{ mm}$) to a single neuron or group of neurons (see Figure 2). If multiple neurons are recorded, the action potentials (spikes) are sorted into groups based on amplitude, width, and other characteristics in order to assign each spike (and spike time) to a series of similar spikes believed to originate from an individual neuron. 300 Hz - 6000 Hz is the nominal range for the band-pass filter used to enable capturing individual action potentials with standard thresholding and template matching.

Local field potentials (LFPs), on the other hand, are typically obtained by low-pass filtering (below $\sim 300 \text{ Hz}$) signals from extracellular electrodes with the goal of obtaining a signal that reflects neural population dynamics in the region. LFP signals (see Figure 3) are believed to reflect the sustained currents, such as the synaptic and

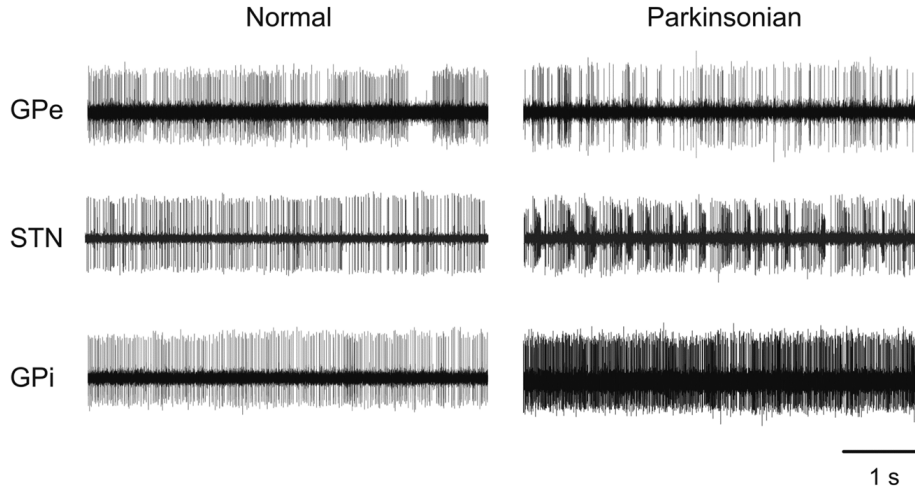


*Figure 2: Neurons have characteristic patterns of firing in normal versus parkinsonian conditions that can be seen in the above signals captured at a high sampling rate (40 kHz) with microelectrodes placed in close proximity to individual neurons [39]. Reprinted from *Clinical Neurophysiology*, vol. 119, no. 7, Adriana Galvan and Thomas Wichmann, “Pathophysiology of parkinsonism”, pp1459-1474, Copyright © 2008, with permission from Elsevier.*

somato-dendritic currents, in the region of the electrode.

Cortical signals may be recorded using either of the above approaches. However, electrocorticography (eCoG) electrode grids, or epidural or non-invasive electroencephalographic (EEG) electrodes (usually with a lower signal-to-noise due to attenuation of the signal by the skull) are also used. In this dissertation, spike times, or more precisely, inter-spike time intervals (ISIs) were used for the work in Chapter 3, while LFPs and EEGs were analyzed for the remaining work. Figure 3 shows example STN LFPs from two different monkeys recorded in baseline (normal) conditions, mild parkinsonism, and moderate parkinsonism.

2.2.2 Rate characterization

Rate methods, so-called because they rely on neuron firing rate related measures of PD, typically look at the behavior of single cells and networks of cells. Because of this they are more constructive in nature. The general theory behind these approaches is that PD-related dopamine loss causes changes in the firing rate of individual cells;

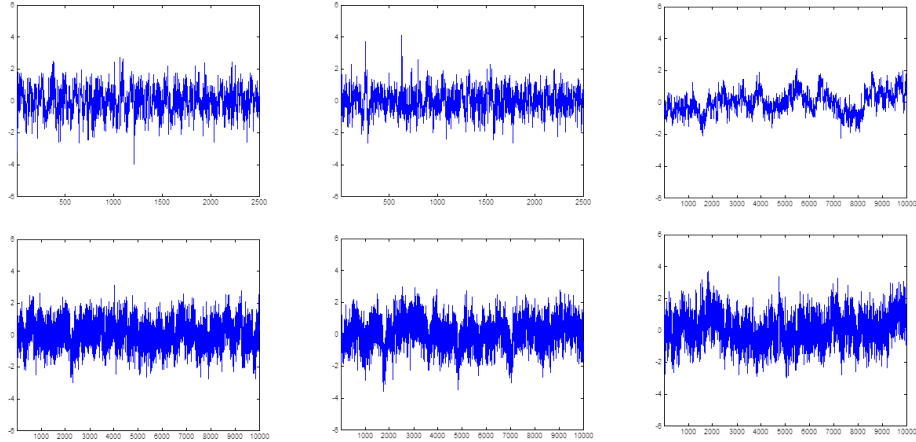


Figure 3: It can be difficult to determine the presence and degree of parkinsonism when electrodes are not close to parkinsonian single cells, as shown in these Local Field Potential (LFP) examples. Top row shows z-scored LFPs in the pre-parkinsonian condition, then in mild, and moderate parkinsonism (left to right) for Monkey 1. Bottom row shows the same categories of z-scored LFP examples for Monkey 2. Each sample shows 10 seconds of activity. The y-axis for each sample ranges from -8 to +8.

these firing rate changes, in turn, impact downstream neurons and propagate throughout the brain. Rate approaches may consider various firing rate statistics such as mean, standard deviation, or coefficients of variation (CV). Typical analysis methods include peristimulus time histograms (PSTH), auto- and cross-correlations, and coherences [13].

Early studies of basal ganglia firing abnormalities focused on changes in the mean discharge rate of basal ganglia neurons, with the finding that GPe firing rates were reduced, while GPi and STN firing rates were increased in animal models of the disease (e.g.,[4, 8, 29, 34, 88, 120].) Basal ganglia neurons show a greater-than-normal tendency to discharge in bursts in the parkinsonian state, as has been shown in animal models [8, 10, 88, 90, 118, 121].

2.2.3 Oscillation characterization

Oscillation approaches, which rely on frequency analysis methods, typically look at the composite behavior of cells in a region through population signals such as LFPs

or EEGs. Thus, these approaches tend to be more top-down in nature.

Basal ganglia neurons often fire in oscillatory firing patterns. These patterns of activity have been documented in the basal ganglia since at least the early 1980s [8, 41, 49, 87]. Following the discovery of strong beta band oscillations in LFP recordings from the STN in parkinsonian patients [14], many current authors see these oscillations as the predominant electrophysiological abnormality in the parkinsonian brain. Oscillations are primarily identified in STN, GPi, and GPe [8, 75, 74, 73], although other areas of the basal ganglia-thalamocortical circuitry also show oscillatory discharge [46, 48, 95, 97]. The generation of these oscillatory activity patterns has not been clarified, but experimental and modeling studies have suggested that they are the product of network interactions and pathological synchronizations rather than due to oscillations at a single basal ganglia location [41, 49, 53, 82, 84, 83].

Oscillation methods for decoding electrical brain activity often focus on average power in various frequency bands. However, average power approaches have been shown to yield conflicting results, particularly when looking at data across different individuals [92, 38]. Such average power changes are not found at all in some PD patients (and in some of the rodent and primate models of PD), even in the presence of clear and convincing parkinsonism.

In spite of these sometimes conflicting results, average power methods have uncovered a few PD features, such as elevated power in oscillations at frequencies between 13 and 30 Hz, known as the beta band, that have been observed in many patients [49, 35]. However, in the results presented, frequency coupling power was a better predictor of PD pathology than average power in a band.

2.2.4 Classification

In this document, “classification” refers to the process of separating data into classes using machine learning and/or statistical techniques. Binary classification, known

as discrimination, was performed with Support Vector Machine (SVM) techniques. SVMs are “supervised classifiers”, meaning that the class boundaries are defined using training data. An SVM separates data into classes in N-dimensional space by finding the hyperplane that provides the maximum margin between “support vectors” (boundary points) at the class boundaries in the training data. Non-linear classification can be performed with SVMs using kernels that effectively map the N-dimensional data into a higher dimensional space. This work used the kernel most commonly paired with SVM techniques, the Gaussian radial basis function kernel.

When more than two classes were involved, Linear Discriminant Analysis (LDA) was used in order to simplify visualization of results. LDA is also a supervised classification technique. In this approach, a multivariate normal density is fit to each class in the training set. The classification boundaries are then determined by the relative probability densities associated with each class.

Classification performance results in this work were calculated using k-fold cross-validation. In this method, the data is repeatedly divided into k different subsets of equal size, chosen randomly. Each subset is then tested using the classifier trained on the remaining k-1 subsets [54]. In most cases $k = 5$ in this work. The reported results are the average performance of the classifier over all the different subset permutations.

2.2.5 Neural feature selection

Feature selection refers to the process of identifying “features”, or measurable attributes, that are useful for analysis of events, systems, or classes of objects from which the features are measured. Although some progress in understanding neural activity has been made by analyzing simple features such as firing rate statistics and oscillatory power in particular frequency bands, a richer set of features will be needed to begin to delve further into the complexity of the human brain and to decipher the variety of neural encoding mechanisms employed there. This work uses

optimal feature selection methods from classical signal processing to consider both novel and standard features and to determine which features contain the information most useful for discriminating between pathological states. Not surprisingly, the work shows that multiple types of features are more useful than features from a single category, and that the most informative features vary by brain structure. A novel implementation of one particularly useful class of features, phase-amplitude cross-frequency-coupling was created and examined in detail.

2.2.6 Cross-frequency-coupling

Several new measures have been created recently to quantify the interactions between oscillations [7, 79]. Studies using these features typically analyze the data in averaged trials relative to a stimulus event [19]. In the work described in the following chapters, novel methods were developed for analyzing stimulus-independent oscillation interactions based on cross-frequency-coupling (CFC) measures extracted from Complex Continuous Wavelet Transform (CCWT) coefficients.

The following CCWT formulation was used:

$$X_w(c, n) = \frac{1}{\sqrt{c}} \int_{-\infty}^{\infty} x(t) \psi^* \left(\frac{t - n}{c} \right) dt$$

where “c” represents the scale factors and “n” represents the time points at which the CWTs are evaluated, and $\psi(t)$ is the complex Morlet wavelet:

$$\psi(t) = \kappa (e^{-\frac{t^2}{BW}}) (e^{2i\pi fct})$$

Composite signals were created by pooling the wavelet coefficients corresponding to the wavebands of interest. Phase and amplitude data were then extracted from the composite signals and used to compute the CFC measures as follows.

CFC evaluates how the amplitude or phase of one waveband changes as a function of the amplitude or phase of a second waveband. In this work, we use phase-amplitude CFC quantified with a modulation index (MI) calculation. In order to obtain the

MI, the phase and amplitude data of the wavebands are examined in a pair-wise fashion. The phase values of the first waveband of interest are divided into 18 bins, and the amplitudes in the second waveband that co-occur with the phases from the first waveband are averaged over each bin. If no cross-frequency-coupling is present (only random fluctuations), the values in the 18 bins will be similar (appear uniform). However, if there is cross-frequency-coupling, then the values will not be uniform. The divergence from uniform is evaluated using the two-sided Kullback-Leibler divergence between two discrete distributions,

$$D_{\text{KL}}(P\|Q) = \sum_i \ln \left(\frac{P(i)}{Q(i)} \right) P(i).$$

where $Q(i)$ indicates the uniform distribution that occurs when the amplitudes are distributed randomly across all phases, and $P(i)$ indicates the distribution obtained by normalizing the phase-amplitude coupling calculated as described above. The two-sided divergence was used, i.e., $D_{\text{KL}}(P\|Q) + D_{\text{KL}}(Q\|P)$, in order to give a symmetric measure of the deviation from the uniform distribution.

Figure 4 shows examples of the averaged amplitude (y-axis) versus phase bin (x-axis) values for strong (left) and weak (right) coupling.

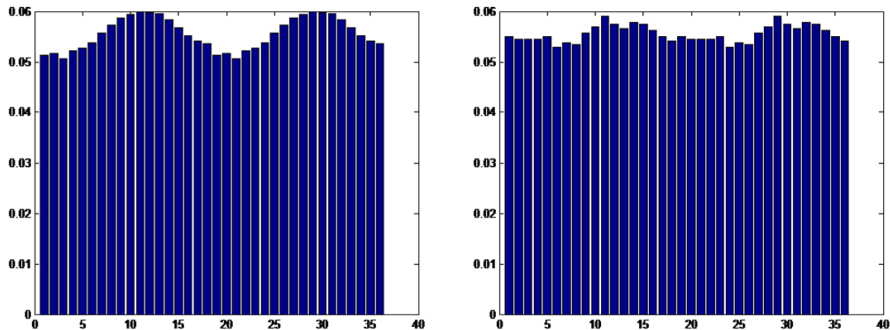


Figure 4: Phase-amplitude coupling

CHAPTER III

PARKINSONISM-RELATED FEATURES OF NEURONAL DISCHARGE IN PRIMATES

Parkinson's disease is known to be associated with abnormal electrical spiking activities of basal ganglia neurons, including changes in firing rate, bursting activities, oscillatory firing patterns, and changes in entropy. We explored the relative importance of these measures through optimal feature selection and discrimination analysis methods. Key characteristics of basal ganglia activity were found that predicted whether the neurons were recorded in the normal or parkinsonian states. Starting with 29 features extracted from the spike timing of neurons recorded in normal and parkinsonian monkeys in the internal or external segment of the globus pallidus (GPI, GPe), or the STN, a computationally intensive method that incorporates a support vector machine was used to find feature combinations that optimally discriminate between the normal and parkinsonian states. The results demonstrate that the discrimination power of combinations of specific features is higher than that of single features, or of all features combined, and that the most discriminative feature sets differ substantially between structures. Each nucleus or class of neurons in the basal ganglia may react differently to the parkinsonian condition and the features used to describe parkinsonism should be adapted to the neuron type under study. The feature most predictive of the parkinsonian state, the STN intra-burst frequency, was found to have a significantly changed relationship to STN oscillations under parkinsonism. Interestingly, this feature was not correlated with parameters describing oscillatory firing properties in recordings made in the normal condition, but was significantly correlated with spectral power in specific frequency bands in recordings from the

parkinsonian state (specifically with power in the 8-13 Hz band). The work presented in this chapter has been published in [106].

3.1 Motivation

It is well known that parkinsonism results in firing abnormalities of basal ganglia neurons, specifically in the subthalamic nucleus (STN) and the internal and external pallidal segments (GPi and GPe, respectively). It is very likely that such abnormalities are ultimately linked to the generation of the motor signs of Parkinson's disease, given the remarkable antiparkinsonian effects of pallidotomies and other surgical interventions aimed at the basal ganglia ([5, 70, 76, 81, 119]). Early studies of basal ganglia firing abnormalities focused on changes in the mean discharge rate of basal ganglia neurons, with the finding that the average firing rates of GPe neurons were reduced, while the average firing rates in GPi and STN were increased in animal models of the disease (e.g., [4, 8, 29, 34, 37, 88, 120]), as well as patients ([55, 89]). Recent optogenetic studies have reinforced the idea that global changes in basal ganglia output contribute to parkinsonism ([64]). More recent studies have emphasized changes in firing patterns. For instance, basal ganglia neurons have a greater-than-normal tendency to discharge in bursts in the parkinsonian state, as has been shown in animals [8, 10, 37, 88, 90, 118, 121] and humans [55]. A subset of these bursts may represent rebound (or low threshold spike) bursts, presumably driven by activation of T-type calcium channels in the basal ganglia and thalamus. Abnormal bursting in the basal ganglia and thalamus may not only be related to the motor signs of parkinsonism, but may also underlie some of the arousal deficits in Parkinson's disease [6, 43]. Another parkinsonism-related property of spiking activities of basal ganglia neurons is that these neurons often fire in oscillatory firing patterns. These patterns of activity have been documented in the basal ganglia since at least the mid-1980s [8, 41, 49, 87]. Following the discovery of strong β -band oscillations

in local field potential recordings from the STN in parkinsonian patients [14], many current researchers see these oscillations as the predominant electrophysiological abnormality in the parkinsonian brain. Oscillations are primarily identified in STN, GPi, and GPe [8, 75, 74], although other areas of the basal ganglia-thalamocortical circuitry also show oscillatory discharge [46, 48, 97]. The source of these oscillatory activity patterns has not been clarified, but experimental and modeling studies have suggested that they are the product of network interactions rather than being generated at specific basal ganglia locations [41, 49, 53, 82, 84]. Most recently, several studies have observed that the spiking activity of neurons in the individual basal ganglia nuclei differs in terms of entropy and other non-linear characteristics of firing [41], and that these changes are affected in parkinsonian patients by treatment with dopamine receptor agonists or with deep brain stimulation in animal models of parkinsonism. The relative preponderance and importance of these firing abnormalities in the dopamine-depleted state, and their relationship to parkinsonism is not clear, in part because most studies in this field tend to focus on individual changes (such as changes in firing rates, bursts, or oscillations). In order to develop a better understanding of the relative strength of these changes, we carried out an analysis in which we evaluated the ability of combinations of multiple descriptors of single-cell discharge in the basal ganglia to predict parkinsonism, using recordings in STN, GPe and GPi from normal and MPTP-treated (parkinsonian) monkeys.

3.2 Methods

Some of the data used in this analysis were also used in previous studies [110, 121]. The activity in GPe, STN and GPi was first recorded in the normal state, and then again after the animals had been treated with MPTP to induce parkinsonism. The state of wakefulness was monitored throughout all experiments, and recordings were discarded if the animal showed signs of drowsiness. After completion of the recording

sessions, the location of the neurons was verified by histologic analysis. Inter-spike interval (ISI) data from the recorded cells were then analyzed to measure the firing rate, descriptors of burst discharges, entropy, or oscillatory activity. These analyses resulted in 29 features (listed in Table 1) which were fed into different feature selection algorithms to identify single features, or combinations of them, that would best discriminate between neurons recorded in the normal and parkinsonian states, separate for each of the three structures.

3.2.1 Animals

The two Rhesus monkeys (*Macaca mulatta*, 4-5 kg) that were used for these studies were housed under conditions of protected contact housing, with free access to standard primate chow, water, and supplemental fruit and vegetables. Prior to the recording sessions, the animals were adapted to the laboratory environment, and trained to sit in a primate chair and permit handling by the experimenter. All experimental protocols were performed in accordance with the NIH Guide for the Care and Use of Laboratory Animals (Anonymous, 1996), the PHS Policy on the Humane Care and Use of Laboratory Animals (amended 2002), and the American Physiological Societys Guiding Principles in the Care and Use of Animals (revised, 2000). All experiments were approved by the Institutional Animal Care and Use Committee of Emory University.

3.2.2 Surgical procedures

After completion of behavioral conditioning, stainless steel chambers for chronic recording (inner diameter 16 mm) were stereotaxically positioned over trephine holes under aseptic conditions and isoflurane inhalation anesthesia (1-3 percent). Chambers directed at the pallidum (GPe, GPi) were placed at an angle of 50 from the vertical in the coronal plane and chambers aimed at the STN were placed at an angle of 36 anterior to the vertical in the sagittal plane. The chambers were affixed to the

Table 1: Neuronal Discharge Features

<p><i>Basic descriptors of firing</i></p> <ol style="list-style-type: none">1. mean ISI2. SD of ISIs3. CV of ISIs4. firing rate <p><i>Integrated Spectral power</i></p> <ol style="list-style-type: none">5. 1-3 Hz range6. 3-8 Hz range7. 8-13 Hz range8. 13-30 Hz range9. 30-100 Hz range <p><i>Entropy Measures</i></p> <ol style="list-style-type: none">10. H111. H212. H313. H414. H515. zc116. zc217. zc318. zc419. zc5 <p><i>Measures describing bursting</i></p> <ol style="list-style-type: none">20. burst-free rate21. mean spikes per burst22. median spikes per burst23. mean intra-burst frequency24. median intra-burst frequency25. proportion of time in bursts26. proportion of spikes in bursts27. proportion of rebound bursts28. proportion of LTS bursts29. proportion of rebound LTS bursts
--

skull with dental acrylic. Stainless steel head holders were also embedded into the acrylic cap to permit stabilization of the head during the recording sessions.

3.2.3 Electrophysiology

All recordings were done with the animal seated in a standard primate chair, with its head restrained. Recordings were only conducted if the animal was fully awake (verified by direct observation). The neuronal activity in GPe, GPi and STN was recorded

extracellularly with tungsten microelectrodes (Frederick Haer Co., Bowdoinham, ME; impedance 0.5-1.0 M at 1 kHz). The microelectrodes were lowered into the brain with a microdrive (MO-95B, Narishige, Tokyo, Japan), using a guide tube that was positioned with its tip barely penetrating the surface of the brain to protect the electrodes as they passed through the dura. The electrical signals were amplified (DAM-80 amplifier, WPI, Sarasota, FL), filtered (400-10,000 Hz, Krohn-Hite, Brockton, MA), displayed on a digital oscilloscope (DL1540, Yokogawa, Tokyo, Japan), made audible via an audio amplifier, and recorded as digital signals, using a video recording adapter (model 3000A; Vetter, Rebersburg, PA; sampling rate: 40 kHz). Neurons in the basal ganglia were identified by generally accepted characteristics such as high frequency discharge with pauses in GPe, tonic high frequency discharge in GPi, and tonic and regular discharge in an area of high background activity in the STN (see [9]). We did not discriminate between specific functional territories within the basal ganglia in these recordings, thus, records from motor and non-motor areas were included in the analysis.

3.2.4 Administration of MPTP

After completion of recordings in the normal state, the animals received MPTP, injected under general isoflurane anesthesia (1-3%) into the right common carotid artery with the external carotid artery occluded, so that the toxin reached the brain via the internal carotid artery (0.5 mg/kg per injection; one monkey received two injections separated by two weeks, while the other received a single one). Both animals developed similarly obvious signs of moderate parkinsonism (bradykinesia, rigidity, flexed posturing of arm and leg) contralateral to the injections. The animals did not receive any dopaminergic medications throughout these experiments. The recordings in the parkinsonian state started 2 months after the MPTP injection. Throughout the post-MPTP period, the behavioral state of the animals remained

stable, as assessed with routine behavioral observations ([63, 110, 122]). After stable parkinsonism was established, electrophysiological recordings resumed on the left side (contralateral to the MPTP-administration).

3.2.5 Histology

At the conclusion of the experiments, the monkeys were killed by induction of deep anesthesia with an overdose of sodium pentobarbital, followed by transcardial perfusion with saline and 4% paraformaldehyde in 0.1 M phosphate buffer (pH 7.2). The brains were removed and cryoprotected in 30% sucrose solution in 0.1 M phosphate buffer. The fixed brain was sectioned in coronal planes (50 μ m). One of every four sections was stained with cresyl violet for localization of microelectrode tracks. The results of the histologic examinations are documented in our previous publication [110].

3.2.6 Data analysis

Preliminary steps. We included cells in the analysis only if the reconstruction of their location, based on stereotaxic information, micromanipulator readings during the recordings, and the results of postmortem histologic analysis, confirmed that they were located within one of the target structures (GPe, GPi, or STN). For inclusion into the analysis, cells also had to be adequately isolated throughout the record, as defined by a signal-to-noise ratio of their signals of 3 or greater. The recorded activity was processed with a template-matching spike sorting device (Alpha-Omega, Nazareth, Israel) which extracted the timing of spike occurrence. The data were stored as ISIs. The ISI data were imported into Matlab (MathWorks, Natick, MA) for further analysis. For confirmation of adequate signal isolation, we constructed ISI distribution histograms for quality control. In addition, raster displays of the spontaneous firing of each cell were carefully examined and episodes of stationary discharge were selected in a blinded fashion. As shown in detail in Table 2, the

Table 2: Data Segments.

Structure	State	Number of cells	Number of events mean \pm SD (range)	Length of records (s) mean \pm SD (range)
GPe	Normal	44	36894.2 \pm 16194.1 (5102 - 72182)	554.3 \pm 169.4 (72.1 – 842.3)
	MPTP	40	26157.2 \pm 13572.1 (9108 – 71191)	547.7 \pm 126.0 (286.7 – 830.5)
GPi	Normal	33	38073.7 \pm 14633.9 (5182 – 61656)	523.0 \pm 151.7 (63.3 – 644.8)
	MPTP	34	44380.6 \pm 17070.5 (12689 – 107684)	568.9 \pm 159.0 (164.9 – 1201.2)
STN	Normal	15	11260.9 \pm 5379.7 (2783 – 23626)	498.4 \pm 166.1 (73.4 – 671.7)
	MPTP	28	21104.3 \pm 7594.6 (8054 – 37870)	561.8 \pm 95.2 (225.5 – 640.9)

eventually processed data segments were 546.9 ± 146.4 s long (mean \pm SD, range: 63-1201 s), and included 31932 ± 16906 ISIs (range: 2783–107684 ISIs).

3.2.6.1 Feature extraction

The ISI data were used to extract different descriptors of neuronal discharge. In addition to basic features (average, standard deviation and coefficient of variation of ISIs, firing rate), we analyzed the oscillatory properties of neuronal discharge within the spectral range of 1-100 Hz, as described in our previous publication [110]. The power in portions of the spectrum was then integrated over the 1-3 Hz, 3-8 Hz, 8-13 Hz, 13-30 Hz and 30-100 Hz regions of the spectrum, and expressed as proportion of the total spectral power in the 1-100 Hz range. We also calculated measures of entropy, following the algorithm proposed by Dorval et al. (parameters H1-H5, and zc1-zc5, see [32, 31]). In addition, we used the Poisson surprise method [71] to determine the onset and offsets of bursts in discharge in the recorded data streams, using a surprise value of 3 to identify bursts [121]. Bursts detected with this method were used to calculate the average and median number of spikes per burst, the average and median intra-burst firing rate, the proportion of time which the cell spent bursting,

and the proportion of spikes in bursts. We also examined all ISIs that were not part of bursts to determine the cells background (i.e., burst-free) firing rate. Each burst preceded by a long pause (i.e., an ISI that was at least 500 ms long) was classified as a rebound burst, and bursts following classic electrophysiologic features of T-type calcium channel dependent bursting [130] were called LTS bursts. We then calculated the proportion of rebound bursts that fulfilled LTS burst criteria. The surprise method can also be used to identify pauses in discharge. We initially used this fact to calculate the average pause duration, and the SD of pause durations, the proportion of spikes that flanked pauses, and the proportion of time a cell spent in pauses. However, these data could not be used for the subsequent classification analysis (below), as many cells did not show pauses in their discharge. Eventually, 29 features, available from all neurons in all three nuclei, were used for the classification analysis. These features were meant to encompass the characteristics typically used to analyze neuronal discharge, along with a few novel features. As such, the set contains some features that are linearly dependent. For instance, firing rate was included because it is historically the most commonly analyzed feature. However, the mean and standard deviation of ISIs were also included, as well as their combination (CV) to see how the individual features would compare to the combination of the two. The optimal feature selection method in this study allows ranking of the usefulness of combinations of the dependent features for discriminating between recordings from the parkinsonian and normal states.

3.2.6.2 Feature analysis

The general goal of the following data analysis was to identify combinations of the previously extracted features that would best discriminate between the normal and parkinsonian states. All analyses of the discrimination success were carried out with a support vector machine (SVM) classification method (see below). In order to find

optimal combination of features for each nucleus, individual features were cumulatively added to the SVM analysis, according to an order that was established by one of four methods which are described (and compared) below. The simplest method was a naive feature selection approach in which I first determined the SVM discrimination performance for each feature individually, and then added them one at a time in the order of their performance (from best to worst) into the feature set used for the eventual SVM discrimination. The second method ranked features based on their respective F-scores [21], the third method explicitly considered feature relevance and redundancy, and the fourth was an empirical iterative method which I refer to as the best n features method. All feature selection methods were implemented with custom MATLAB scripts.

3.2.6.3 Support vector machine discrimination

SVMs optimize the separation between classes of data (such as data generated in the normal and parkinsonian states) in an N-dimensional feature space by choosing a class boundary that maximizes the margin between points from each class that lie closest to the boundary. The fractional correct SVM discrimination (discrimination performance) is then the fraction of data points separated into the correct classes with the chosen boundary. In this paper, SVMs were used to optimize class separation for features individually ($N = 1$), reduced subsets of features ($1 < N < 29$), and for the total number of features in the dataset ($N = 29$) in order to compare how different number and composition of features affected the discrimination performance. In order to reduce the potential for over-fitting, the data was divided into training and test sets containing equal proportions of normal and parkinsonian data. The SVM classifier was trained (i.e. the boundary was chosen) using the training data. The discrimination performance was then evaluated by applying the trained classifier to the test data. The method of 5-fold cross-validation was used for selecting the

training and test sets. This method repeatedly divides the data into 5 different subsets of equal size and each subset is tested using the classifier trained on the remaining 4 subsets [54]. Classification of data that are not linearly separable in standard N-dimensional feature space can be performed through use of a non-linear kernel, such as the radial basis function [113]. The RBF kernel was employed for the analysis in this paper, not only because it allows non-linear classification, but also because it has been successfully used in other studies involving the classification of neuronal discharge [40]. The SVM algorithms were implemented using the LIBSVM library, with α and γ parameters optimized via a search over a set of discrete (α, γ) points in a bounded region (grid search, [20]).

3.2.6.4 F-score method

One of the methods used to generate a rank order of features for the subsequent SVM classification was the F-score method. For a given set of features x_i , $i = 1 \dots N$ related to two classes denoted by $'$ and $*$, the F-score is defined as

$$F(i) = \frac{(\bar{x}'_i - \bar{x}_i)^2 + (\bar{x}^*_i - \bar{x}_i)^2}{\frac{1}{m'-1} \sum_{k=1}^{m'} (x'_{k,i} - \bar{x}'_i)^2 + \frac{1}{m^*-1} \sum_{k=1}^{m^*} (x^*_{k,i} - \bar{x}^*_i)^2}$$

For our study, the data were either recorded in the normal or parkinsonian state, hence, the two classes were normal and parkinsonian, while the features were the $i = 129$ features described previously. The numerator of the F-score for each feature was computed by summing the square of the difference between the mean of the normal feature data and the overall mean of the feature data (from both classes) and the square of the difference between the mean of the parkinsonian feature data and the overall mean of the feature data. Similarly, the denominator summed the variances for the normal and parkinsonian feature data for each feature. The end result was an F-score for each feature, indicating how well that feature separated the two classes of

data. Higher F-scores reflect features with good separation relative to the uncertainty (variance) of the feature. The features were ranked from highest to lowest F-score and added in a cumulative manner to the SVM discrimination process.

3.2.6.5 Relevance and redundancy method

The F-score approach does not reveal mutual information between features [21], a problem that can lead to incorporation of redundant features in a given feature selection algorithm. In order to overcome this disadvantage, we tested a feature ranking method that considers the relevance and redundancy [128] of the selected features. For this approach, an SVM classifier was used to estimate the relevance of each feature, along with a cross correlation coefficient measure between features to estimate its redundancy with other features. Visual inspection of the cross correlation map (Figure 5) to gain insight into the feature selection process was a helpful aspect of this method. The relevance score for each feature was defined as its individual RBF SVM discrimination performance, P_i , between the normal and parkinsonian states. The standard Pearson correlations, r_{ij} , were selected as the basis for the redundancy measure, where

$$r_{ij} = \frac{\sum_{k=1}^m (x_{k,i} - \bar{x}_i)(x_{k,j} - \bar{x}_j)}{\sqrt{\sum_{k=1}^m (x_{k,i} - \bar{x}_i)^2 \sum_{k=1}^m (x_{k,j} - \bar{x}_j)^2}}$$

The absolute values of the Pearson correlations for each feature vs. each of the other features were summed, normalized, and subtracted from 1 to obtain a score ranging from 0 (maximum redundancy) to 1 (no redundancy):

$$R_i = 1 - \frac{1}{n-1} \sum_{j=1}^{n, n \neq i} |r_{ij}|$$

Next, the relevance and redundancy scores were added and the features ranked from

high to low based on this composite score ($C_i = P_i + R_i$). The features were then incorporated in a cumulative manner to the support vector machine (SVM) discrimination process based on their C_i ranking.

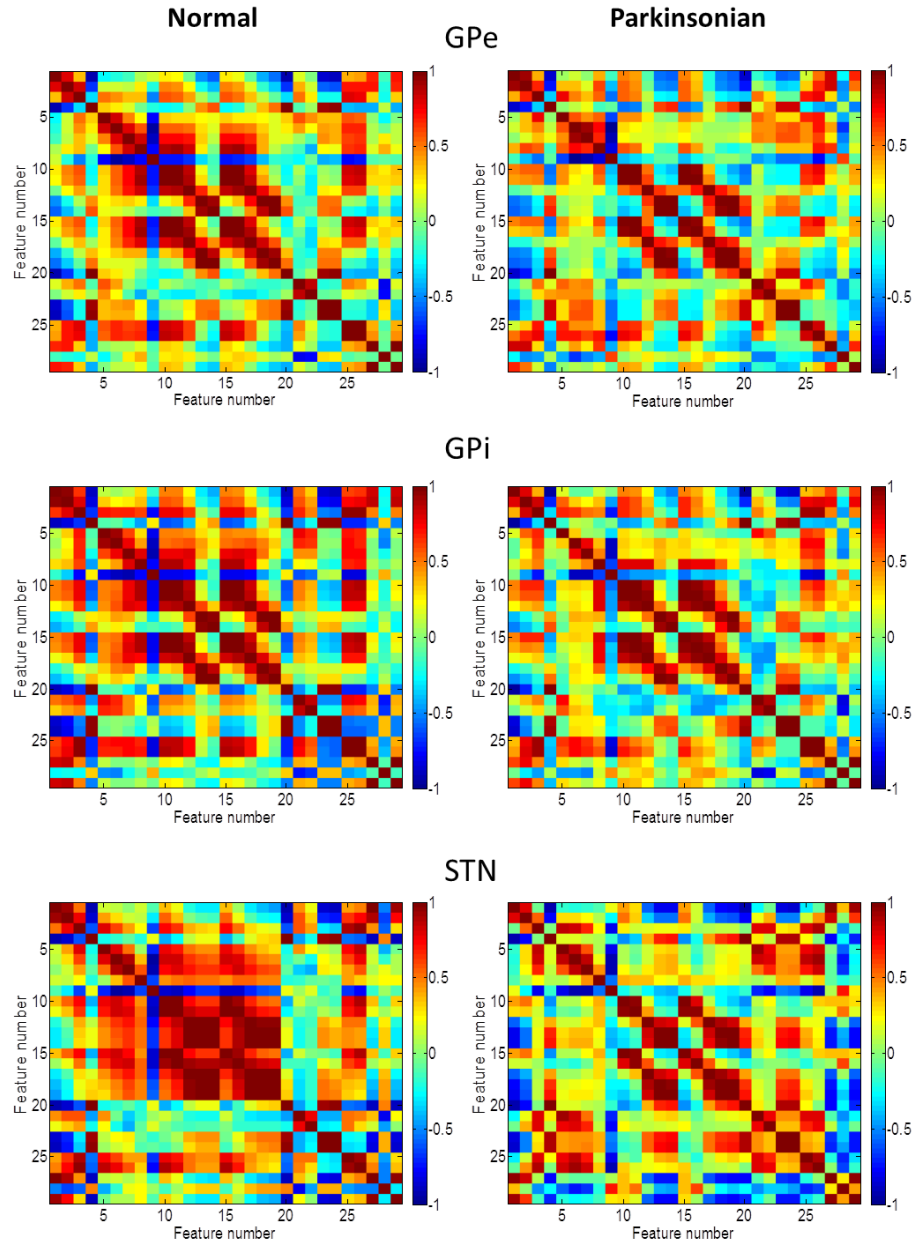


Figure 5: Pearson Cross Correlations

3.2.6.6 *Best n features method*

The best n features method used an empirical iterative process that selected the individual feature providing the highest fraction of correct SVM discrimination as the first optimal feature. At each subsequent step, an exhaustive search was used to find the j features (singly, j = 1, or pairwise, j = 2) that provided the most improvement in composite SVM discrimination, with features considered in order of their individual SVM discrimination performance. The j features that provided the most improvement at each step were then added to the best feature list, and the process repeated until all features were included. This required computing the SVM discrimination achieved by incorporating all possible combinations of j features over all m remaining features for each step ($\frac{m!}{j!(m-j)!}$). After all 29 features were included, the list of ordered features was then truncated to the 1 through n features necessary to reach the point of maximum SVM discrimination, i.e. the best n features.

3.3 *Results*

The data set consisted of data from GPe, GPi and STN, recorded before and after treatment of the animals with MPTP. The basic data characteristics are shown in Table 2. The Pearson correlation between features (Figure 5), gives a qualitative overview of the discriminability of the data. In the figure, varying patterns of feature correlation can be seen between the normal (left column of plots) and parkinsonian states (right column of plots) in GPe, GPi, and STN. Note the large contrast between features based on STN data from the normal state, compared to features based on STN data from the parkinsonian state, the two classes of data that yielded the best discrimination results in all of the discrimination algorithms tested here (see below).

3.3.1 Discrimination achieved using results of different feature ranking algorithms

Figure 6 shows the ranking of features obtained using the four different feature selection processes, applied to data from GPe. For each method, the x-axis lists the features from best to worst individual discrimination performance and the line shows the performance achieved by incorporating the k best performing features, for $k = 129$. The naive feature selection approach ("A" in Figure 6) achieved a peak performance of 80% for the GPe data, 79% for the GPi data, and 86% for the STN data. As in all parts of Figure 6, the figure shows that the addition of certain features (even those ranked highly by these methods) actually reduced the cumulative discrimination performance. Parts "B" and "C" of Figure 6 illustrate the respective discrimination performance when features were added to the SVM analysis in the rank order as indicated by the F-score and the Relevance and redundancy methods. For both, the maximal level of discrimination was higher than that possible with the naive method. Finally, Part D demonstrates the results of the best n features method. Adding iteratively the single feature that gave the most improvement in discrimination increased the discrimination success beyond that achieved with the other methods. Additional increases were seen by bringing in the two best features at each step (pairwise best n features). This method resulted in a performance curve that peaked at 91% for the GPe data (10 features), 86% for the GPi data (10 features), and 95% for the STN data (6 features). Note that the performance increased until a maximum was reached, and then declined, indicating no additional discrimination capability was provided by the remaining features. The higher peak and the monotonically increasing and then decreasing nature of the performance curve led us to choose the optimal features selected using this method for further analysis. Table 3 shows the feature sets that yielded the maximum performance using this approach for each nucleus.

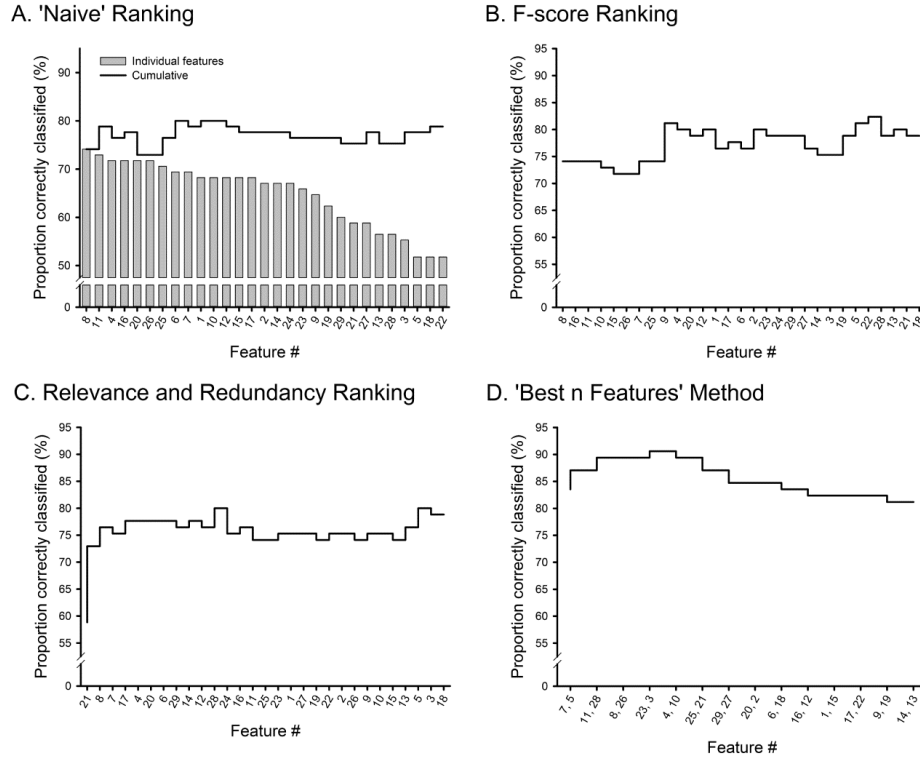


Figure 6: Discrimination results for four different feature ranking methods

3.3.2 Comparison of features selected by the different methods

As shown in Part A of Figure 7, the single feature discrimination performances typically varied substantially from one feature to another. The single feature discrimination performances also varied widely between the different nuclei for some features. Part B of Figure 7 shows a comparison of the discrimination performance of combinations of features, added in order of their ranking by the different feature selection algorithms used in this study. For each approach, the results reflect the performance obtained by including the set of features that produces the highest level in the respective performance graph. When the full set of 29 features was used (All features), 81% correct discrimination between the normal and parkinsonian states was achieved for the cells in the STN data set, and 79% was achieved for both the GPe and GPi data sets. Although each of the methods for feature selection improved on the all features

approach, the figure shows that the pairwise best n features method generated the rank order of features that resulted in the best discrimination performance. The top features selected with each of the associated methods were not necessarily the same. However, within a particular nucleus, many features were seen to be common across methods. For example, in the GPe data, 3 of the top 11 features (4, 7, 8) were common across all methods, with feature 7 (spectral power in the 8-13 Hz band) being the strongest. Four of the remaining 8 were common among three methods (10, 11, 25, 26). For the GPi data, 3 of the top 11 features appeared in all four methods (21, 22, 28), with feature 28 (proportion of LTS bursts) as the strongest feature. Four of the remaining 8 features were common among three methods (3, 24, 25, 26). In the STN data, 6 of the top 11 features appeared in all methods (features 4, 7, 14, 20, 23, 24), with feature 24 (median intra-burst frequency) being the single strongest feature.

3.3.3 Top features for each nucleus

Figure 8 shows scatterplots of the two top ranked features for discrimination for each of the three nuclei, as selected by the best n features method. Although more than two features were necessary for peak discrimination, the two-dimensional scatterplots provide a visual indication of how the neuronal discharge patterns changed under parkinsonism, and how much discrimination is achievable using only the two features that were most changed. Standard linear discrimination analysis (LDA) of the two-dimensional data yielded 76% discrimination for the GPe, 71% for the GPi, and 82% for the STN data (lines show LDA discrimination). As can be seen, the top features in each nucleus were related to either bursting or fractional spectral power. For GPe, the top two features were the fractional spectral power in the 8-13 Hz (feature 7) and 1-3 Hz (feature 5) bands. Under baseline conditions, the mean 8-13 Hz fractional power was 0.03 ± 0.016 (i.e., approximately 3% of the entire power in

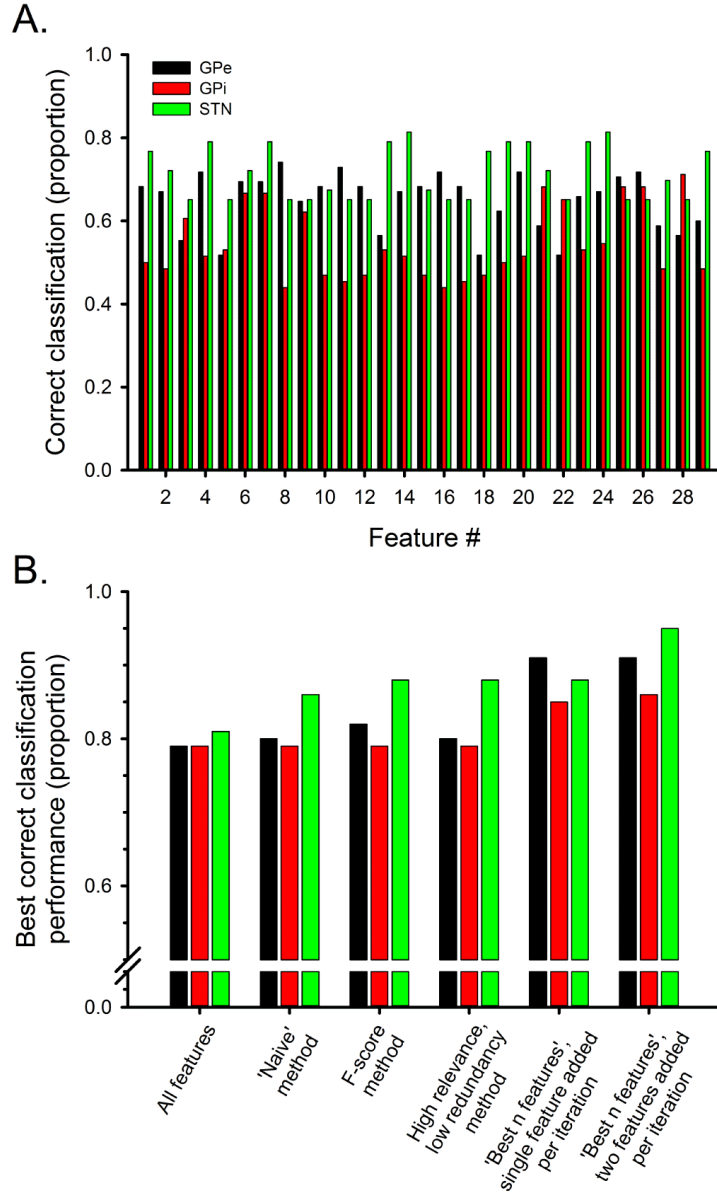


Figure 7: Summary Results. A: Single feature discrimination. B: Discrimination using optimal feature selection approaches.

the 1-100 Hz range was in this band; mean \pm SD). Under parkinsonian conditions, the mean increased to 0.06 ± 0.041 . The mean 1-3 Hz fractional power decreased from 0.04 ± 0.026 (baseline) to 0.03 ± 0.016 (parkinsonism). For the GPi data, the two highest ranking features were the fraction of LTS bursts (feature 28) and the mean intra-burst frequency (feature 23). Under baseline conditions, the fraction of

LTS bursts was 0.27 ± 0.059 (i.e., 27% of all bursts were designated as LTS bursts). In the parkinsonian state, the mean decreased to 0.20 ± 0.070 . The mean intra-burst frequency increased from 185.06 ± 41.147 spikes/s at baseline to 204.03 ± 43.881 spikes/s in the parkinsonian state. For the STN data, the two top features were the median intra-burst frequency (feature 24) and the spectral power in the 8-13 Hz band (feature 7). Under baseline conditions, the median intra-burst frequency was 74.37 ± 24.934 spikes/s. Under parkinsonian conditions, the mean increased to 119.15 ± 33.599 spikes/s. The mean fractional power in the 8-13 Hz range increased from 0.05 ± 0.012 (baseline) to 0.08 ± 0.028 (parkinsonism). The minimum and maximum values, and the data distributions for the top two features from each nucleus can be seen in the scatterplots in Figure 8. The individual (and two-dimensional) feature distributions for the baseline and parkinsonian conditions overlapped. However, as seen in Part D of Figure 6, the ability to discriminate between the data increased as more features were included. Although increased bursting occurred in all three nuclei, the observed changes differed between the STN and the two pallidal segments. The GPe and GPi data showed large increase in the average proportion of spikes in bursts (feature 26), while in STN, the major effect was the increased intra-burst frequency. The median intra-burst frequency (feature 24) increased by approximately 60% in the STN in the parkinsonian state as compared to the normal condition, although the average proportion of spikes in bursts only increased by about 7%. In contrast, the median intra-burst frequency in the GPe decreased by 16% while the average proportion of spikes in bursts increased by 80% in the parkinsonian state. In the GPi, the median (and mean) intra-burst frequency increased by 10% while the average proportion of spikes in bursts increased by 50%. Some spectral characteristics were shared between nuclei while other spectral features showed significant differences. For example, the 30-100 Hz fractional spectral power in each band for GPe, GPi, and STN was reduced, while the fractional power in the 3 to 30 Hz frequency bands was higher

in the parkinsonian state. In the GPi, characteristics of burst discharges (features 23-26), and fractional spectral power in the 3-100 Hz frequency bands (features 6-9) were not significantly correlated in either the normal or parkinsonian states ($p \geq 0.1$). In the GPe, these sets of features were related, but the significance (and direction) of correlation between them was similar for both states ($p \leq .008$; 30-100 Hz [negatively correlated with bursting], 3-8 Hz and 8-13 Hz [positively correlated with bursting]). Thus, there was no parkinsonism-related change in the relationship between burst features and spectral power in either pallidal segment. This was different for the STN, however. In this nucleus, the intra-burst frequency (features 23 and 24) and the power in the 3-100 Hz bands were not correlated under normal conditions ($p > 0.3$, see flat solid least square fit lines in Figure 9). In contrast, in the parkinsonian state, the intra-burst frequency correlated negatively with the power in the 30-100 Hz band ($p = 0.002$, Part A of Figure 9, dashed line) and positively with the power in the bands between 3 and 30 Hz ($p = .01$ for 3-8 Hz [Part B of Figure 9], $p = 0.009$ for 8-13 Hz, and $p = .04$ for 13-30 Hz).

3.3.4 Reproducibility of results

Recognizing the importance of reproducibility in generating a set of best features for each nucleus, we re-ran the best n features algorithm using half of the data, randomly selected, for training and optimizing parameters, then used SVM prediction to classify the other half of the data. We then repeated the process, swapping the training and testing data sets. As can be expected, the performance results were slightly lower, (81-83% for the GPe data set, 68-75% for the GPi data set, and 77-86% for the STN data set), but the list of best features did not change significantly. In particular, the top features for each nucleus remained the same.

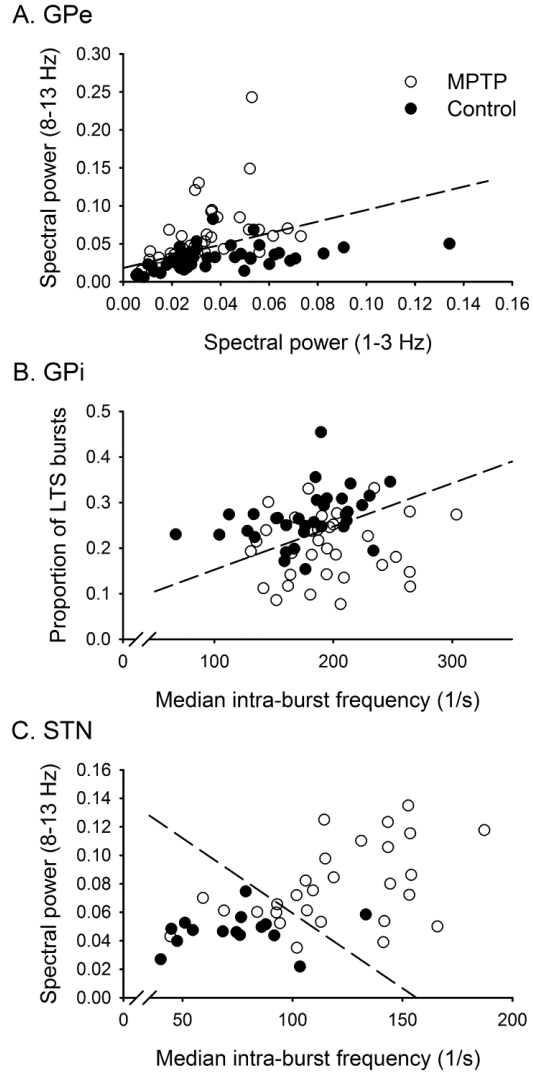


Figure 8: Top two features providing the best discrimination for *A. globus pallidus externa* (GPe), *B. globus pallidus interna* (GPi), and *C. Subthalamic nucleus* (STN).

3.3.4.1 Discrimination between nuclei

We also explored whether the best n features method could be used to discriminate single cell spiking recorded in the different nuclei. Under baseline conditions, the discrimination between GPe and GPi was 83.1%, between STN and GPe was 98.3%, and between STN and GPi was 100%. The top features for discrimination were, for GPe/GPi: *zc3*, CV of ISIs, H3, SD of ISIs, and mean spikes per burst; for STN/GPe:

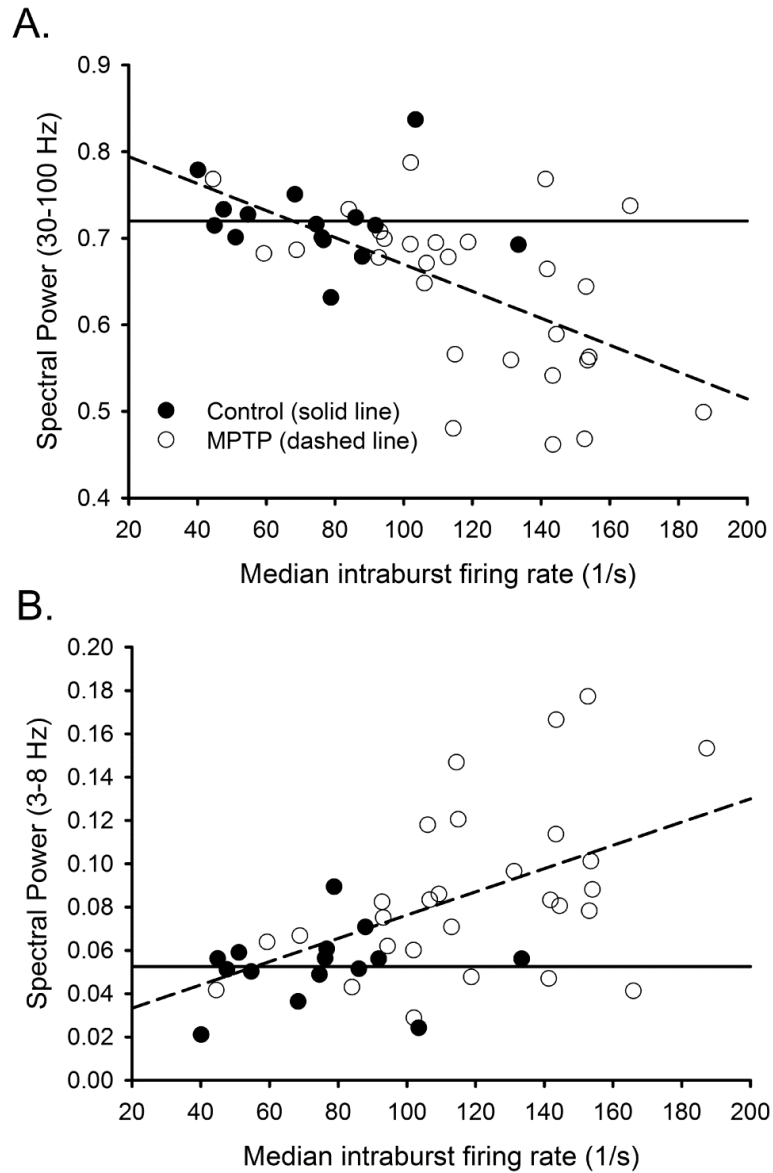


Figure 9: Data and trend lines for STN fractional spectral powers versus median intraburst firing rate; A. High frequency (30-100 Hz), and B. Low frequency (3-8 Hz) spectral power

median intra-burst frequency, 13-30 Hz power, and firing rate; and for STN/GPi: H1, zc5, and firing rate. In the parkinsonian condition, the corresponding accuracies were 89.1%, 97.0%, and 96.8% respectively. Concerning the GPe/GPi discrimination, the best features were the mean intra-burst frequency, 13-30 Hz power, and mean ISI; for STN/GPe discrimination, the best features were 13-30 Hz power, H1, and zc1; and

for the discrimination between STN and GPi, the best features were 13-30 Hz power, median intra-burst frequency, and *zc2*.

3.4 Discussion

We found that SVM discrimination between ISI features from extracellular recordings in the STN, GPe and GPi allowed successful discrimination between the normal and parkinsonian states and between the three nuclei in monkeys. Combining the SVM discrimination techniques with optimal feature selection methods enabled quantitative analysis of the most changed features, and the relationships between them, in the three basal ganglia regions under dopamine depletion conditions. As seen in Figure 7, the best *n* features method provided the highest discrimination percentages of the feature selection approaches tested. The top features identified using that method were also highly ranked by most of the other methods, adding to our confidence that the features identified and discussed in the following are important for distinguishing between the normal and parkinsonian conditions.

3.4.1 Best feature sets for discriminating between normal and parkinsonian states in different basal ganglia nuclei

As shown in Table 3, the set of best features included multiple categories of features for all three basal ganglia nuclei, reinforcing the idea that it is relevant to examine different aspects of cellular activity to gain optimal information. As suggested by the summary results, the best number of features for this type of discrimination may be approximately 6-10. The optimal feature sets did not include all features in any one category, indicating that some of the features in each category were redundant (and were thus removed). For example, optimal feature lists included the ISI CV (feature 3), but not the ISI mean and standard deviation (features 1 and 2), likely because the former is a linear function of the latter two. The feature categories most

relevant for discrimination were the bursting statistics and fractional power of oscillations (spectral power), although firing rate/ISI statistics and entropy measures were also useful. Interestingly, the relationship between oscillatory activities and bursting may be different in the STN and the GPe/GPi. The burst statistics indicated that, although increased bursting occurs in all three nuclei in the parkinsonian state, the effect in the STN was an increase in intra-burst frequency, while the GPi and GPe data showed larger increases in the proportion of spikes in bursts. Our analysis showed that the fractional spectral power in the 8-13 Hz and 13-30 Hz bands was higher on average in the parkinsonian condition for all 3 nuclei, agreeing with previous findings of prominent oscillations in the beta band in the parkinsonian state (see, for instance [8, 49]). The STN intra-burst frequency feature was not correlated to the oscillatory power in these frequency bands at baseline (normal), but under parkinsonian conditions, became positively correlated for bands between 3 and 30 Hz and negatively correlated for the 30-100 Hz band. This significant change in the correlation between bursting and spectral power is likely the reason better discrimination was possible for the STN as compared to the GPe and GPi data. It also suggests a link between the increased burst intensity of STN neurons and the parkinsonian profile of increased beta and reduced gamma oscillations. Although increased fractional spectral power in the 3 to 30 Hz frequency bands was also seen in GPe and GPi, the magnitude and direction of correlation between burst features and fractional spectral power in these structures did not change significantly in the parkinsonian state as compared to the normal state. We found that the proportion of LTS bursts (feature 28), the top ranked feature for GPi discrimination, was smaller in the parkinsonian state than in the baseline condition in the GPi data, indicating that, at least for GPi cells, the increased bursting is substantially different from typical LTS bursting activity. This result may be understandable by the fact that LTS bursts tend to be associated with increased membrane hyperpolarization. While several structures within the

basal ganglia-thalamocortical network of connections are hypothesized to be subject to greater phasic or tonic GABAergic inhibition and may thus be prone to develop LTS bursts, this is not the case for GPi which, according to the classic models of basal ganglia activity changes in Parkinson’s disease, is, instead, subject to an increased excitatory drive from the STN (see, e.g., [39]). As seen in Table 3, three of the most relevant features from the GPe and GPi data sets were based on measures of entropy (features 10, 11, and 15). H1 (feature 10) is the entropy calculated considering only single ISIs, while H2 (feature 11) takes all sets of two consecutive ISIs into account. Zc1 (feature 15) is calculated by extrapolating the entropy to infinite signal length through regression of H1 (see [32]). The entropy features indicate the general level of variability in the cell firing [13]. It is interesting to note that entropy features did not appear in the STN best feature set even though the STN data allowed the best overall discrimination. Even for GPi and GPe, entropy measures did not appear in the top two features. Thus, while measures of entropy may be helpful when used in conjunction with other features, they do not perform as well as other features for the type of discrimination performed in this study, and, if the ease of discrimination is considered a proxy for importance, may be less important than other features. Although basic descriptors of firing were not top-ranked features for any nucleus, the firing rate, and mean, standard deviation, and CV of the ISIs ranked fairly high in the single feature discrimination performance for all nuclei (see Part A of Figure 6, features 1-4). In our study, no firing rate related features were necessary for optimal discrimination of the STN data, however, the CV of the ISIs (feature 4) was included in the optimal feature lists for both the GPe and GPi data sets (see Table 3). These features continue to be widely used in models of the pathophysiology of parkinsonism, perhaps in part because they are easily quantifiable smoothed statistics that reflect the underlying bursting activity that this study found most relevant for distinguishing between the normal and parkinsonian states. Our analysis showed that the optimal feature sets

Table 3: Table of Best Features

	GPe	GPi	STN
Firing rate/ISI statistics	CV of ISIs, firing rate	CV of ISIs	-
Fractional spectral power	1-3 Hz, 8-13 Hz, 13-30 Hz	1-3 Hz, 13-30 Hz	1-3 Hz, 8-13 Hz, 30-100 Hz
Entropy measures	H1, H2	H1, zc1	-
Burst statistics	mean intra-burst frequency, proportion of spikes in bursts, proportion of LTS bursts	median intra-burst frequency, mean spikes per burst, median spikes per burst, proportion of spikes in bursts, proportion of LTS bursts	median intra-burst frequency, proportion of rebound bursts, proportion of rebound LTS bursts

differed substantially between neurons recorded in the different structures. Discriminating neurons recorded in the normal and parkinsonian states was easiest for the STN data, possibly due to the previously discussed significant correlation between the median intra-burst frequency and spectral features that occurs under parkinsonism. Records from GPe and GPi were consistently more difficult to categorize, resulting in lower rates of correct discrimination. These differences are likely due to the different membrane properties, afferent synaptic connections, and receptor and neurotransmitter distributions found in the GPe, GPi, and STN nuclei. The different optimal feature sets hint at the general response properties of the cell types under parkinsonian conditions. Whereas the STN cells have a clearly discernible pattern of increased intra-burst frequency and spectral changes, the pallidal cells responses appear to be more varied and complex.

3.4.2 Discrimination between nuclei

Trained investigators can easily distinguish between STN, GPi and GPe activities, using on-line audio representations or oscilloscope displays of single cell activities

recorded from these nuclei. The analysis of the inter-nuclear discrimination of the chosen analysis method was therefore included as a positive control experiment, demonstrating that the chosen analytical methods are capable of discriminating GPe, GPi, and STN activities. Not surprisingly, the discrimination between the relatively slow-firing STN cells and the high-frequency pallidal cells was found to be excellent, while distinction between the two (relatively similar) pallidal segments was less accurate. In all cases, three to five features were adequate for maximum discrimination. However, the best features for discriminating between nuclei differed between the control and parkinsonian states, supporting the notion of significant parkinsonism-related changes of single cell activities in these nuclei. Note that, in the parkinsonian state, discrimination between the STN and GPi became less accurate while discrimination between the GPe and GPi became more accurate.

Figure 8 shows scatterplots of the two top ranked features for discrimination for each of the three nuclei, as selected by the “best n features” method. Although more than two features were necessary for peak discrimination, the two-dimensional scatterplots provide a visual indication of how the neuronal discharge patterns changed under parkinsonism, and how much discrimination is achievable using only the two features that were most changed. As can be seen, the top features in each nucleus were related to either bursting or fractional spectral power. For GPe, the top two features were the fractional spectral power in the 8-13 Hz (feature 7) and 1-3 Hz (feature 5) bands. For the GPi data, the two highest ranking features were the fraction of LTS bursts (feature 28) and the mean intra-burst frequency (feature 23). For the STN data, the two top features were the median intra-burst frequency (feature 24) and the spectral power in the 8-13 Hz band (feature 7). Standard linear discrimination analysis (LDA) of the two-dimensional data yielded 76% for the GPe, 71% for the GPi, and 82% for the STN data (lines show LDA discrimination). In contrast, when the optimally selected set of features were used, SVM discrimination achieved 91%

for the GPe data (10 features), 86% for the GPi data (10 features), and 95% for the STN data (6 features).

Although increased bursting occurred in all three nuclei, the observed changes differed between the STN and the two pallidal segments. The GPe and GPi data primarily showed large increases in the average proportion of spikes in bursts (feature 26), while in STN, the major effect was the increased intra-burst frequency. The median intra-burst frequency (feature 24) increased by approximately 60% in the STN in the parkinsonian state as compared to the baseline condition, although the average proportion of spikes in bursts time spent bursting only increased by about 7%. In contrast, the median intra-burst frequency in the GPe decreased by 16% while the average proportion of spikes in bursts increased by 80% in the parkinsonian state. In the GPi, the median (and mean) intra-burst frequency increased by 10% while the average proportion of spikes in bursts increased by 50%.

Some spectral characteristics were shared between nuclei while other spectral features showed significant differences. For example, the 30-100 Hz fractional spectral power in each band for GPe, GPi, and STN was reduced, while the fractional power in the 3 to 30 Hz frequency bands was higher in the parkinsonian state. In the GPe and GPi, the correlation between bursting features and fractional power in frequency bands was similar in both the baseline and parkinsonian states. However, for the STN neurons recorded in the parkinsonian state, increased intra-burst frequency correlated negatively in a linear fashion with the power in the 30-100 Hz band ($p = 0.002$) and with positive linearity for the power in the bands between 3 and 30 Hz ($p = .01$ for 3-8 Hz, $p = 0.009$ for 8-13 Hz, and $p = .04$ for 13-30 Hz) . There was no correlation between these parameters in the STN neurons recorded in the normal state ($p = 0.5$ to 0.8).

3.5 Conclusion

Using multiple feature selection methods tested against a set of neuronal discharge features from three basal ganglia regions, we found that the features that most effectively discriminate the neuron activity in the parkinsonian and normal states differ between the STN and the two segments of the globus pallidus. Although the reasons for these differences remain speculative, it is possible that the cellular responses are strongly influenced by local factors, such as the membrane properties of specific groups of cells, or by the synaptic connections between the recorded neurons and their respective afferents. We found that concentration on any one feature of single cell firing (such as firing rates or oscillatory properties) to characterize the parkinsonian state in all nodes of the basal ganglia-thalamocortical network is less accurate than an analysis of multiple nucleus-specific descriptors to predict changes of activity patterns in the basal ganglia-thalamocortical network.

3.6 Contributions to work

The animal experiments and recordings in this chapter were performed by Jesus Soares and Thomas Wichmann. Previously published analysis of the original data was performed by Thomas Wichmann and Jesus Soares. The analysis of optimal features for discrimination was performed by Teresa Sanders with input from Mark Clements. The manuscript was prepared by Teresa Sanders and Thomas Wichmann with feedback from Mark Clements.

CHAPTER IV

PARKINSONISM-RELATED FEATURES FROM SUBTHALAMIC NUCLEUS LOCAL FIELD POTENTIALS AND CORTICAL ELECTROENCEPHALOGRAMS

Synchronized neural oscillations underlie the precise timing associated with coordinated movements [107]. These normal baseline oscillation patterns have been shown to be disrupted in many disorders [115]. The following four studies, described in Chapters 4 and 5, analyze the relationships between six frequency bands in subthalamic nucleus (STN) local field potentials (LFPs) and primary motor cortex (M1) electroencephalographic (EEG) signals recorded from rhesus monkeys as they progressed from the baseline state to moderate parkinsonism. The original datasets, used for the findings described in studies one (Section 4.1) and three (Section 5.1), consisted of two MPTP monkey models. Later, data from a third monkey was obtained and used for confirmation of the findings, as described in the second (Section 4.2) and fourth study (Section 5.2).

In the first study, discrimination between baseline and varying stages of parkinsonism was accomplished with $> 84\%$ accuracy using only amplitudes of the LFP wavelet packet transform (WPT) envelope from each of the six frequency bands. In the second study, similar performance results were achieved using the complex continuous-time wavelet transform (CCWT). A novel mapping technique was then developed to show the progression of parkinsonism over time using phase-amplitude cross-frequency-coupling (CFC) features [7, 17, 18, 114]. One unique feature of the mapping technique was that the CFC features were extracted from the CCWT coefficient phases and amplitudes for the six frequency bands, rather than simply from

bandpass-filtered signals. The maps generated using this technique revealed similar CFC feature changes in the progression of parkinsonism for three monkeys.

In the third study, canonical correlation was used to show that weighted combinations of the phase-amplitude CFC features (also known as Modulation Indices (MIs)) correlated significantly with the individual and composite motor scores for the STN-LFP signals. Statistically significant correlation was also found using the EEG MIs. In the fourth study, the correlations between the composite motor scores and the MIs were compared to correlations between the motor scores and standard statistical measures from the same six frequency bands.

4.1 Discrimination between normal conditions and parkinsonism based on wavelet packet transform analysis of electroencephalographic (EEG) and subthalamic local field potential recordings

Parkinsonism is believed to be associated with increased inter-neuronal synchronization in the basal ganglia and cortex of parkinsonian patients and dopamine-depleted animals, but the relationship between changes in neuronal synchronization and the severity of the disease remains unclear. The following study examined this issue by analyzing changes in subthalamic LFPs and cortical EEG signals in two Rhesus monkeys that developed parkinsonism in response to chronic systemic treatment with the dopaminergic neurotoxin MPTP. LFPs were recorded acutely, along with EEG signals from the primary motor cortex (M1) as the monkeys progressed from their behavioral baseline to moderate parkinsonism. Based on scoring of behavioral observations, the level of parkinsonism was classified as slight, mild, or moderate.

Since LFP and EEG oscillations fluctuate in both frequency and duration, non-windowed discrete-time Fourier transform methods, which rely on frequency components that exist over all time points, do not adequately capture the dynamics of the data. Bases sets that support jointly varying frequency and time representations, such as wavelets or multi-taper methods [58], are more appropriate for such analyses. Fast Fourier transform, continuous wavelet transform and statistical properties of wavelet spectra have been used successfully to evaluate important features of STN LFPs aligned to movement activities such as finger-tapping exercises [69]. For this study, we hypothesized that changes in the LFP and EEG oscillations might be detectable without the presence of a known aligning activity or stimulus. We chose to analyze the time-frequency signal representations using the wavelet packet transform (WPT) since this allowed evenly spaced frequency (scale) bands and easy transformations from the time domain to the frequency domain and back. Scaling was adjusted to

match the frequency bands commonly used in EEG analysis literature [98, 61] (delta, theta, alpha, beta, and gamma). Based on features used successfully in [85], WPT envelope features of the recorded LFP and EEG data were analyzed. Standard scores (also known as z-scores) of the 1000 Hz LFP and EEG signals for each recording day were calculated. Next, a 90 Hz low pass filter was applied to the z-scored data and the data was downsampled by 4. (Downsampling was performed to reduce the required computations; the resulting 250 Hz signal more than supported the maximum frequencies of interest.) The remainder of the processing used the methods described in [85] which are summarized as follows. WPTs were used to filter the downsampled data into 6 band-filtered signals from the following frequency bands: Delta (3-4Hz), Theta (5-7 Hz), Alpha (8-11 Hz), Low Beta (12-19 Hz), High Beta (20-30 Hz), and Low Gamma (31-40 Hz). The envelope of each of the 6 band filtered signals was calculated using the Hilbert transform. The data for each of the band filtered signals were then averaged over 100 ms frames, and finally split into groups containing 5 consecutive averages for each of the 6 frequency bands (corresponding to 500 ms of data). Each group was then a feature vector of length 30 and was subsequently used for classification. Linear discriminant analysis (LDA) classification with radial basis function kernel and 5-fold cross-validation were used to discriminate between the LFP/EEG feature vectors associated with normal brain function and those associated with the varying levels of parkinsonism. LDA discrimination accuracy between the baseline and parkinsonism was 78% to 98% for Monkey 1 and 59% to 75% for Monkey 2 using the STN LFP data, and 74% to 78% (Monkey 1) and 70% to 75% (Monkey 2) using the M1 EEG data. See Figure 10. Note that, in each case, the performance shown is for binary discrimination between the baseline condition and the indicated stage.

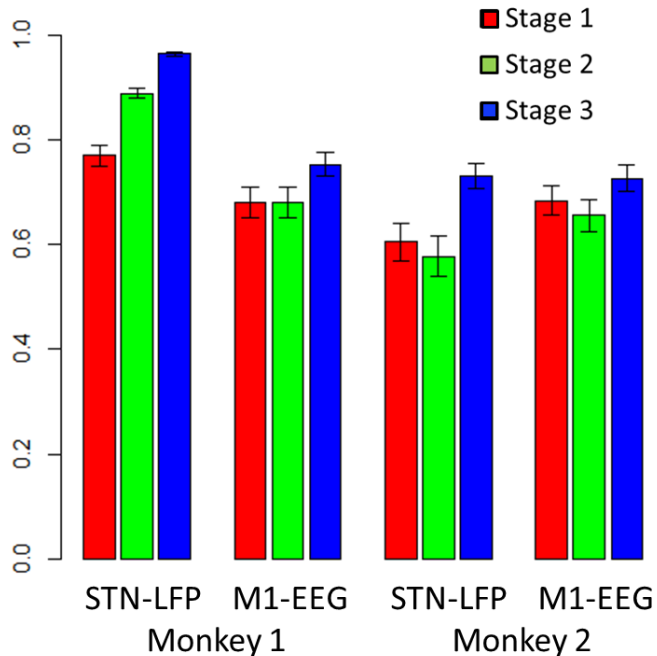


Figure 10: Fraction correct discrimination between the baseline condition and three stages of parkinsonism using Wavelet Packet Transform (WPT) features. Shown for features extracted from both STN LFP and motor cortex electroencephalogram (EEG) data for Monkey 1 (left set of bars) and Monkey 2 (right set of bars). Error bars indicate the standard deviation for the 5-fold cross-validation.

4.2 Classification of four stages of parkinsonism based on complex continuous wavelet transform phase-amplitude coupling features

Although the WPT approach used in the previous study allowed discrimination between baseline and each parkinsonian stage, classification into the four stages was not possible with high accuracy. In order to provide classification between multiple stages, new and/or expanded features were needed. In order to incorporate phase information, in addition to the magnitude features considered in the previous discussion, the complex continuous-time wavelet transform (CCWT) approach was employed. The use of a complex wavelet atom accurately preserved phase information, allowing both frequency and phase analysis.

Before transitioning from the WPT to the CCWT for frequency pre-processing, the envelope features previously obtained with the WPT approach were extracted using the CCWT, and the performance was compared to the results in Section 4.1 to ensure no loss of discrimination capability occurred due to the non-orthogonality of the CCWT or other unforeseen issues. Subsequent analysis then used the CCWT amplitude and phase information to create phase-amplitude cross-frequency-coupling (CFC) features. The detailed methods for calculating these features will be described in Section 5.1.2.

4.2.1 Introduction

The motor signs commonly seen in Parkinson’s disease patients are well documented. However, the electrophysical characteristics of the disease and its progression are still the subject of debate. In this work, phase-amplitude CFC features were extracted from LFPs recorded in the subthalamic nucleus of three monkeys in order to characterize the electrophysiologic progression of parkinsonism. ANOVA analysis showed marked increases in beta phase modulation of amplitude in mild to moderate parkinsonism for three monkeys despite inconsistent trends in average beta power across monkeys. In addition to the beta phase modulation of amplitude, delta phase modulation of amplitude was seen. Specifically, the delta phase modulation was reduced in parkinsonism as compared to the baseline condition for all three monkeys.

4.2.2 Methods

The animal experiment methods for this study, including the wakefulness assessment and parkinsonism scoring, were performed using the methods described in Section 5.1.2. Prior to the following analysis, the LFPs were preprocessed to remove any segments where the monkey was not in a wakeful state.

CFC features known as modulation indices (MIs) were calculated from the phase and amplitude of the STN-LFP CCWT coefficients in 6 frequency bands (see Section

5.1.2 for detailed methods). The frequency bands used were as follows: Delta (3-4 Hz), Theta (4-8 Hz), Alpha (8-13 Hz), Low Beta (13-16 Hz), High Beta (16-30 Hz), and Gamma (30-58 Hz). A few different frequency band divisions were tested (including the divisions used in the previous study in 4.1). However, the divisions above were selected since they are the standard frequency bands used for clinical EEG analysis, and also because they showed the changes in the electrophysiology most clearly. The MIs were z-scored and placed in an image array with colors corresponding to the z-scored MI value and indexed by (parkinsonism score, MI feature number).

Figure 11 shows the MIs for one parkinsonism score in a two-dimensional array (left) and in the vector configuration (right) used in this study. The MI vectors were arranged in order of increasing parkinsonism score and a 2-dimensional Wiener filter applied to create the MI map images shown in this analysis (Figure 12). Z-scoring the MIs was performed in order to visually balance the 36 MI rows to a common range. (Variations between different rows occur due to power differences in the frequency bands.)

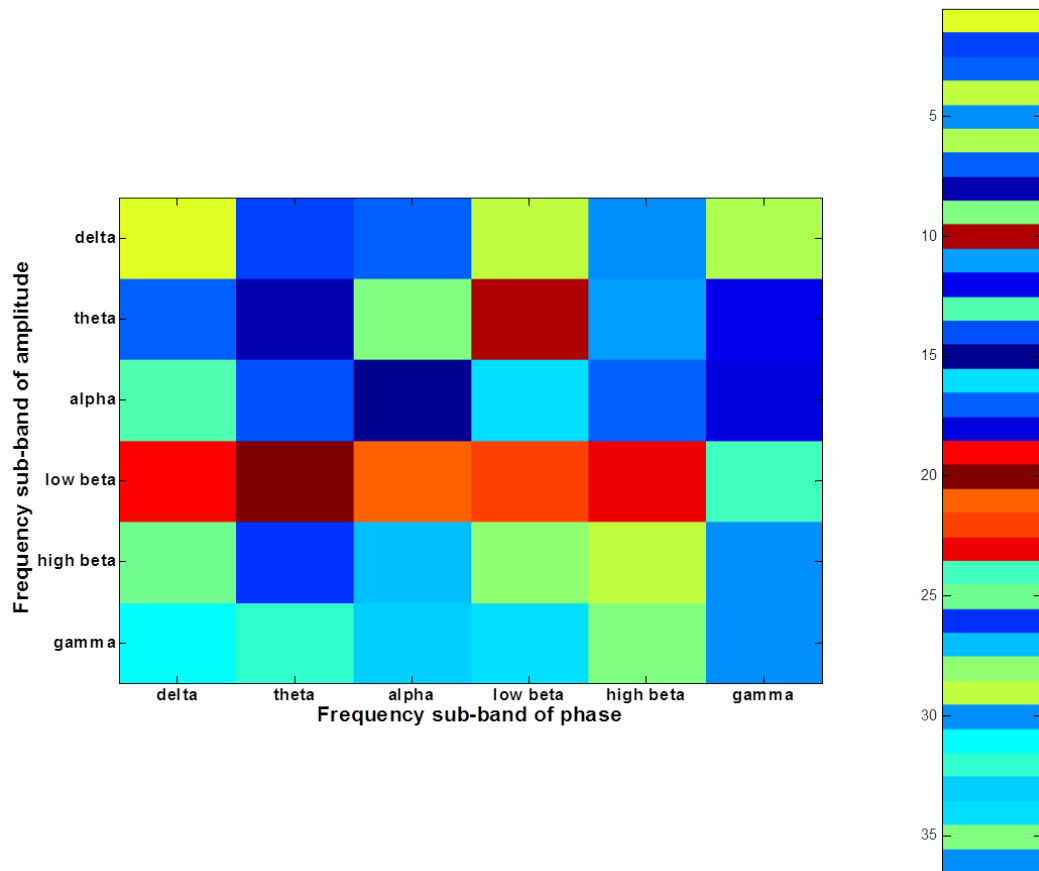


Figure 11: Example Modulation Index (MI) feature images for a single parkinsonism score. Red corresponds to a high degree of cross-frequency-coupling, while dark blue corresponds to an absence of cross-frequency-coupling. The 36 MI features can be displayed in a 6x6 array (left) or in a column vector (right). This analysis used the column vector configuration in order to show changes in the features with increasing parkinsonism.

One-way ANOVA analysis was used to find the MIs with the highest statistical significance across data grouped by parkinsonism scores. Multiple comparisons with Bonferroni adjustments [33] were then used to find the MIs with the most statistically significant differences across all motor scores.

4.2.3 Results

Figure 12 shows the modulation indices related to each motor score as the monkeys progressed from baseline to parkinsonism. Colors represent the z-scored degree of phase-amplitude CFC in each of the phase sub-bands indicated on the y-axis, showing the amplitude modulation of each band by the phase of each of the six modulating bands. Each column shows the CFC features averaged over one recording session.

The x-axis corresponds to gradually worsening parkinsonism, as indicated by the labeling. Several regions of reduced (blue) or enhanced (red) modulation activity can be seen.

Four common patterns in the data were visible. First, in the baseline region, there was little beta phase modulation of the amplitudes at any frequency. This is particularly evident by noting the large dark (blue) patches in the baseline MIs shown in Figure 12. For Monkey 1 and Monkey 3 the blue patch was most apparent in the low beta phase modulation region, while for Monkey 2 it was seen most clearly in the alpha/low beta phase modulation. Secondly, as the degree of parkinsonism increased, the beta phase modulation increased (blue patches disappear). Although not always a linear increase, the beta phase modulation continued to increase with increasing parkinsonism until reaching scores of approximately 7 to 10. The beta phase modulation then generally decreased. This is best seen in the top image in Figure 12 which shows a bright orange/yellow region where the phase modulation peaked at a parkinsonism score of 8, followed by a return to "blue" levels at a score of 12. The z-scored MI values and shape of the low beta MI patterns were similar for all three monkeys as shown in the left side of Figure 13. Note that the Monkey 2 MIs in the low beta band follow this characteristic pattern, even though the minimum baseline phase modulation occurs in the alpha band for Monkey 2 (see Figure 12).

The third common characteristic seen in Figure 12 was the elevated delta phase modulation at baseline (red patches) which decreased overall from left to right. The

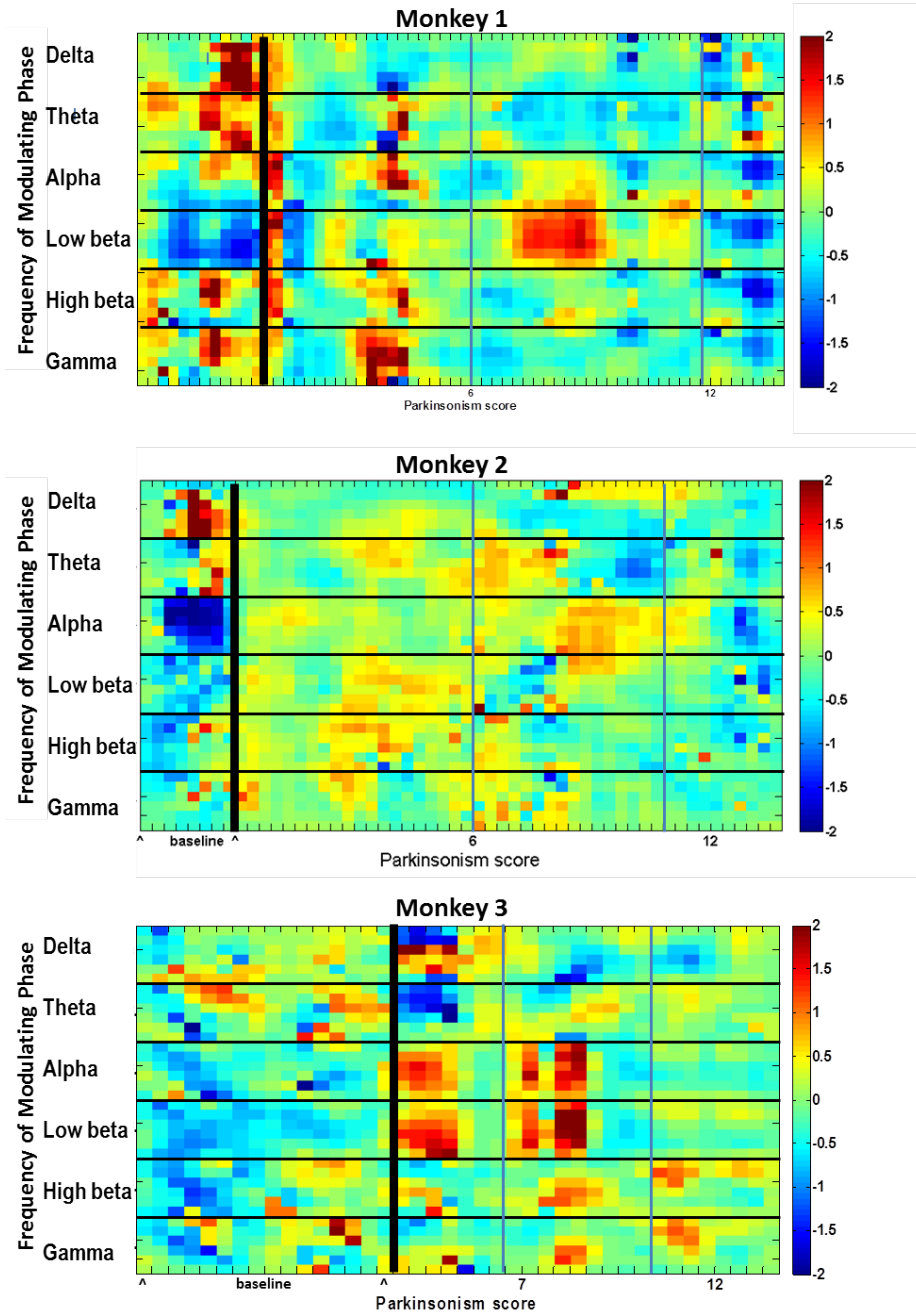


Figure 12: Phase-Amplitude Coupling features versus degree of parkinsonism for Monkey 1, Monkey 2, and Monkey 3. Vertical lines indicate columns of data belonging to each of the four stages of parkinsonism: Baseline (beginning to bold line), Stage 1, Stage 2, and Stage 3. Horizontal lines group the features by modulating phase. Within each phase group, the amplitude band increases from top to bottom.

right side of Figure 13 shows the generally decreasing delta phase modulation for all three monkeys. Finally, at the highest parkinsonism score measured for all three monkeys (12), decreased phase modulation can be seen across all frequency bands.

Taken together, these characteristics were used to partition the parkinsonism progression into four stages as indicated by the vertical lines in Figure 12. The baseline stage was characterized by low beta phase modulation and high delta phase modulation. Note that approximately twice as much baseline data was recorded for Monkey 3 compared to the other two monkeys. The second stage (scores (0-6]) showed medium-high level modulation for all frequencies, with Monkeys 1 and 3 showing some regions of low delta/theta modulation. The third stage (scores (6-10]) had the opposite characteristics of the baseline pattern (high beta, low delta). The fourth stage (scores of (10-12.5]) showed reduced modulation at all frequencies.

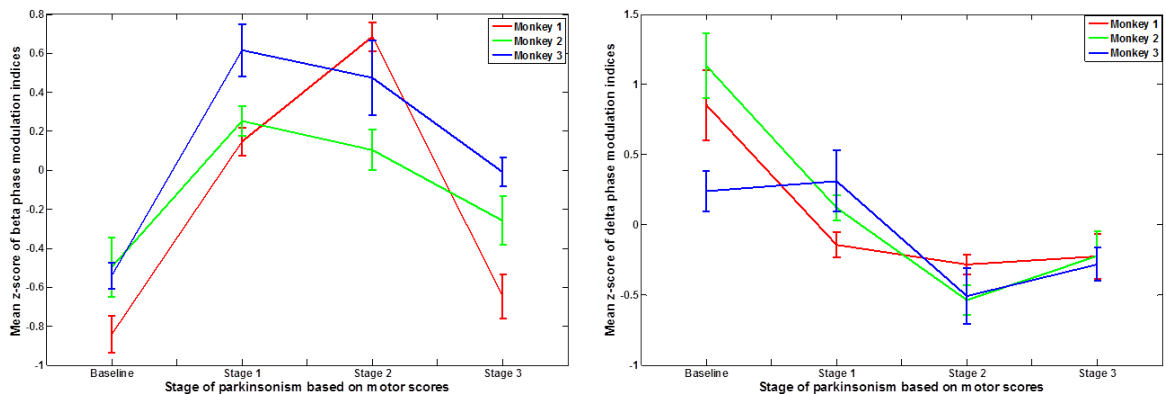


Figure 13: Left: mean beta phase-amplitude cross-frequency-coupling (CFC) MIs; Right: Mean delta phase-amplitude CFC MIs; Monkey 1 (red), Monkey 2 (green), and Monkey 3 (blue).

4.2.3.1 Comparison with beta power statistics

The beta MI changes showed a similar pattern that was statistically significant for the baseline stage and for other parkinsonism scores for all three monkeys. The left column of Figure 14 shows the distributions of the summed low beta and high beta phase-amplitude CFC MIs across parkinsonism scores using Bonferroni multiple

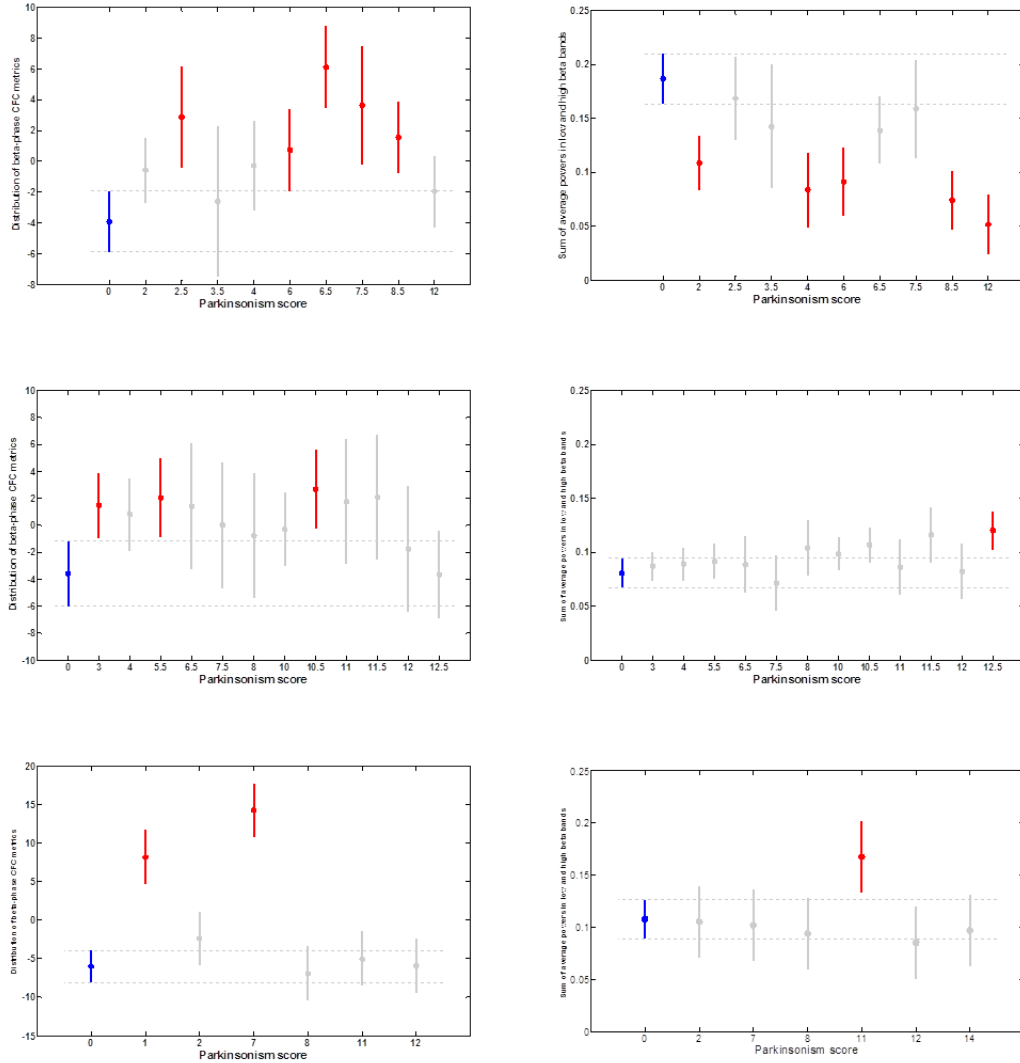


Figure 14: Summed beta phase-amplitude CFC features (left) and beta powers (right) for Monkey 1 (top), Monkey 2 (middle), and Monkey 3 (bottom). The beta CFC features (left column) show low values under baseline conditions (0) and at maximum parkinsonism (12-12.5), with elevated beta values in between, while the beta powers (right column) do not show a consistent trend across the three monkeys.

comparison analysis. The blue and red vertical lines indicate statistically significant differences between the baseline and other parkinsonism scores. The same analysis performed for the average beta powers failed to show any statistical significant common trends (right column of Figure 14).

It is important to note that the mean baseline MI values for any of the three

monkeys could be used as the reference point for detecting parkinsonism in the other monkeys. Figure 15 illustrates this for the raw low beta phase modulation of the alpha amplitude MI. The data shown is from the set of STN recordings captured simultaneously with GPi recordings. The horizontal lines correspond to the mean value under baseline conditions for this MI for the three monkeys. The figure shows that the range of raw scores was similar for all three monkeys, and that increased MI scores (reflecting parkinsonian activity) in any one of the monkeys would exceed any of the three means.

4.2.4 Discussion

This work was unique in several aspects. First, no aligning trigger was present in this data. However, even in the absence of any aligning stimulus markers, steady state patterns in parkinsonian brain activity were detectable using this approach. Second, by displaying the CFC features in concatenated vector format, the resulting image allowed a view of the progression of parkinsonism over time. Third, studies of CFC features often only consider phase modulation of amplitudes at higher frequencies, since this is a more understandable model of signal behavior. However, all combinations were included in this work, since the modulation results were not symmetric and many statistically significant pairings were found for which the phase frequency was greater than the amplitude frequency. Future work will explore the physical processes that might underlie such interactions.

The assessed parkinsonism scores for the three monkeys were not uniformly spaced throughout the range of possible scores (0-12.5) and the number of data samples for each assessed score differed as well. This created some difficulty in aligning and comparing the data between the monkeys. However, the results for the baseline and maximum parkinsonism scores were similar for all three monkeys, and the progression of parkinsonism between the two extremes appeared to share similar stages.

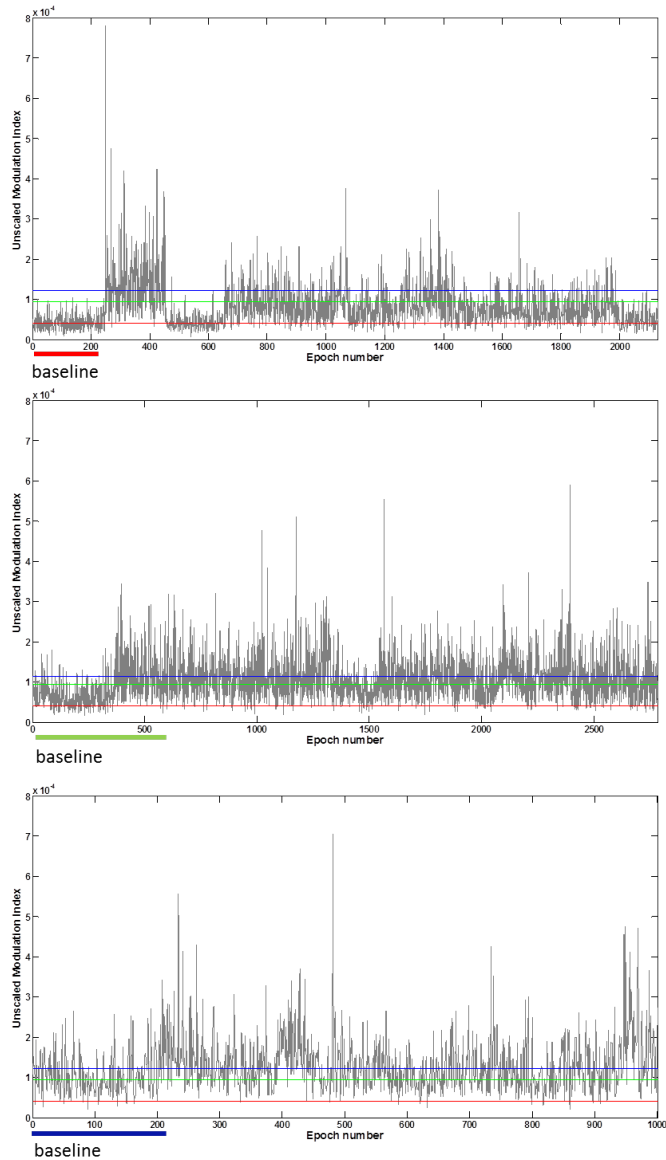


Figure 15: Raw modulation index (MI) values per 10 second epoch for 1 of the 36 features (low beta phase modulation of the alpha amplitude) for Monkey 1 (top), Monkey 2 (middle), and Monkey 3 (bottom). Horizontal lines indicate the average baseline value for each monkey. The length of the baseline data segment is indicated underneath each graph.

Although four stages of parkinsonism were detectable in the three monkeys, the increases and decreases that occur in the raw MI data (see Figure 15) suggest that there are acute effects associated with increasing parkinsonism, in addition to the chronic effects that allowed the parkinsonism staging examined in this study. For

example, the precipitous changes that occurred for all 36 CFC MI features with the first MPTP dose (see values immediately to right of the baseline stage (bold line) in Figure 12 and Figure 15) indicate that the CFCs are impacted strongly and immediately by the initial exposure to the neurotoxin. We did not find correlations between the degree of CFC and the strength and timing of MPTP dosages beyond the first dose. Still, it may be of interest to see how the CFC MIs correlate with brain injury in other animal models.

The most prominent features in the CFC map are the very low values of phase modulation under baseline conditions for certain frequencies (blue patches) which occur with greater phase modulation in lower frequencies. This pattern was unique to the baseline condition and may characterize healthy STN activity. It would be of interest to see if these healthy patterns can be restored after administration of anti-parkinsonism treatments such as levodopa.

It is also interesting that the characteristic baseline pattern was seen more strongly in the low beta region for monkeys 1 and 3, while it was more visible in the alpha region for Monkey 2, suggesting that there may be individual differences in characteristic operating frequencies in the baseline condition. If so, this has important implications for diagnosis and treatment of disorders involving the basal ganglia.

4.2.5 Conclusion

STN-LFP MI characterization of parkinsonism in MPTP monkey models showed statistically significant increased beta phase modulation compared to baseline conditions for mild to moderate parkinsonism, followed by decreased beta phase modulation for the maximum parkinsonism condition assessed in all three monkeys. The characterization also showed decreased delta phase modulation with increasing parkinsonism. Taken together, these patterns characterized four stages of parkinsonism.

Several studies have shown prominent beta band power in PD patients who were

“off” treatment, and reduced beta power, accompanied by improved symptoms, when patients resumed treatment [68, 125]. However, statistically significant elevation of average beta power was not consistently observed in the monkeys in this study. On the other hand, the beta MI features did show statistically significant changes that followed a similar pattern for all three monkeys. Based on this study, we believe that modulation indices are useful for characterizing the progression of parkinsonism, and that the characterization may be generalizable across multiple individuals.

4.2.6 Contributions to work

The animal experiments and recordings in this chapter were performed by Annaelle Devergnas. The approach for constructing CFC features using CWT coefficients in this and following chapters was designed and implemented by Teresa Sanders. Data analysis and software coding were performed by Teresa Sanders. The chapter was written by Teresa Sanders with feedback from Thomas Wichmann and Mark Clements.

CHAPTER V

CORRELATION BETWEEN MOTOR SCORES AND PHASE-AMPLITUDE COUPLING FEATURES IN PARKINSONISM PROGRESSION

5.1 Canonical correlation to estimate the degree of parkinsonism from local field potential and electroencephalographic signals

In this study, published in [105], modulation index (MI) features derived from Local Field Potential (LFP) recordings in the subthalamic nucleus (STN) and EEGs from the primary motor cortex were used to estimate the degree of motor impairment in a monkey model of parkinsonism. MI features are phase-amplitude cross-frequency-coupling (CFC) measures between frequency sub-bands within a signal. Six sub-bands were extracted with complex wavelet transforms to calculate the features for both the LFP and EEG signals. Using the method of canonical correlation, weighted combinations of the features produced estimates of parkinsonism motor impairment that correlated significantly with behavioral measures of parkinsonian signs, specifically scores on a scale for parkinsonian disability. Additionally, a subset of the STN LFP features were reconstructed from the EEG features.

5.1.1 Motivation

Deep Brain Stimulation (DBS) is a highly effective treatment for parkinsonism. DBS treatment involves the implantation of an electrode into specific brain regions (often the STN). The electrode is subsequently used to apply small electrical currents, generated from a pacemaker-like implanted battery-driven impulse-generator device. Typically, DBS therapy is continuously administered, without regard for the presence

or absence of parkinsonian signs or symptoms. The recent realization that the implanted DBS electrodes can also be used to record electrical activity [124] in humans has led to interest in pursuing approaches to modulate DBS based on measurements of brain activity in these regions. If successful, use of this ‘closed-loop DBS’ approach could lead to significant savings in battery power of the implanted pulse generator devices, as they could potentially be switched off or run with reduced duty cycles for periods of less severe parkinsonism. While LFPs recorded from the STN are the most commonly discussed biological feedback signal for closed-loop DBS, such signals are difficult to record in the real-life situation, particularly during stimulation, because of the presence of electrical stimulation artifacts. This study examined whether not only STN-LFPs, but also EEG signals recorded from M1 in the MPTP model of primate parkinsonism could be used for measuring parkinsonism, and whether STN LFP and M1 EEG features are related. Compared to STN-LFP data, measuring the severity of parkinsonism based on M1-EEG data would be advantageous, because EEG signals would be less encumbered by stimulation artifacts than the STN LFP signals. MIs [7, 19, 18, 114], which are measures of phase-amplitude CFC between frequency sub-bands within EEGs or LFPs were calculated for a series of recordings from two monkeys. Using canonical correlation [59], the correlation between the LFP and EEG MI features and the parkinsonism rating scores (a validated measure of the severity of parkinsonism) was maximized, and the LFP features that correlated most strongly with the parkinsonism scores were analyzed. Next, the canonical correlation between these LFP features and the full set of EEG MI features was computed. The resulting weights were then used to reconstruct the LFP MI features from the EEG MI features. Finally, the parkinsonism estimates obtained using the LFPs and EEGs were compared with the observation-based ratings of the severity of parkinsonism.

5.1.2 Methods

5.1.2.1 *Animals, surgical procedures*

Two rhesus monkeys (*Macaca mulatta*, 6-10 kg) were used for this electrophysiological experiment. Note that the two monkeys correspond to Monkeys 1 and 2 from the previous analysis. The results for Monkey 3 are not shown here (but are summarized in the next section) since this study occurred before the data for Monkey 3 was available. The animals were housed in pairs, with ad libitum access to food and water. All experiments were performed in accordance with the National Institutes of Health Guide for the Care and Use of Laboratory Animals and the United States Public Health Service policy on humane care and use of laboratory animals. All studies were approved by the Institutional Animal Care and Use Committee of Emory University. After initial behavioral conditioning, the animals were surgically prepared for chronic recordings, by affixing two standard metal recording chambers to their skull with dental acrylic. One of the chambers was positioned to give us access to the STN, using a sagittal approach (36° from the vertical). Head fixation bolts were also embedded into the acrylic. In addition, multiple epidural EEG electrodes were implanted.

5.1.2.2 *MPTP treatment*

After completion of the recordings in the normal state (see below), the animals were rendered progressively parkinsonian through weekly administration of MPTP (0.3-0.6mg/kg im). Monkey 1 received 21 injections (9.4mg/kg total), Monkey 2 received 26 injections (10.2mg/kg total) before it developed stable motor signs of parkinsonism. To assess the degree and stability of the MPTP induced motor disability, Annaelle Devergnas carried out a 15 minute observation of the animal's behavior every week. During this observation, motor impairment was scored (rating bradykinesia, freezing, extremity posture, frequency of arm movements, and finger dexterity) as well as trunk posture, home cage activity, and balance. Composite scores were formed

from the individual impairment scores and ranged from 0 (baseline) to 16 (moderate parkinsonism).

5.1.2.3 Recordings and Vigilance Analysis

LFP and EEG signals were recorded once weekly before and throughout the period of MPTP treatment. After electrophysiologic mapping of the STN, the dorsal sensori-motor portion of the nucleus was targeted for LFP recordings [94]. LFPs were recorded with bipolar electrodes (SNEX-100, Rhodes Medical Instruments Inc, CA). EEG signals were recorded as bipolar signals, using chronically implanted epidural electrodes. EEG, LFPs and video monitoring were recorded simultaneously. LFPs and EEG signals were amplified, band-pass filtered, sampled at 1000Hz and stored on a hard drive using a data acquisition interface (Power 1902 and 1401; CED, Cambridge, UK) and commercial software (Spike2, CED) for off-line analysis.

Vigilance stage scoring was manually performed offline on Spike2 (CED) using the sleepscore program, based on the analysis of consecutive 10 second epochs. Each epoch was labeled as representing either wakefulness, drowsiness or light sleep. For the present analysis, only the wakefulness epochs were used. Wakefulness was considered when the monkey was attentive to the surroundings with eyes open and with low-amplitude mixed-frequency EEG.

5.1.2.4 Complex Continuous Wavelet Transform

As previously discussed, wavelet methods are appropriate for analyzing LFP and EEG signals, since wavelet bases allow representation of signals that vary in both frequency and duration. For this study, complex continuous wavelet transforms were used in order to allow extraction of phase information.

First, z-scores of the 1000 Hz signals for each recording day were calculated. The z-scored data was then low-pass filtered and downsampled by a factor of 4 prior to complex Morlet wavelet transform (CWT) decomposition, calculated as follows:

$$X_w(c, n) = \frac{1}{\sqrt{c}} \int_{-\infty}^{\infty} x(t) \psi^* \left(\frac{t - n}{c} \right) dt$$

where “c” represents the scale factors and “n” represents the time points at which the CWTs were evaluated. The range of scales chosen was $c = 1:512$ since this range supported the frequency bandwidths of interest, n was set to 1:2500 to capture each full 10 second epoch at 250 Hz., and $\psi(t)$ was the complex Morlet wavelet:

$$\psi(t) = \kappa (e^{-\frac{t^2}{BW}}) (e^{2i\pi f_c t})$$

with BW as the wavelet bandwidth, f_c as the center frequency, and $\kappa = (\pi BW)^{-\frac{1}{2}}$ as a normalization constant. Currently, $BW = 1$, and $f_c = 3$.

Previous studies have documented parkinsonism-related changes in theta-, beta- and gamma-bands in LFP and EEG signals [14, 101, 49, 73, 27, 108]. In order to capture effects in these and neighboring bands, composite signals were created by pooling the wavelet coefficients corresponding to each of the following wavebands: delta (3-4Hz), theta (5-8 Hz), alpha (8-11 Hz), low beta (12-19 Hz), high beta (20-30 Hz), and gamma (31-60 Hz).

5.1.2.5 Cross-frequency-coupling and modulation index

Cross-frequency-coupling (CFC) is defined as the interaction between oscillations in multiple frequency bands and can include phase-amplitude, phase-phase, or amplitude-amplitude coupling. Phase-amplitude coupling analysis has uncovered features of interest in several recent studies, particularly event-related theta band phase modulation of gamma band amplitudes [19], and beta band phase modulation of both narrowband gamma band oscillations in STN and broadband gamma band oscillations in M1 [27]. For this work, phase-amplitude coupling was calculated by averaging the amplitude in the modulated frequency band corresponding to phase values for the modulating frequency band. We used phase values from $0-2\pi$, divided into 18 equal width phase bins. In order to facilitate comparisons of phase-frequency coupling over time, various measures have been developed. We used the MI calculation proposed by Tort [114] based on the Kullback-Leibler divergence between two distributions:

$$D_{\text{KL}}(P\|Q) = \sum_i \ln \left(\frac{P(i)}{Q(i)} \right) P(i).$$

where $P(i)$ indicates the uniform distribution that occurs when the amplitudes are distributed randomly across all phases, and $Q(i)$ indicates the distribution obtained by normalizing the phase-amplitude coupling calculated as described above. The two-sided divergence was used, i.e., $D_{\text{KL}}(P\|Q) + D_{\text{KL}}(Q\|P)$, in order to give a symmetric measure of the deviation from the uniform distribution. This measure is more indicative of true sinusoidal modulation than other methods, such as height differences, which only measure the distance between two points on the distribution (usually the minimum and maximum).

MI's were calculated for each 10 second epoch. Next, the MI's were averaged across all epochs within a file. These average MI's from each file were used to correlate with the motor scores as described in the next section.

5.1.2.6 Canonical correlation

The goal of canonical correlation is to choose a set of weights \mathbf{a} and \mathbf{b} that maximize the correlation between samples from two vectors of random variables, \mathbf{X} (e.g., MI features) and \mathbf{Y} (e.g., motor scores).

The function to be maximized can be written:

$$\rho = \frac{\mathbf{a}'\Sigma_{\mathbf{X}\mathbf{Y}}\mathbf{b}}{\sqrt{\mathbf{a}'\Sigma_{\mathbf{X}\mathbf{X}}\mathbf{a}}\sqrt{\mathbf{b}'\Sigma_{\mathbf{Y}\mathbf{Y}}\mathbf{b}}}. \quad (1)$$

where $\Sigma_{\mathbf{X}\mathbf{X}}$, $\Sigma_{\mathbf{Y}\mathbf{Y}}$ are the covariance matrices for \mathbf{X} and \mathbf{Y} respectively, and $\Sigma_{\mathbf{X}\mathbf{Y}}$ is the covariance matrix between \mathbf{X} and \mathbf{Y} .

Observing that the solution is not affected by scaling, the optimization problem can be solved by maximizing the numerator in (1) subject to:

$$\mathbf{a}'\Sigma_{\mathbf{X}\mathbf{X}}\mathbf{a} = 1 \quad (2)$$

$$\mathbf{b}'\Sigma_{\mathbf{Y}\mathbf{Y}}\mathbf{b} = 1 \quad (3)$$

The maximization problem can be solved in multiple ways with the most common approaches using either singular value decomposition alone [86] or in combination with QR factorization (decomposition of a matrix \mathbf{A} into a product $\mathbf{A}=\mathbf{Q}\mathbf{R}$ of an orthogonal matrix \mathbf{Q} and an upper triangular matrix \mathbf{R}), as done in the MATLAB Statistical Toolbox used for our analysis.

5.1.3 Results

Our analysis included 5373 10 second epochs of data recorded on 13 days over the 6 months during which Monkey 1 progressed from the baseline (normal) state to a

state of moderate parkinsonism. For Monkey 2, the analysis included 5779 10 second epochs recorded over a similar progression from baseline to moderate parkinsonism.

For each monkey, the weightings that resulted in maximum correlation between the motor scores and the modulation indices were calculated. For both monkeys, the weighted combination of LFP modulation indices correlated well with the composite motor score ($p < 0.0001$), as well as subscores for balance and bradykinesia ($p < 0.01$), and freezing ($p < 0.001$). Figure 16 shows the weighted motor scores and LFP MIs for Monkey 1 for each recording file. Figure 17 shows the relationship between the weighted sum of the LFP MIs and the balance motor scores for Monkey 2.

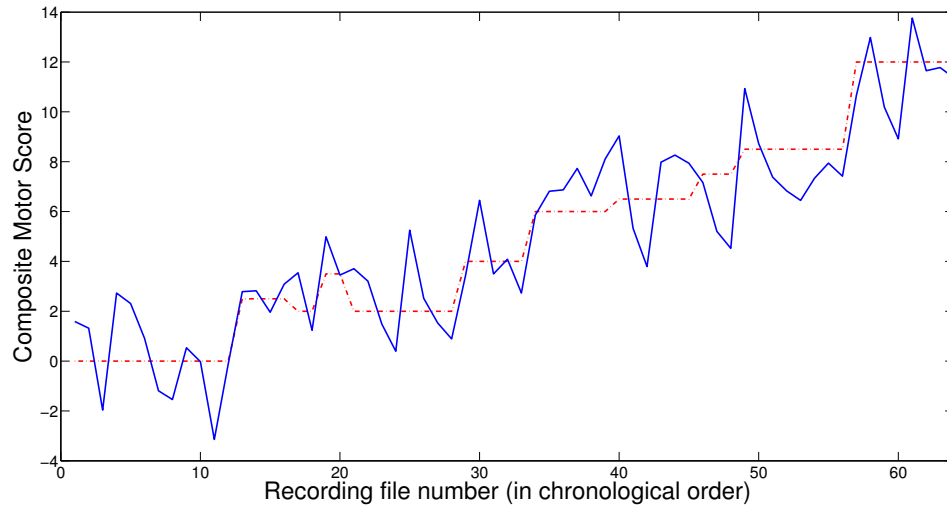


Figure 16: Comparison between measured composite motor scores (dashed line) and motor scores estimated from the sum of the optimally weighted LFP MIs (solid line) for Monkey 1.

The weighted combination of EEG modulation indices correlated well with the composite motor scores ($p < 0.000001$), the balance and bradykinesia ($p < 0.000001$), and the specific rating for freezing ($p < 0.000001$). Figure 18 compares the weighted EEG modulation indices and the composite motor scores for each recording file for Monkey 1. Figure 19 shows the relationship between the weighted modulation indices and the freezing motor scores for the Monkey 1 EEG data.

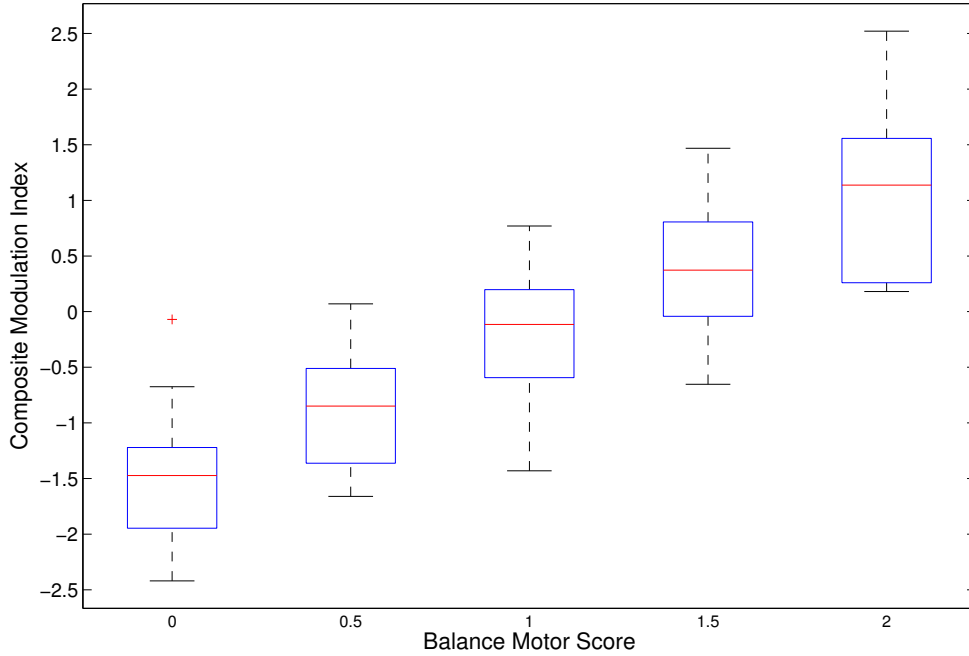


Figure 17: Distributions of the sum of the optimally weighted LFP MIs (composite modulation index) for each of the measured balance motor scores (x-axis) for Monkey 2. For each box, the central mark is the median, while the edges of the box are the 25th and 75th percentile. “Plus” symbol is an outlier.

For both monkeys, the optimally weighted canonical correlation between the EEG MIs and the composite motor scores were similar to those between the LFP MIs and the composite motor scores, (for Monkey 1, 0.9428 and 0.9205, respectively; for Monkey 2, 0.9000 and 0.9185, respectively). The EEG MIs and the LFP MIs were also highly correlated with each other (optimally weighted canonical correlation of 1.0 for Monkey 1 and 0.9856 for Monkey 2, $p < 0.0001$). In particular, it was possible to reconstruct the two STN LFP MIs that most strongly correlated with the motor scores (8-11 Hz / 12-19 Hz and 8-11 Hz / 8-11 Hz) from the EEG MIs for Monkey 1 as shown in Figure 20. Note that the raw STN-LFPs and EEGs are different from each other in appearance and uncorrelated (cross correlation coefficients < 0.05).

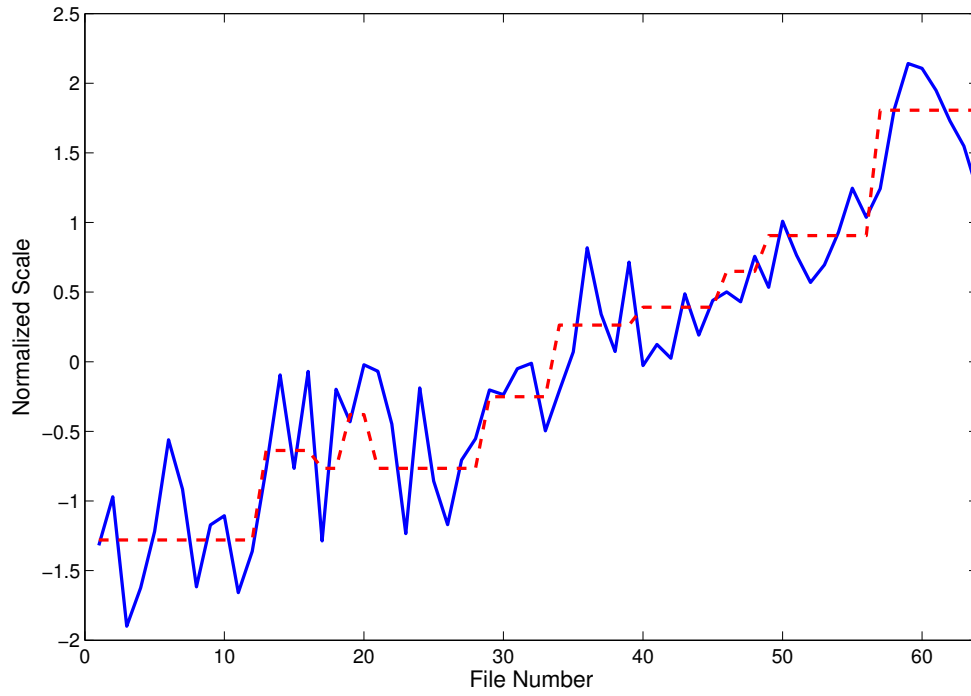


Figure 18: Comparison between weighted EEG MIs (solid line) and composite motor scores (dashed line) for Monkey 1.

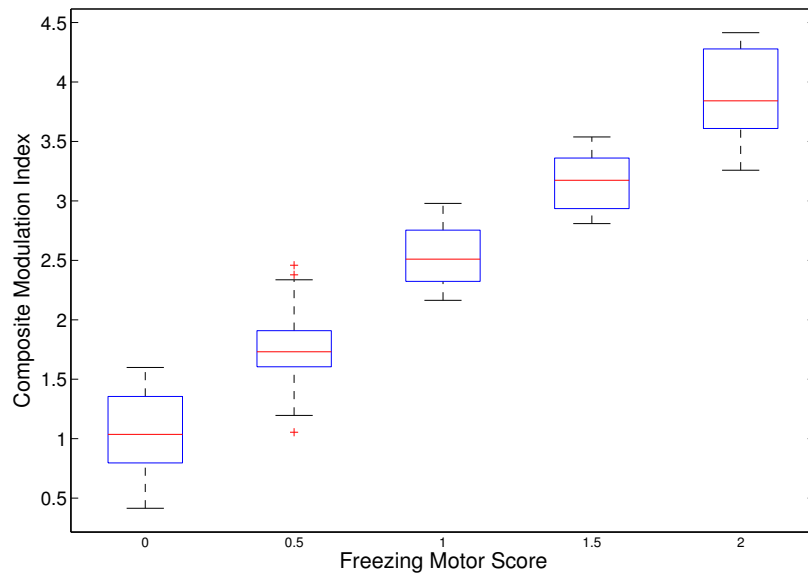


Figure 19: Distributions of the weighted EEG MIs corresponding to the freezing motor scores for Monkey 1.

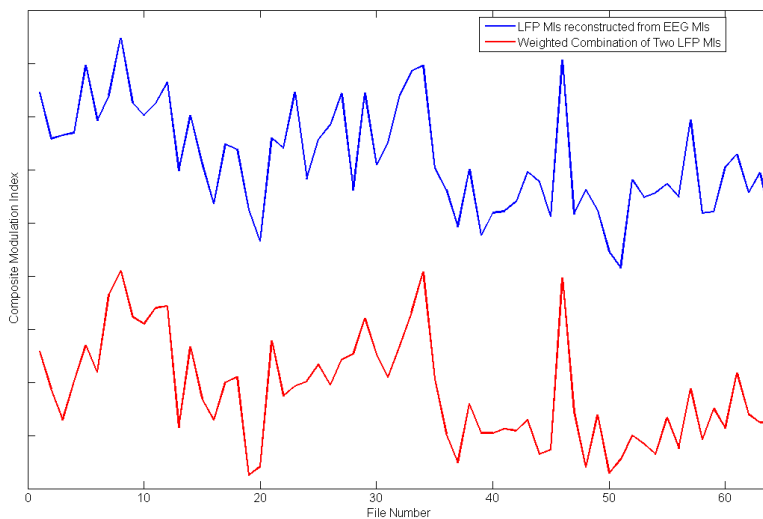


Figure 20: Comparison between 2 STN LFP MIs and their reconstruction with EEG MIs for Monkey 1.

While modulation indices from particular frequency bands did not appear to be associated with individual motor component scores, there were several frequency bands that correlated well with multiple motor scores, and many frequency bands that interacted with each other to form the most highly weighted modulation indices. In particular, two LFP (phase / amplitude) modulation indices, (12-19 Hz / 12-19 Hz) and (8-11 Hz / 12-19 Hz), yielded statistically significant correlation with both composite motor scores and subscores.

Table 4 summarizes the accuracy of the motor score estimates calculated using the LFP and EEG MIs as compared to the motor scores. The comparison includes both the full LFP MI estimates as well as the estimates obtained using the subset of two statistically significant LFP MIs mentioned previously. The entries in the table are $1 - NRMSE$ (normalized root mean square error):

$$1 - \frac{\sqrt{\frac{\sum(\text{estimated score}(i) - \text{actual score}(i))^2}{n}}}{(\text{max score} - \text{min score})}$$

The asterisks indicate the statistical significance of the canonical correlation underlying each estimate.

Table 4: Accuracy of Motor Scores Estimated using Weighted Modulation Indices.

Motor Score Type	Monkey 1			Monkey 2		
	All STN LFP MIs	All EEG MIs	2 LFP MIs: (12-19 Hz/12-19 Hz) and (8-11 Hz/12-19 Hz)	All STN LFP MIs	All EEG MIs	2 LFP MIs: (12-19 Hz/12-19 Hz) and (8-11 Hz/12-19 Hz)
Composite	0.89****	0.92****	0.77****	0.87****	0.86***	0.87**
Subscores:						
Balance	0.86**	0.90****	0.72*	0.88****	0.85***	0.87***
Freezing	0.88***	0.91****	0.75**	0.89****	0.84**	0.87***
Bradykinesia	0.89****	0.90****	0.80****	0.86**	0.86**	0.86*
Home Cage Activity	0.91****	0.90****	0.79****	0.84 ^{ns}	0.85*	0.82*

* p < .05, ** p < .01, *** p < .001, **** p < .0001

The accuracies show that statistically significant estimates of the degree of parkinsonism were obtained from each of the following for both monkeys: weighted combinations of the STN LFP MIs, the EEG MIs, and a subset of two LFP MIs. Additionally, estimates of the balance, freezing, and bradykinesia subscores were possible with lower statistical significance. The Monkey 1 estimates using the full set of 36 MIs were more accurate than the Monkey 2 scores. The Monkey 1 EEG MIs provided the most accurate estimates while the Monkey 2 EEG MIs provided the least accurate estimates obtained with all 36 features. Finally, the set of two optimal LFP MIs provided good estimates for Monkey 2, but were less accurate for Monkey 1.

5.1.4 Discussion and conclusions

We have shown that canonical correlation methods can be used to estimate Parkinsonian motor scores from STN-LFP and primary motor cortex EEG modulation indices. This finding provides further support to the hypothesis that parkinsonism is associated with changes in cross-frequency coupling patterns that can be detected both in cortex and in associated basal ganglia areas. The high correlation between the MI features from simultaneous STN-LFPs and M1 EEGs, and the ability to estimate

parkinsonism motor scores and subscores using weighted MI features from STN-LFP and EEG signals, are novel findings. These results suggest that EEG signals could be used for classifying the severity of parkinsonism, and possibly as control signals for on-demand DBS [2, 13]. As stated above, the advantage of using EEG measurements rather than the more frequently considered LFPs from the DBS electrodes is that EEG signals are less prone to stimulation artifacts, so that monitoring of parkinsonism may be accomplished not only when the DBS pulse generator is off, but also during stimulation.

It is a limitation of the current analysis that the parkinsonism estimate is based on the full data set and that we achieved our results by studying relatively long data segments (multiple 10 second epochs of data within each recording file). Predicting parkinsonism in a test set using weights calculated from a training set, and examining whether shorter epochs suffice to predict the degree of parkinsonism will be of interest in future studies.

5.1.5 Contributions to work

The animal experiments and recordings were performed by Annaelle Devergnas. The signal processing was designed, analysis software written, and data analysis performed by Teresa Sanders. The manuscript was prepared by Teresa Sanders with feedback from Thomas Wichmann, Mark Clements, and Annaelle Devergnas.

5.2 Comparison between phase-amplitude coupling features and standard statistical measures for estimating the degree of parkinsonism

In the previous section (5.1), parkinsonism motor scores for two MPTP-treated rhesus monkeys were estimated using weighted CFC MI features from 6 frequency bands. In this section, data from the same two monkeys and a new third MPTP-treated rhesus monkey were used. The weighted CFC MI estimates were calculated for all three monkeys and then compared to weighted standard statistical estimates calculated from the same 6 frequency bands using the same optimal weighting method. The standard statistical features used were the mean magnitudes for each of the 6 frequency bands and the mean of the variances for each of the 6 frequency bands. For both the MI approach and the standard statistical approach, the features were calculated for each 10 second epoch and then averaged for each recording file.

5.2.1 Methods

The animal experiment methods used to collect the STN-LFP and M1-EEG data analyzed in this study were described in Section 5.1.2. The data used for this study was a representative subset of the data analyzed in Section 5.1, along with data from a third monkey that became available after completion of the previous study. Specifically, the data for this work consisted of the set of subthalamic nucleus (STN) and M1 data collected simultaneously with recordings from the globus pallidus, corresponding to approximately half of the full data set. This subset of data was chosen because the CFC MI features had already been extracted for a previous analysis, and because it lessened the time required to calculate the CFC MIs and standard statistical features for the 3 brain regions and 4 feature types compared in this study. It is representative of the entire data set because it was collected under the same conditions and for all of the recording days and degrees of parkinsonism used in the full data set.

The methods for filtering the data into 6 frequency bands using the CWT are

described in Section 5.1.2.4. The frequency bands used were the same: delta (3-4Hz), theta (5-7 Hz), alpha (8-11 Hz), low beta (12-19 Hz), high beta (20-30 Hz), and gamma (31-60 Hz). The methods for obtaining the optimal correlation, ρ , between the parkinsonism score and the CFC MIs and estimating the parkinsonism score using CFC MIs are described in Section 5.1.2.5.

The methods for calculating the standard statistical features were as follows.

For each of the 6 frequency bands, the mean magnitude was computed for each epoch,

$$\mu(freq. band, epoch) = \frac{1}{m} \sum_{i=1}^m |s_i(freq. band, epoch)|$$

where “s” are the band-filtered signal samples and “m” is the number of signal samples in each 10 second epoch. The means for each file, $\overline{\mu(freq. band, file)}$, were then computed by averaging over all epochs in the file.

For each of the 6 frequency bands, the variances were computed for each epoch,

$$\sigma^2(freq. band, epoch) = \frac{1}{m-1} \sum_{i=1}^m (s_i(freq. band, epoch) - \mu(freq. band, epoch))^2$$

where “s” is the band-filtered signal and “m” is the number of signal samples in each 10 second epoch.

The average variances for each file, $\overline{\sigma^2(freq. band, file)}$ were then computed by averaging over all epochs in the file.

5.2.2 Correlation between Modulation Indices and Motor Scores

As shown in Figure 21, the weighted CFC MI combinations correlated with the overall motor score for all three monkeys ($\rho > 0.73$). Plots of the weighted sum of the features as a function of the composite motor score also show that the CFC MIs yield a good estimate of the degree of parkinsonism for Monkey 1 (Figure 22) and Monkey 3 (Figure 23).

As can be seen in Figure 21, the weighted mean and variance features also correlated in most cases. However, with the exception of the Monkey 2 cortical data

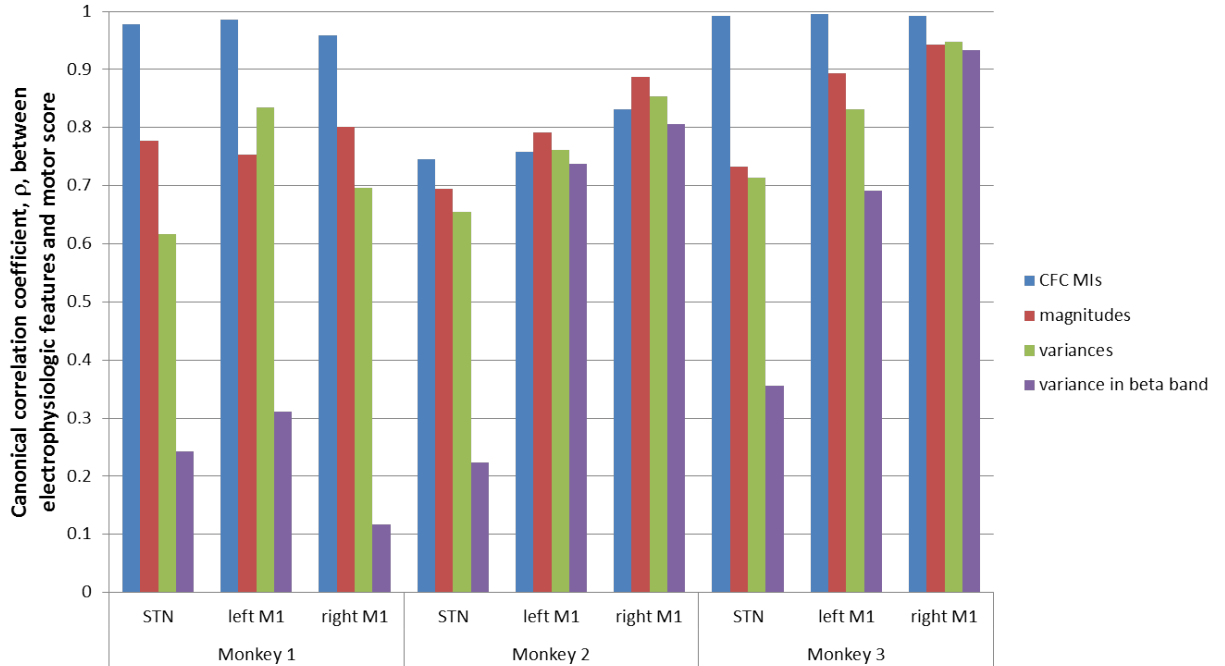


Figure 21: Correlation of parkinsonism rating with CFC MIs and standard statistical features extracted from band-filtered STN-LFP and M1-EEG data. As shown in the legend, the 3 standard statistical measures used were: magnitude of signal in all 6 bands, variance of signal in all 6 bands, and variance of signal in the beta band.

(Figure 24), the weighted CFC MIs provided a more accurate estimate than did the weighted mean or variance estimates. Tables 5, 6, and 7 shows the statistical significance of each of these correlations as well as a control statistical significance for a random same-length sequence.

5.2.2.1 Mean and variance features

The mean magnitude and variance features changed similarly with increasing parkinsonism score, likely because of the initial z-scoring of the raw LFPs and EEGs. Accordingly, the mean and variance weighted sums correlated similarly with the parkinsonism rating (Figure 21). In part because of these similarities, the following results and discussion will focus on comparing the variance features to the MI features. Showing the variance results also allows a comparison that is relevant to other recent work that assesses parkinsonism using the variance (and/or coefficient of variation) of the

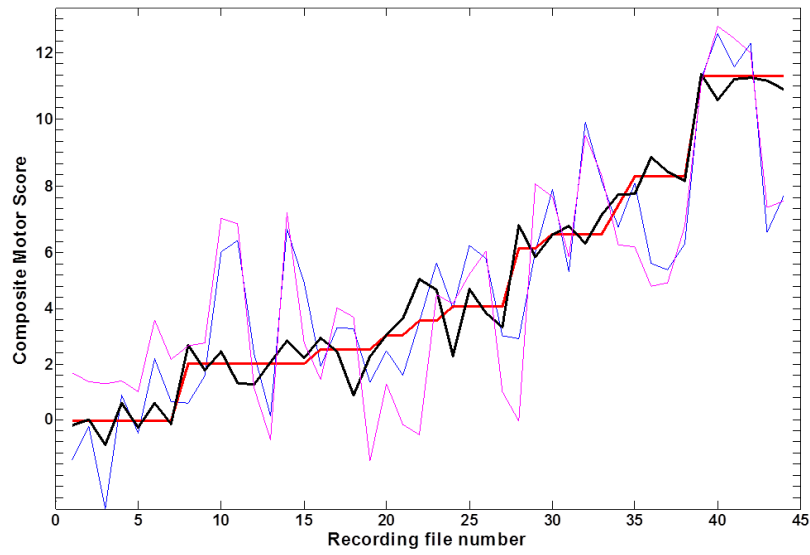


Figure 22: Parkinsonism estimates using CFC MI features (black), magnitude within frequency bands (magenta), and variance within frequency bands (blue). The visually rated parkinsonism scores are shown in red. (Monkey 1 left cortex data)

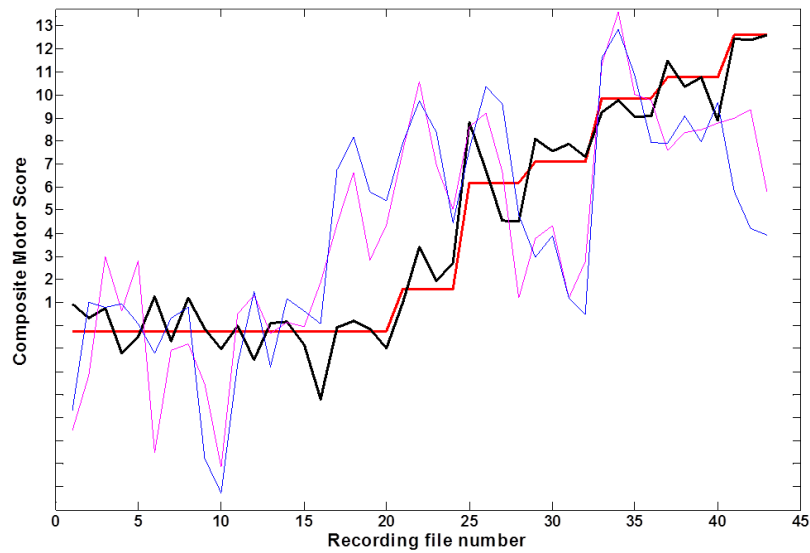


Figure 23: Parkinsonism estimates using CFC MI features (black), magnitude within frequency bands (magenta), and variance within frequency bands (blue). The visually rated parkinsonism scores are shown in red. (Monkey 3 STN data)

Table 5: Statistical significance for Monkey 1 Canonical Correlation

Monkey 1	Subthalamic Nucleus, STN			Left Motor Cortex, M1			Right Motor Cortex, M2		
	Correlation with motor scores	p value, (Statistical significance)	p control, (Significance when correlated with a random sequence)	Correlation with motor scores	p value, (Statistical significance)	p control, (Significance when correlated with a random sequence)	Correlation with motor scores	p value, (Statistical significance)	p control, (Significance when correlated with a random sequence)
CFC MI	0.9787	1.1x10 ⁻⁴	0.6239	0.9865	4.4x10 ⁻⁶	0.4252	0.9595	0.006	0.2522
Magnitude	0.7779	2.5x10 ⁻⁶	0.2057	0.8352	2.2x10 ⁻⁸	0.6183	0.8015	4.4x10 ⁻⁷	0.1587
Variance	0.6174	0.0047	0.3625	0.7529	1.2x10 ⁻⁵	0.9361	0.6962	2.4x10 ⁻⁴	0.2008
Variance in beta bands	0.2424	0.2891	0.8059	0.3111	0.1241	0.3425	0.1167	0.7549	0.5235

Table 6: Statistical significance for Monkey 2 Canonical Correlation

Monkey 2	Subthalamic Nucleus, STN			Left Motor Cortex, M1			Right Motor Cortex, M2		
	Correlation with motor scores	p value, (Statistical significance)	p control, (Significance when correlated with a random sequence)	Correlation with motor scores	p value, (Statistical significance)	p control, (Significance when correlated with a random sequence)	Correlation with motor scores	p value, (Statistical significance)	p control, (Significance when correlated with a random sequence)
CFC MI	0.7452	0.0012	0.4107	0.7583	4.4x10 ⁻⁴	0.8097	0.8313	1.4x10 ⁻⁷	0.2522
Magnitude	0.6942	5.6x10 ⁻¹²	0.8308	0.7916	1.3x10 ⁻¹⁸	0.8187	0.8880	2.6x10 ⁻³⁰	0.4156
Variance	0.6552	4.7x10 ⁻¹⁰	0.4619	0.7621	3.0x10 ⁻¹⁶	0.6261	0.8542	3.0x10 ⁻²⁵	0.2008
Variance in beta bands	0.2230	0.0781	0.1080	0.7372	9.3x10 ⁻¹⁸	0.5525	0.8062	1.6x10 ⁻²³	0.7622

beta band filtered signal [77, 78].

As mentioned previously, in most cases, the weighted sum of variance estimates were not as accurate as those obtained using the weighted sum of the CFC MIs. However, the weighted sums of the variances allowed estimation of the parkinsonism rating in the cortical data with $\rho > 0.69$ (see Figure 21). Since calculation of the variances is less computationally costly than computation of the CFC MIs, parkinsonism estimation with the variance data may be beneficial for situations where computational power and time are limited.

Table 7: Statistical significance for Monkey 3 Canonical Correlation

Monkey 3	Subthalamic Nucleus, STN			Left Motor Cortex, M1			Right Motor Cortex, M2		
	Correlation with motor scores	p value, (Statistical significance)	p control, (Significance when correlated with a random sequence)	Correlation with motor scores	p value, (Statistical significance)	p control, (Significance when correlated with a random sequence)	Correlation with motor scores	p value, (Statistical significance)	p control, (Significance when correlated with a random sequence)
CFC MI	0.9787	2.3x10 ⁻⁴	0.4597	0.9958	2.8x10 ⁻⁷	0.3723	0.9915	4.7x10 ⁻⁷	0.1012
Magnitude	0.7999	1.7x10 ⁻⁶	0.3682	0.8940	2.6x10 ⁻¹⁰	0.9918	0.9429	6.6x10 ⁻¹⁶	0.1339
Variance	0.7024	0.0080	0.4972	0.8315	2.7x10 ⁻⁷	0.8806	0.9484	1.1x10 ⁻¹⁶	0.1154
Variance in beta bands	0.4324	0.1731	0.5538	0.6916	5.9x10 ⁻⁶	0.9203	0.9334	1.6x10 ⁻¹⁶	0.1119

As can be seen in Figures 22, 23, and 25, the variance features yielded a more noisy estimate of the degree of parkinsonism over time than the CFC MI features. However, it is interesting to note in Figure 25 that the variances of the second, third, and fourth frequency bands (alpha through low beta) generally increase with parkinsonism in the cortex, while the same features decrease with parkinsonism in the subthalamic nucleus for all three monkeys, indicating the responses to increasing parkinsonism in M1 and STN are anticorrelated. (See the left to right change from shades of blue to red/yellow in the second, third, and fourth row of the top set of images, and the change from red/yellow to blue for the same three rows in the bottom set of images.) The decreasing / increasing trend for the low beta variance features in the STN / M1 data can be seen in the top plot in Figure 26.

5.2.3 Discussion

The frequency band statistical features required less time to compute than the CFC MI features, and were helpful for estimating the degree of parkinsonism, as shown in Figure 21. Since the simple frequency band statistical changes can be computed more quickly, they may be useful for real-time applications such as closed-loop deep brain stimulation (DBS). However, as shown in Figure 21, the estimates based on the CFC

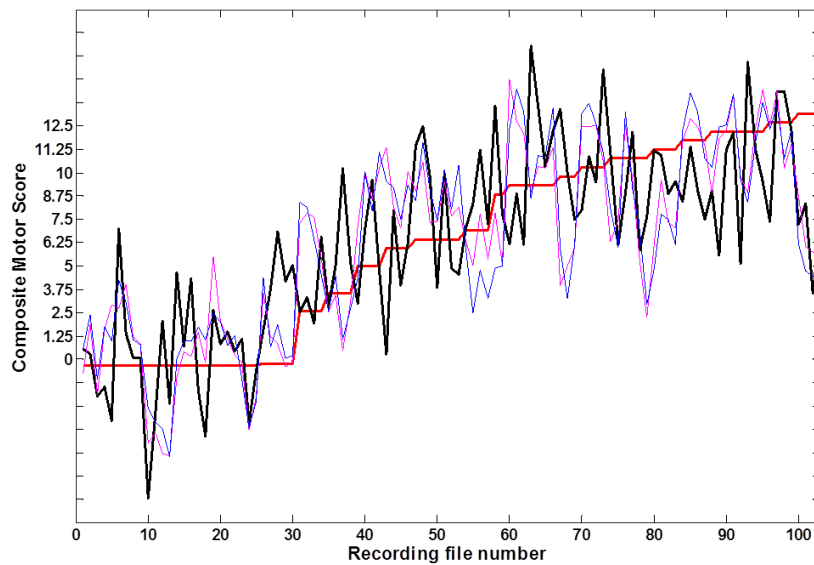


Figure 24: Parkinsonism estimates using CFC MI features (black), magnitude within frequency bands (magenta), and variance within frequency bands (blue). The visually rated parkinsonism scores are shown in red. (Monkey 2 right cortex data)

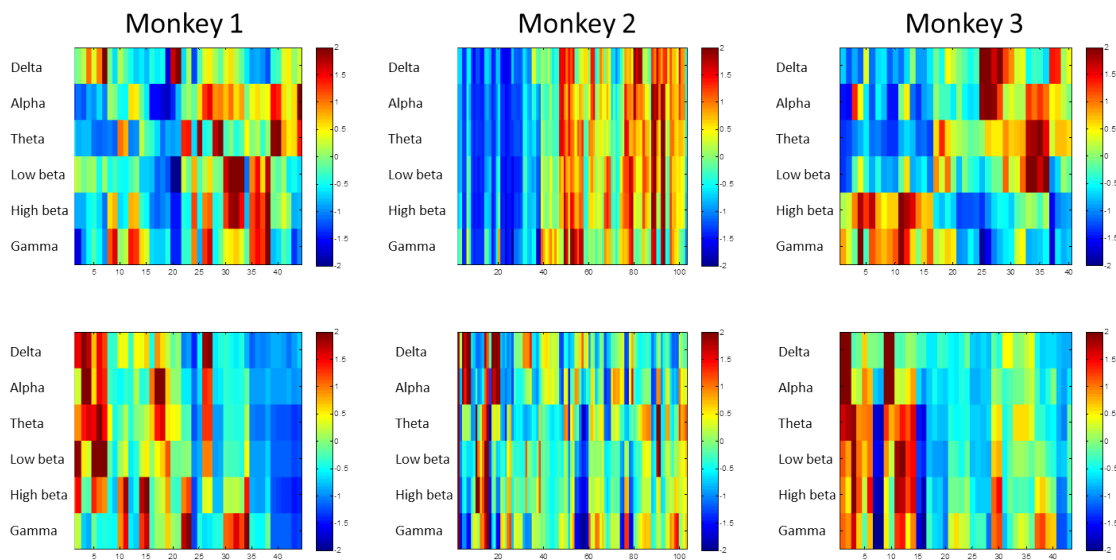


Figure 25: Z-scored variances in the 6 frequency bands for increasing parkinsonism (left to right). The x-axis denotes the data file number. Top row shows cortical variances. Bottom row shows STN variances. Left to right images show Monkey 1, Monkey 2, and Monkey 3, respectively.

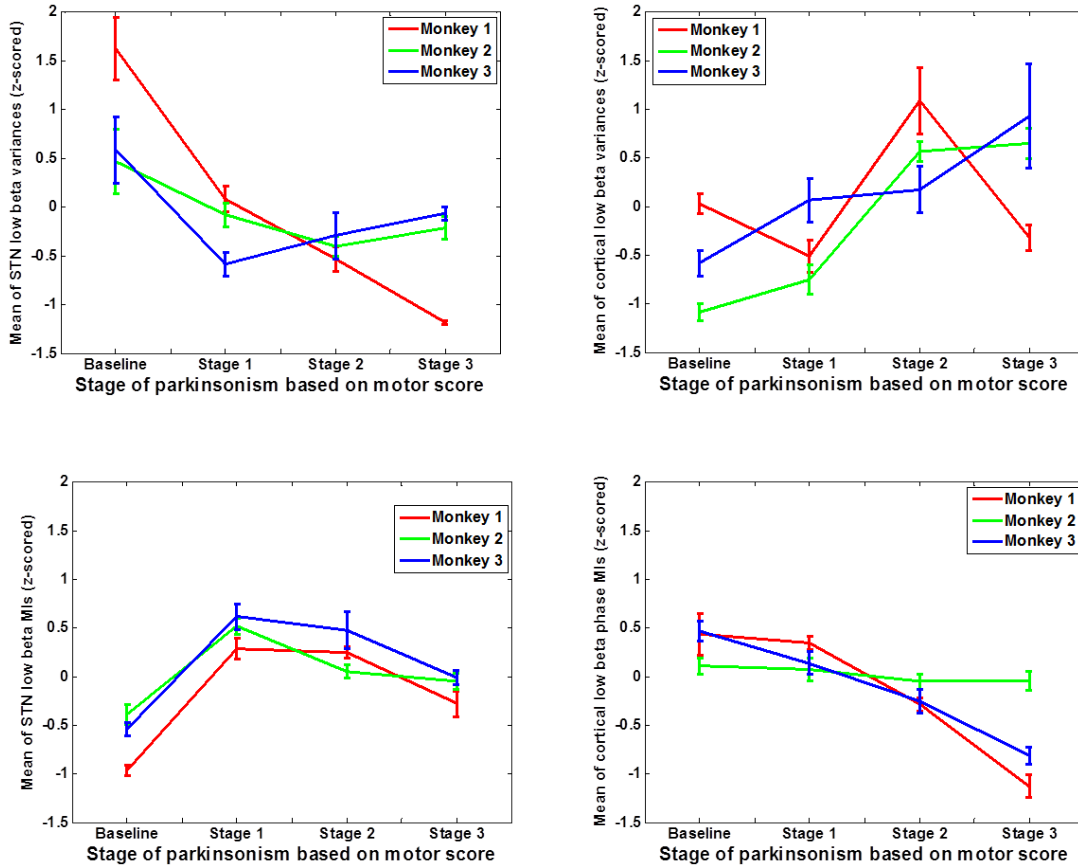


Figure 26: Low beta STN (left) and cortical (right) variance (top row) and MI features (bottom row) for Monkey 1 (red), Monkey 2 (green), and Monkey 3 (blue) for increasing stages of parkinsonism. Note that the Monkey 2 cortical beta phase CFC MI plot (green trace in lower right figure) does not follow the same trend as Monkeys 1 and 3. This is consistent with the less accurate estimate of parkinsonism obtained using the Monkey 2 cortical MIs.

MI features were more accurate in all cases except the Monkey 2 M1-EEG data. This can also be seen by observing that the error bars for the low beta phase MI curves (bottom row) are smaller than those for the low beta variance curves (top row).

Another advantage of the CFC MI features is that the range of the raw (non-z-scored) features were similar for the three monkeys. This was previously shown for the STN-LFP low beta phase modulation of the alpha amplitude in Figure 15 and can also be seen for the M1-EEG low beta phase MIs in the lower graph in Figure 27. In comparison, the raw standard statistical features varied more across individuals as can be seen in the upper graph in Figure 27.

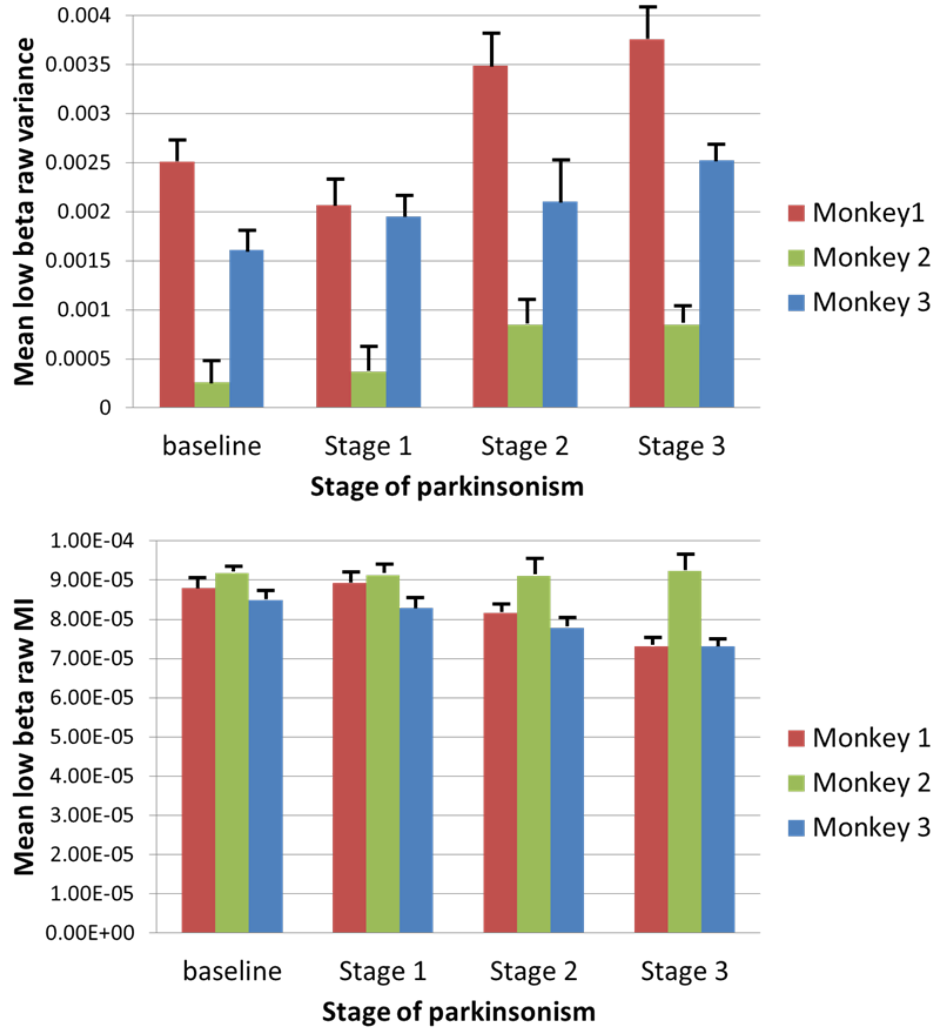


Figure 27: Mean raw (non-z-scored) cortical low beta variances (top row) and MIs (bottom row) for Monkey 1 (red), Monkey 2 (green), and Monkey 3 (blue) for increasing stages of parkinsonism. The variance features are dissimilar for the three monkeys, while the MI baseline features are similar for all monkeys. As previously shown in Figure 26, the Monkey 2 cortical MI features do not follow the same trend as the cortical MI features for the other two monkeys.

The analysis in this section focused on longer-term time (5-20 minute) averages of electrophysiological features in order to determine whether CFC MIs provide a more stable and accurate estimate of the overall degree of parkinsonism than standard statistical measures. For the purpose of applications such as closed-loop DBS, another important question may be whether CFC MIs provide a better estimate for shorter time intervals. Although this question is not addressed directly here, the greater

accuracy of the long-term estimates suggest that the short-term CFC MIs, if they can be detected over small enough time intervals, may also provide a more accurate estimate than standard statistical measures. Since the analysis in Chapter 4 shows that CFC MIs allow discrimination between normal and parkinsonian stages for 500 ms samples, CFC MIs may provide a more accurate realtime feedback signal for DBS adjustments than standard statistical measures such as those used in [77, 78].

5.2.4 Conclusion

The CFC MI features based on CCWT coefficients from LFPs and EEGs changed in predictable ways with the degree of parkinsonism in monkeys and allowed reliable estimation of the parkinsonism score. The raw CFC MI features were more similar for the three monkeys than were the raw variance features. With the exception of the Monkey 2 EEG data, weighted CFC MI features provided a more accurate estimate of the parkinsonism score than the mean or variance features.

CHAPTER VI

MULTIMODAL MONITORING SYSTEM FOR NEUROLOGICAL DISORDERS

Sections 6.1 through 6.3 were published in [104]. Copyright © 2013 Association for Computing Machinery, Inc. Reprinted by permission.

6.1 Motivation

Motor disorder symptoms such as tremor, bradykinesia (slow movement), postural instability, and gait disturbances (such as freezing, where the patient cannot complete a desired movement) can be alleviated with drug treatments or deep brain stimulation (DBS); however, these treatments need to be appropriately adjusted over time. Monitoring the disease severity during intermittent physician visits for this purpose is notoriously imprecise. Mobile, continuous monitoring of the severity of parkinsonism in these patients could therefore significantly improve the patient's health and quality of life.

Current mobile monitoring systems typically only consider tremor [60, 72], or are designed to be used under supervision while the patient performs scripted movements, such as the Timed Up and Go (TUG) test [11], or finger tapping exercises. While these devices can be useful, they do not allow continuous long-term monitoring of patient symptoms during normal daily routines, nor do they evaluate the brain electrophysiologic aspects of their condition.

Based on our previously discussed successful results detecting stages of parkinsonism with high accuracy in EEG data from monkeys, we hypothesized that it might be possible to detect similar patterns in ambulatory human EEGs collected periodically

during home health care visits. If so, the EEG readings could be used together with continuous gyroscope and accelerometer movement measurements to allow improved management of Parkinson’s disease (PD) treatments.

In order to enable investigation of the hypothesis that such a system could improve PD treatments, we proposed and built a system for portable monitoring of PD in humans using EEG signal features and movement signals from gyroscopes and accelerometers. While the former is useful for staging the severity of PD under controlled conditions in the context of clinical neuroprotection trials, the latter will allow monitoring of treatment response fluctuations in patients with advanced PD. The system utilizes commercial smartphones, off-the-shelf attachments, and custom-programmed software. A major new goal of the system is to provide continuous monitoring of movement (including spontaneous voluntary movement, as well as involuntary movements such as tremor and dyskinesia), using combined readings from the smartphone gyroscope and accelerometer and the wrist accelerometer. The initial system description was published in [104] and is presented here with only minor changes reflecting updates to the system since publication.

6.2 Background

With the development of ubiquitous small sensors, measuring different types of human movement such as walking, running, and other forms of exercise has become an area of high interest and rapid growth. The interest in measuring human movement has spilled over into medical application development with a few recent attempts at detecting and measuring movement abnormalities.

One standard test for mobility and motor function in PD patients is the Timed Up and Go test (TUG). The TUG test measures the time a person takes to rise from a chair, walk three meters, turn around, walk back to the chair, and sit down. Although the test is simple, it enables measurement of both static and dynamic

movement, and was shown to give consistent results among trials for each individual. Analysis of motion during TUG testing has been demonstrated previously [103, 15, 57, 93, 51]. Typical methods for analyzing the different time phases of the TUG test include Hidden Markov models [93] and Dynamic Time Warping [3]. Recently, a few algorithms [11, 116] have been developed that allow instrumentation of the TUG test using inertial sensors similar to those available in many smartphones.

Tremor assessment applications (apps) [60, 72] are another recent development of interest for smartphone PD evaluation. These apps typically use existing seismic measurement applications to estimate tremor magnitude from smartphone accelerometer readings. For example, assessment of tremor at rest using smartphone accelerometers has been accomplished with iSeismo by ObjectGraph LLC which uses the iPhone accelerometer to measure movement in the X, Y, and Z axes relative to the device. Although limited in scope, tremor estimates using these measures have been shown to be similar in quality to laboratory EMG tremor assessments [47].

Despite these recent developments, none of the current approaches allow the type of comprehensive mobile monitoring possible with our prototype system. Our prototype combines limb tremor assessment with unsupervised trunk motor sign detection and EEG monitoring in a mobile, wireless system.

Controlling PD symptoms is difficult, particularly in patients 5-10 years or more post diagnosis. Our approach for monitoring allows long-term assessment of symptoms in an environment that is convenient and accessible for the patient. It provides valuable information needed by physicians to diagnose PD and optimize patient treatment protocols, thereby improving the quality of life for patients, and reducing the likelihood of subsequent hospitalizations due to improperly adjusted medication and/or patient falls.

6.3 Methods

6.3.1 Overview

The prototype system, known as the PD-3, includes a Samsung Galaxy S3 smartphone, an EZ430-Chronos watch with tri-axial accelerometer, and a 14-channel Epoc Emotiv EEG headset (system shown conceptually in the following figure and discussed in detail in [4]). The smartphone and watch are controlled and interfaced over a secure RF link via two Java apps running on the Samsung Galaxy S3, where the sensor data is collected and stored for later download. I created the watch-smartphone interface and watch data collection app from scratch, and modified an existing app [129] to collect the smartphone sensor data in parallel. The EEG data collection is currently performed via a wireless link to a laptop. The smartphone and watch data can be downloaded from the smartphone wirelessly, by direct connection, or through transfer from the memory card for off-line analysis. Performance results for detection of tremor and trunk motor signs (bradykinesia, freezing, and postural instability) are reported in the following chapter. Note that additional sensors can be added to the system with modifications to the software apps.

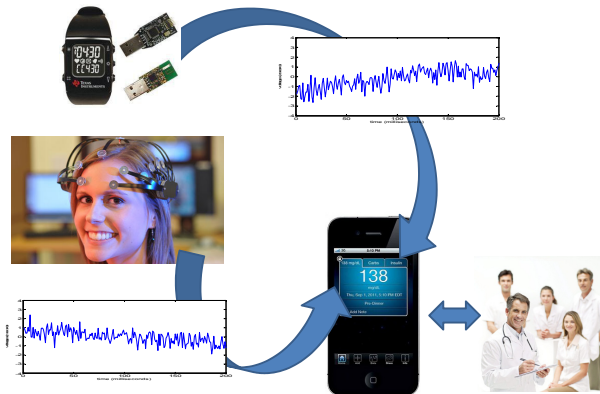


Figure 28: Target system: smartphone with accelerometer and gyroscope, wrist watch with accelerometer, and EEG headset

The system components and their roles in PD monitoring are as follows:

Samsung Galaxy 3: The smartphone accelerometer and gyroscope measure tri-axial acceleration and angular rotation, respectively.

EZ430-Chronos watch: The wristwatch contains a tri-axial accelerometer capable of measuring x, y, and z limb acceleration.

Software: The watch and smartphone were programmed in Java/XML using the Eclipse development tools. Detailed analysis software was implemented in MATLAB.

Emotiv EEG Headset: The EEG PD scores, calculated as described in the following, will be combined with the motor PD estimates on the download computer and compared to physician PD ratings for accuracy.

6.3.2 Data Collection

The initial electrode signals for analysis were the closest EPOC electrodes to the standard International 10-20 defined “C3 - A2” and “C4 - A1” (see Figure 29) since these correspond to the electrode recording locations in the available clinical comparison data and are the electrodes located closest to M1. The EEG signals were captured at a sample rate of 128 Hz using a laptop computer with wireless adapter.

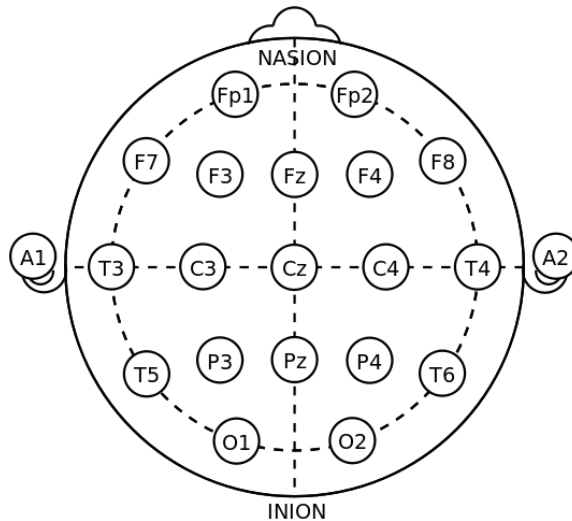


Figure 29: International 10-20 electrode configuration. Note the locations of A1, A2, C3, and C4.

The wristwatch and smartphone accelerometer outputs are of the form \ddot{x} , \ddot{y} , and \ddot{z} , while the smartphone gyroscopes provide measures of yaw, pitch, and roll ($\dot{\theta}_x$, $\dot{\theta}_y$, $\dot{\theta}_z$). Data from the watch is sent to the smartphone using a 915 MHz RF link. The smartphone software stores the accelerometer and gyroscope readings from its own sensors, along with the accelerometer samples from the wristwatch, for later download and processing either at a local computer or remote location.

6.3.3 EEG Analysis

6.3.4 Complex Continuous Wavelet Transform

In the work with non-human primates described in Section 4.4, composite signals from the delta (3-4 Hz), theta (5-7 Hz), alpha (8-11 Hz), low beta (12-19 Hz), high beta (20-30 Hz), and gamma bands (31-60 Hz) were constructed. Based on the analysis of the human EEG data (and since the EEG sampling rate is 100 Hz for the clinical data; 128 Hz for the EPOC data), the initial frequency delineations for the 14 channel EEG data analysis were slightly modified as follows: low delta (2-3 Hz), high delta (3-4 Hz), theta (4-12 Hz), low beta (12-16 Hz), high beta (16-30 Hz), and gamma (30-50 Hz). The upper limit on the bands is reduced to 50 Hz to ensure all frequencies fall within the bounds dictated by the Nyquist sampling rate, while the combination of the theta and alpha band into a new theta band was chosen based on recent results showing important modulated activity in this 4-12 Hz band for other cortical signals associated with deep brain activity [62, 100]. CFC MIs were extracted from EEGs as described in the methods in Section 4.4.2. The MI features were used to stage the PD using the approach in Section 4.5.

6.3.5 Motor Data Analysis

The motor signs obtained by visual inspection in animal models and human patients can be estimated with gyroscopic and accelerometer measurement approaches. Our assessment of tremor at rest using the wristwatch accelerometer data is based on the

approach taken in [47]. Our non-scripted trunk motion analysis uses a hierarchical approach. The activity type is determined first, then activity-dependent trunk motor data analysis for obtaining measures of bradykinesia, angle of stoop, gait smoothness, and freezing subscores is performed using a single fixed body sensor approach [116].

Once the limb tremor, bradykinesia, angle of stoop, gait smoothness, and freezing of the body near the center of mass component measures have been calculated, the PD stage can be assessed using the corresponding motor assessment items from Part III. of the Unified Parkinson's Disease Rating Scale (UPDRS) [45].

6.3.6 Conclusion

The PD-3 systems capability for detailed analysis of multi-day monitoring of unscripted motor activities is expected to be valuable for the success of symptomatic antiparkinsonian treatment, as it may provide detailed and previously unavailable information regarding the timing of treatment response fluctuations throughout the day. The PD-3 analysis will enable physicians to use a data-driven approach for optimizing treatments, and may help physicians confirm initial diagnoses of PD.

In the previous chapters, I have shown that it is possible to accurately assess the severity of parkinsonism using epidural EEGs in monkeys. In future tests with the PD-3 system, we will examine how accurately this information can be estimated with surface electrodes in human patients, and how the EEG analysis can be used with the motor monitoring capabilities to provide a comprehensive, objective measure of the severity of parkinsonism (or the stage of PD) in patients. Human subject testing of the PD-3 motor monitoring capabilities is discussed in the following section.

6.4 Multi-sensor mobile monitoring human subject study

Recently, it has been shown that data collected from a body-mounted triaxial accelerometer can be useful for evaluating whether or not a patient has Parkinson's disease (PD) when the patient's movement activity type is known [10]. In this work, we considered whether multiple triaxial sensors can improve the ability to discriminate between normal and simulated parkinsonian movement. We also examined whether discrimination between normal movement and simulated parkinsonism is possible when the the type of activity performed by the subject is unknown.

For this study, ten subjects with no known motor disorders were instrumented with a wireless monitoring system consisting of a trunk-mounted smartphone with accelerometer and gyroscope, and a wristwatch with accelerometer. Data from the accelerometers and gyroscope were collected while the subjects moved normally during resting, sitting, rising, walking, and turning. Data was also collected as these subjects performed the same movements while simulating the motor signs of PD. The aims were to: 1) quantify the advantages, if any, of using multi-modal monitoring to detect simulated signs of PD, and 2) determine if the simulated PD signs could be assessed without prior knowledge of an individual's activity type.

We showed that multiple sensors on different body locations allowed more accurate classification of simulated PD than any of the single sensors tested. The wristwatch sensor data allowed accurate detection of simulated limb tremor while the sensors in the body mounted smartphone allowed detection of other simulated PD signs. We also showed that simulated PD signs can be classified without prior knowledge of which activity is occurring, by first using the motor data to classify the activity type and then applying the appropriate PD classification approach for that activity type.

6.4.1 Introduction

A single accelerometer on the trunk can be used to detect PD signs during scripted movements such as the TUG test [11, 116]. However, the classification rate shown in most such studies is less than 85%, even with ground truth knowledge of the timing and type of each patient’s movements [11]. In order for unsupervised remote mobile monitoring to be possible, the pathology of movement must be assessed without prior knowledge of the patient’s activity pattern. Thus, in many cases, it will be necessary to classify both movement type and any corresponding pathology. For this study, our approach was to use the hierarchical classification scheme shown in Figure 30. In this approach, the activity type is classified first, followed by the parkinsonism motor sign classification, and finally the total PD score based on the motor components.

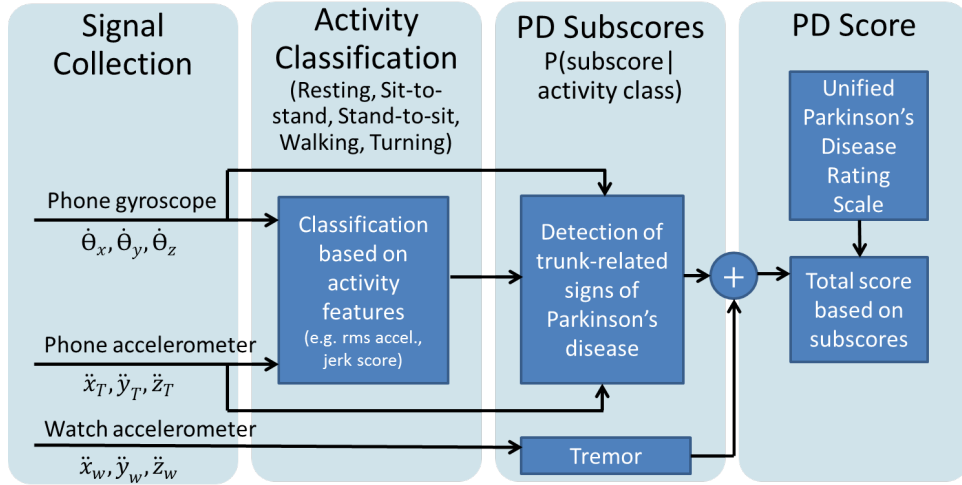


Figure 30: Obtaining the PD score from the motor signals

In previous work, motor signal features such as duration of movement, root-mean-square (rms) acceleration, normalized jerk score, and step duration statistics (mean, standard deviation, and coefficient of variation (CV) were used to assess PD with single accelerometers [93, 11, 116]. For this study, in order to keep the dimensionality at a manageable level, features that preserve the essence of the best performing measures in previous studies were used. After visual inspection of the signals, one

new feature was selected (average number of zero crossings). The motor features used were then as follows: rms of the signal, jerk scores, and statistics related to the maxima, minima, and zero crossings of the x, y, and z components of the gyroscope and accelerometer signals.

6.4.2 Methods

6.4.2.1 *Subjects and Experimental Setup*

Ten subjects ranging in age from 20-75 years of age were examined in this study (6 females and 4 males). None of the subjects had been diagnosed with motor disorders. The subjects were instrumented with PD-3 remote monitoring system [106] components consisting of a belt mounted Samsung Galaxy S3 smartphone and a TI EZ430-Chronos watch. The smartphone was positioned such that the positive x-axis pointed up, the positive y-axis pointed to the subject's right, and the positive z-axis pointed in the forward direction of motion. The accelerations were aligned with these directions, and the gyroscope measures (angular rates) were rotations about these axes.

The subjects were instructed to sit for one minute, then stand up and sit down at a comfortable rate for approximately two minutes, followed by two additional minutes walking across the room, turning and walking back repeatedly, again at a comfortable rate. After completing this five minute task, the subjects were given a summary sheet explaining the following signs of parkinsonism: 4-7 Hz tremor, bradykinesia, postural instability, and freezing. They were then asked to repeat the five minute motor task with simulated parkinsonian movement. They were not told how many times to repeat the activity, or how severely to simulate the symptoms. For this study, the repeated sit-to-stand and stand-to-sit movements were referred to as the 'STS' activity type, while walking with turns was called the 'WWT' activity type.

6.4.2.2 Data collection

The data for each sensor was collected with the default sampling rate for each device. The wristwatch accelerometer data was collected at 30 Hz, the smartphone accelerometer at 100 Hz and the smartphone gyroscope at 200 Hz. The motor sensors were all tri-axial. The wristwatch data was sent wirelessly in realtime to the smartphone across an RF datalink. The smartphone and wristwatch data were collected using two custom-built apps running in parallel on the smartphone, allowing the data sampling to be synchronized to the same clock. Figure 31 shows two examples of the smartphone accelerometer output. The top example shows the output for normal movement while the bottom example shows the output for simulated parkinsonism. Similarly, Figure 32 shows the gyroscope output for normal (top) and parkinsonian movement (bottom).

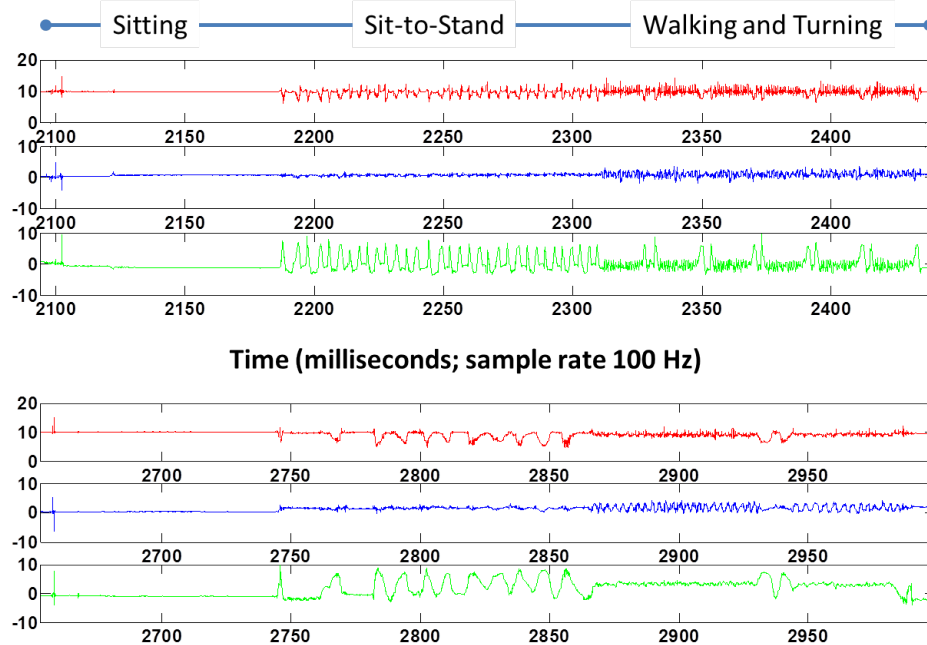


Figure 31: Smartphone accelerometer output. Red, green, and blue lines indicate the x-, y-, and z- accelerations. Top plot shows normal movement. Bottom plot shows simulated parkinsonism.

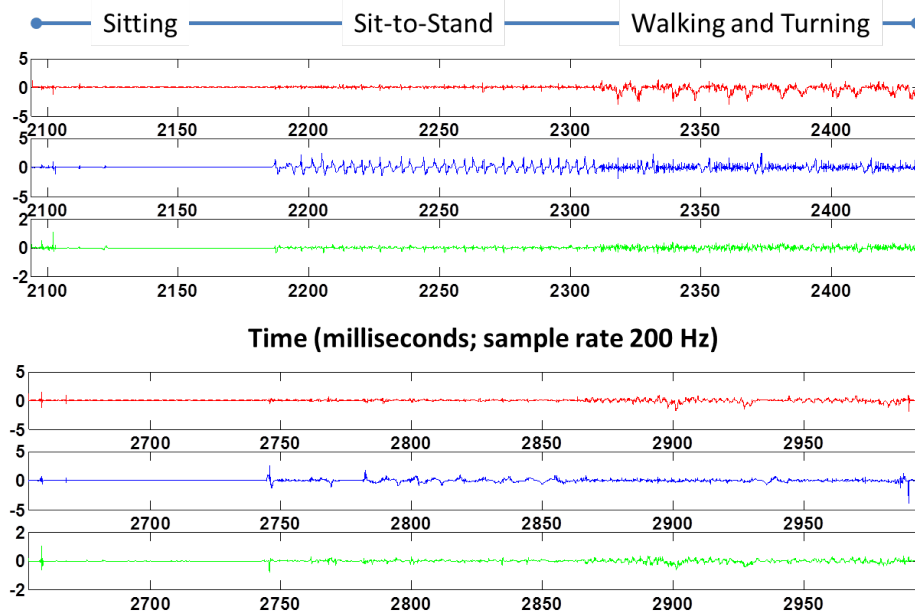


Figure 32: Smartphone gyroscope output. Red, green, and blue lines indicate the angular velocities around the x-, y-, and z-axes. Top plot shows normal movement. Bottom plot shows simulated parkinsonism.

6.4.2.3 Signal Processing

For the watch, the x, y, and z accelerometer signals were passed through bandpass filters to detect oscillations in the nominal parkinsonian tremor frequency band (4-7 Hz). Any oscillations in the expected frequency band greater than twice the average magnitude of the non-tremor baseline were classified as tremor occurrences [56].

For each of the smartphone motor signals, minima, maxima, and zero crossings were identified. Then the measures shown in Figure 33 were calculated as follows:

- 1) The root-mean-square (rms) value of the signal,

$$S_{rms} = \sqrt{\frac{1}{n} \sum_{i=1}^n (s_i - \bar{s})^2}$$

where n is the number of signal samples

\bar{s} is the mean of the s_i and

s_i are the individual signal samples

(from the accelerometer (or gyroscope) x, y, or z signal)

		Features with statistically significant predictive power:		
Measure		Sit-to-stand/ Stand-to-sit (STS)	Walking with Turns (WWT)	Resting
Accelerometer	rms Acceleration	-	-	-
	Positive $\Delta/\Delta t$ accel. (+ Jerk Score)	X***, Z**	-	-
	Negative $\Delta/\Delta t$ accel. (- Jerk Score)	-	-	-
	Number of zero crossings	-	Y****	-
	Mean of maxima magnitudes	-	-	Y*
	Standard Deviation of maxima	Y*	-	-
	Number of maxima	Y*	Y***	-
	Mean of minima magnitudes	Z**	-	-
	Standard Deviation of minima	Y*	-	-
	Number of minima	-	Y****, Z**	-
Gyroscope	rms Gyroscope	Y**	X****, Y**	-
	Positive $\Delta/\Delta t$ angular velocity (+ angular acc.)	-	-	-
	Negative $\Delta/\Delta t$ angular velocity (- angular acc.)	-	-	-
	Number of zero crossings	-	-	X*, Y*
	Mean of maxima magnitudes	-	Z*	X*
	Standard Deviation of maxima	-	-	-
	Number of maxima	Y**	-	-
	Mean of minima magnitudes	-	-	-
	Standard Deviation of minima	-	-	-
	Number of minima	Y***	X**	-

Figure 33: Smartphone accelerometer and gyroscope features with statistically significant discriminative power ($p < 0.05$, ** $p < 0.01$, *** $p < 0.001$, **** $p < 0.0001$)*

For the remaining calculations, subtraction of the mean signal is implied.

2) The positive jerk score (accelerometer), or angular acceleration (gyroscope)

$$J^+ = \frac{1}{m} \sum_{i=1}^m \frac{|s_{max}(i)|}{time(s_{max}(i)) - time(s_{zero}(i-))}$$

where m is the number of local maxima in the signal,

$|s_{max}(i)|$ is the magnitude of the i th maximum,

$time(s_{max}(i))$ is the time when the i th maximum occurred and

$time(s_{zero}(i-))$, the time of the zero crossing

before the i th maximum

3) The negative jerk score (accelerometer), or angular acceleration (gyroscope)

$$J^- = \frac{1}{k} \sum_{i=1}^k \frac{|s_{min}(i)|}{time(s_{min}(i)) - time(s_{zero}(i-))}$$

where k is the number of local minima in the signal,

$|s_{min}(i)|$ is the magnitude of the i th minimum,

$time(s_{min}(i))$ is the time when the i th minimum occurred and

$time(s_{zero}(i-))$, the time of the zero crossing

before the i th minimum

4) The number of zero crossings,

$$N_{zero} = \sum_{i=1}^n 1_{zero}(s_i)$$

where $1_{zero} = 1$ when $s_i = 0$, and $1_{zero} = 0$ otherwise

5-7) The mean, $\overline{s_{max}}$, standard deviation, σ_{max} , and number, N_{max} , of **maxima**

8-10) The mean, $\overline{s_{min}}$, standard deviation, σ_{min} , and number, N_{min} , of **minima**

6.4.2.4 Smartphone signal feature selection and classification

ANOVA was applied to a training sample of the data to determine the statistically significant features for each of the two classification tasks (activity type classification and normal versus PD classification). The results of this analysis for classification between normal and parkinsonian movement are discussed in the following section, and summarized in Figure 33. The most statistically significant features were then extracted from the full dataset for the subsequent analysis. The classification performance results were calculated using linear discriminant analysis (LDA) with 5-fold cross-validation.

6.4.3 Results

6.4.3.1 Classification of PD for each movement category

As shown in Figure 33, the features with the most statistically significant differences based on the ANOVA analysis for the normal versus PD classification were 1) for the Sit-to-stand and stand-to-sit, the X (vertical) positive jerk score and the number of angular velocity (gyroscope) minima for the signal about the Y (medial/lateral) axis and 2) for walking with turns, the number of zero crossings and the number of minima for the Y acceleration signal, and the rms angular velocity about the X axis. For the resting condition, none of the features showed high statistical significance, although the mean magnitude of the Y acceleration maxima, the zero crossings in the angular velocity about the X and Y axis, and the mean magnitude of the angular velocity maxima about the X axis showed slight statistically significant differences between the normal and PD datasets.

Figure 34 shows the results of the LDA 5-fold cross-validation performance testing for discrimination between the normal and parkinsonian state using these most

statistically significant features. The first group of bars shows the discrimination performance when the data is not sorted by activity type (< 0.7 correct discrimination), the following three groups of bars show the normal versus PD discrimination when the data is split into the rest, STS, and WWT movement types, and the best features for each activity type are used. Note that, although the accelerometer features allowed the best discrimination for two of the activity types, the combination of the gyroscope and accelerometer features allowed much better discrimination than the accelerometer for the WWT activity type.

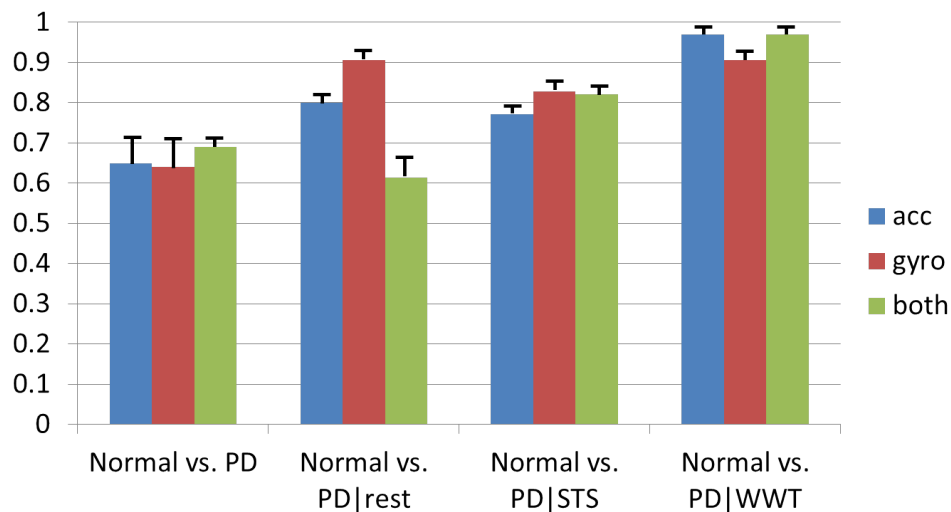


Figure 34: Classification of normal and parkinsonian state based on trunk sensors. The leftmost set of bars shows the discrimination performance when the underlying activity type is unknown. The following 3 sets of bars show the discrimination performance conditioned on the activity type.

6.4.3.2 Classification of activity types

As previously discussed, there were three activity types classified in this study (rest, STS, and WWT). After selecting features using the ANOVA analysis for the three activities, and calculating the LDA 5-fold cross-validation performance, the best 3-way activity discrimination was 0.91 as shown in Figure 35. However, by performing the classification with a hierarchical approach in which rest versus movement was classified first, followed by STS versus WWT, the classification performance increased

to 1.0. The most statistically significant features for discriminating between the training sets for the STS and the WWT were the zero crossings of the signals. For the accelerometer, the X and Z signal zero crossings were the most statistically significant. For the gyroscope, the zero crossings of the angular velocity signal about the X and Y axis ranked highest, along with the X angular velocity rms and number of minima.

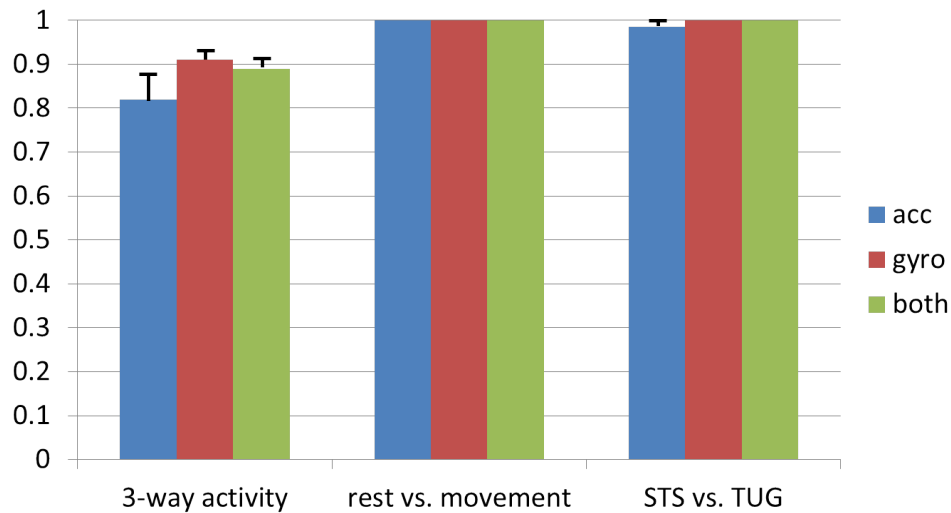


Figure 35: Classification of activity types. Note that a hierarchical classification of rest vs. movement (2nd set of bars) followed by STS vs. WWT (3rd set of bars) gave better results than the 3-way classification of movement (1st set of bars).

6.4.3.3 Hierarchical classification

The classification approach shown in Figure 30, combined with the hierarchical activity type discrimination described in the previous section, allowed better classification than simple discrimination between the normal versus parkinsonian data. The average correct discrimination using this approach was 0.88 as compared to < 0.7 when the data was classified with no regard for the underlying activity type.

6.4.3.4 Tremor Classification

The only parkinsonism sign simulated by the subjects during the resting activity was tremor. The low statistical significance of the features (see Figure 33) and the poor discrimination between the normal and parkinsonian data during rest (≤ 0.78) indicate that the trunk-mounted sensors were not particularly effective for tremor detection. However, as can be seen in Figure 36, tremor classification using the watch accelerometer data was straightforward. In fact, for our simulated data, all tremor data samples were detected. Thus, the tremor classification performance was 1.0.

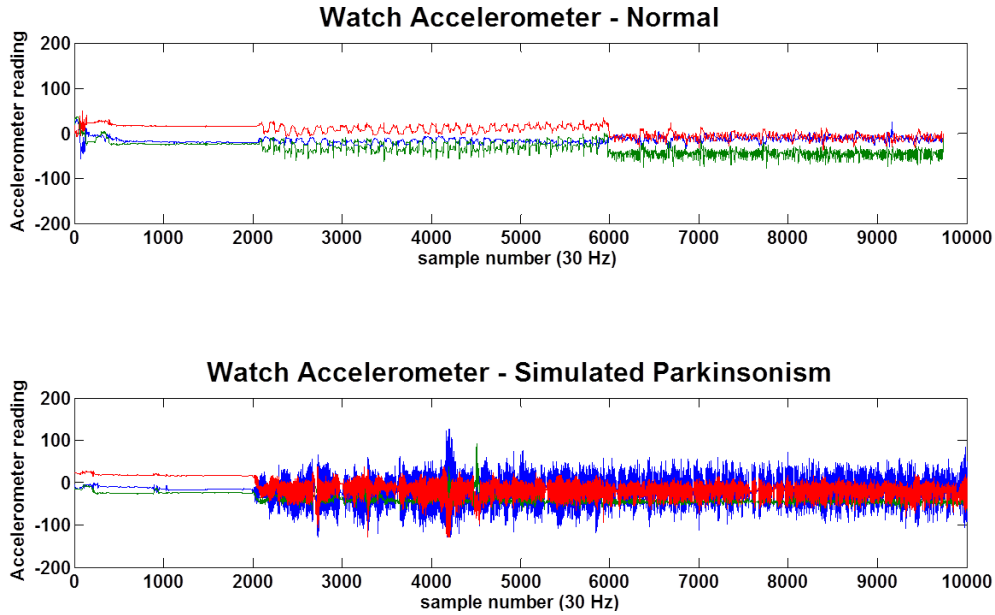


Figure 36: Watch accelerometer output. Note that the sit-to-stand (middle of top plot) and walking-with-turns (right of top plot) activities are visible in the normal (top) accelerometer trace.

6.4.4 Discussion

We had originally hoped to perform this analysis with data from PD patients and controls. However, in retrospect, performing the study with simulated parkinsonism allowed us to better capture the signature of the major signs due to their being repeated multiple times by the subjects. It was also helpful that we knew the types of signs the subjects were simulating, and that we had perfect control data since

each subject served as their own control. How accurately our simulated parkinsonism reflects actual parkinsonism will be considered in future studies.

It was interesting to note the different characteristics of the simulated tremors. All subjects were able to simulate tremor in the desired frequency range, although the spectral peaks varied between individuals (see Figure 37). Some maintained a consistent tremor frequency as shown at left, while others tended to vary the tremor frequency as shown at right. In this study, we wanted to see which axis of movement

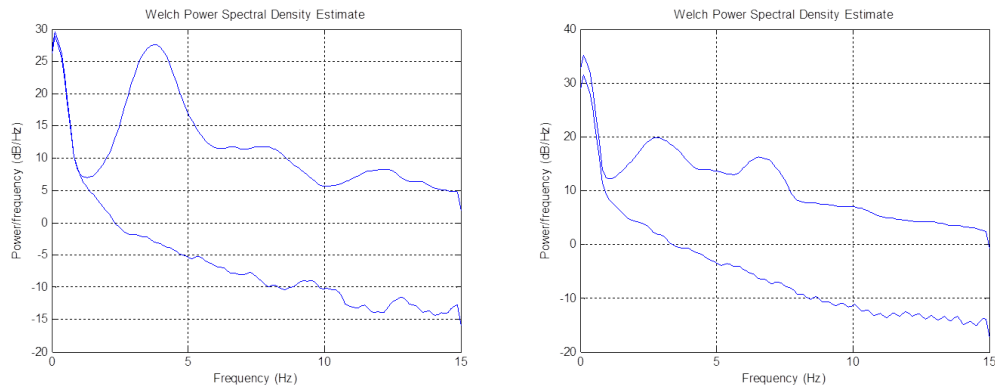


Figure 37: Spectra from the watch accelerometer for two individuals (left and right). For each graph, the upper signal was captured during simulated tremors while the lower signal was captured during the normal movement sequences.

best predicted the different activity types and parkinsonian signatures, so the x, y, and z signals were all considered separately. However, in some cases, the magnitude of the signal may be more useful than the individual x, y, z component scores for discrimination.

Although we did not attempt to analyze the individual signs of parkinsonism in detail in this study, we found that tremor was easy to identify, and it was generally assumed that most of the movements recorded with the trunk sensors were related to bradykinesia. The main reason for the latter assumption was that this was the most consistently simulated (non-tremor) sign. A larger dataset will be needed to determine the characteristics most representative of freezing and postural instability.

The approach shown in Figure 30 indicates that PD subscores and scores will be

assigned based on the signal processing analysis. The subscores and scores were not assigned in this study since we did not have a way to assess their accuracy. However, tremor and trunk symptom subscores could have been calculated based on the distances between the datapoints and the tremor and LDA thresholds, respectively.

6.4.5 Discussion and Conclusions

6.4.5.1 *Advantages of using multi-modal monitoring to evaluate PD signs*

The discrimination accuracy between normal and simulated parkinsonian movement using data from the trunk mounted accelerometer alone was 0.65 when no activity type classification was used. When activity type classification was used prior to discrimination between normal and parkinsonian movement, the discrimination performance increased to 0.78. However, when data from the gyroscope and the two accelerometers were considered, the discrimination accuracy increased to 0.88 when tremor was not present, and to 1.0 when tremor was present. Thus, we have shown that using data from a gyroscope and multiple distributed accelerometers improved the discrimination between normal and simulated parkinsonian movement for subjects performing three different activity types. In particular, since tremor was only poorly detected with the trunk mounted sensors, the wristwatch accelerometers were needed to effectively evaluate this sign. Additionally, the gyroscope sensor data was helpful for detecting parkinsonism during the WWT activity type, and for discriminating between the STS and WWT activity types.

6.4.5.2 *Assessing PD without prior knowledge of movement type*

Discrimination between the normal and simulated parkinsonism data was < 0.7 when attempting to directly classify the two types of data without regard for the underlying activity. However, in our study, it was possible to identify activity types from the accelerometer and gyroscope data with high accuracy (1.0). When the activity type was identified first, it was then possible to discriminate between the two data types

correctly in 0.88 of the data samples.

In our simulated study, there were advantages that would not exist in completely free motion in PD patients. Our study had the advantage of knowing that the activity type was limited to three possibilities. Additionally, multiple repetitions of the activity types provided excellent training data that may not be possible to collect in clinical situations with patients. It is also possible that unintentional biases existed in the data due to the non-blinded nature of the study.

In future studies we plan to test this approach with a larger dataset collected from PD patients and age-matched controls. We will then examine whether the methods in this study can be successfully used to help evaluate clinical cases of parkinsonism. In addition to testing the effectiveness of the methods, the larger dataset will allow consideration of a wider variety of activity types and parkinsonism signs.

6.5 EEG assessment of PD in humans

Chapters 4 and 5 of this work have shown that it is possible to assess the severity of parkinsonism using epidural EEGs in nonhuman primates. With the PD monitoring system, it will be possible to examine whether the assessment of parkinsonism is also possible using surface EEGs in human patients, and whether EEG analysis could be developed into a tool to provide an objective measure of the severity of parkinsonism (or the stage of PD) in patients. A particularly important aspect of the assessment plan was to document the timing and dosing of medications when the EEG signals are collected, as these parameters may influence EEG signals independent of the state of the disease. I am working on collaborations that will enable this type of pre-clinical testing using the system. The target EEG analysis system may eventually help physicians to confirm a diagnosis of PD, and to develop a more objective approach for staging the disease. While this may not be as relevant in the routine care of individual patients, the ability to objectively stage the severity of PD is a highly

important ingredient of neuroprotective clinical trials.

Preliminary analysis of EEG data collected in control subjects during the motor sensor study in Section 6.4 indicated that EEG data may be useful for discriminating between activity types, in addition to potentially staging PD. As shown in Figure 38, using cross-frequency-coupling (CFC) features, three different activity types can be visually separated for a single individual. Figure 39 shows the same three activity types can be observed in CFC features from three different individuals. Although more in-depth analysis is needed to determine how accurately these activity types can be classified across multiple individuals, the initial data suggest that the EEG features may be useful for incorporation in the activity type classification described in Section 6.4.2. Further, knowledge of the appearance of typical EEG patterns for these activity types will be important to consider for neurological disease staging, since any motor pathology assessment should be made relative to the expected baseline features for the underlying activity type. This can be thought of as artifact removal. However, for the multimodal monitoring approach, movement information related to the activity type will not necessarily be removed, but rather be used to evaluate the pathological state conditioned on the activity type ($P(\textit{pathology} \mid \textit{activity type})$).

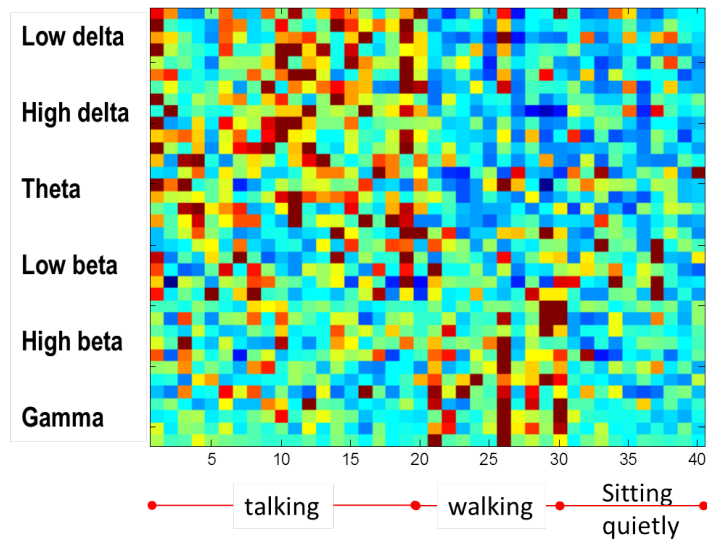


Figure 38: EEG CFC features for a single individual talking, then walking, and finally sitting quietly. Each column represents a 30 second epoch of data.

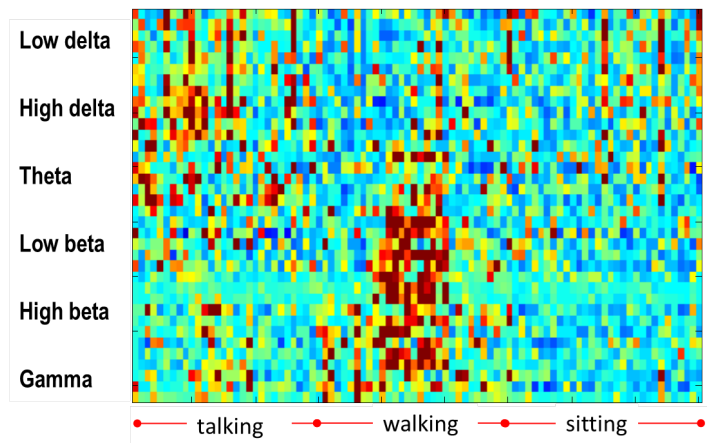


Figure 39: EEG CFC features for three different individuals. The first segment of talking is from individual one, immediately followed by the segments for individual two and three. The data is concatenated the same way for the walking and sitting activities. Each column represents a 30 second epoch of data. The data is z-scored to common μ and σ values for all three individuals.

CHAPTER VII

CONCLUSION

The work presented in this dissertation builds upon established features and methods for signal processing of spike times, EEGs, and local field potentials (LFPs). Previous methods for detecting parkinsonism with electrophysiological data rely on metrics such as firing rate, spectral power and variance within specific frequency bands. In short, previous approaches typically use a single feature or set of related features and assume the features are linearly related to the degree of parkinsonism. The main emphasis in this dissertation is on multiple, optimally selected features that may exhibit non-linear dynamics. The goal of Chapters 3 and 4 was to show that optimally selected features based on basal ganglia electrophysiology can indicate the degree of parkinsonism and that the progression can take similar forms across individuals. In Chapter 5, the goal was to quantify relationships between parkinsonian motor signs and subthalamic nucleus and cortical electrophysiology. In Chapter 6, a step is taken toward translational implementation of these new findings by building and testing a mobile monitoring system for PD.

7.1 Importance of multiple, optimally-selected, non-redundant features.

An approach for selecting optimal, multiple features for characterizing cellular firing and identifying the features most relevant for distinguishing between cells recorded in the parkinsonian versus non-parkinsonian state was presented in Chapter 3. Cells from the subthalamic nucleus (STN) and globus pallidus externa (GPe) and interna (GPi) were examined. Although increased bursting occurred in all three nuclei, the observed changes differed between the STN and the two pallidal segments. Using

multiple feature selection methods tested against a set of neuronal discharge features from three basal ganglia regions, we found the sets of features that most effectively discriminated the neuron activity in the parkinsonian and normal states differed between the STN and the two segments of the globus pallidus. Although bursting features were important for characterizing all three nuclei, the results showed that using any one feature of single cell firing to characterize the parkinsonian state in all nodes of the basal ganglia-thalamocortical network was less accurate than an analysis of multiple nucleus-specific descriptors.

Chapters 4 and 5 discuss features that best discriminate between baseline conditions and parkinsonism in STN LFPs and cortical EEGs. Novel methods were developed for analyzing stimulus-independent oscillation interactions based on phase-amplitude cross-frequency-coupling (CFC) features extracted from Complex Continuous Wavelet Transform (CCWT) coefficients.

7.2 Correlation between motor signs and electrophysiology

Canonical correlation was used to show statistically significant correlation between different weighted sets of these features and the composite motor score as well as bradykinesia, balance, and freezing motor subscores. The analysis showed that phase-amplitude CFCs in STN LFPs and epidural EEGs provide valuable information in the form of characterization of the overall state of the recorded brain area as well as uncovering significant correlation between features in the two brain regions. The CCWT CFC features were shown to be similar across individuals, and superior to standard statistical features for classifying the severity of PD. Based on this work, we believe that phase-amplitude CFCs (also known as modulation indices) are useful for characterizing the progression of parkinsonism, and that the characterization may be generalizable across multiple individuals.

7.3 Multimodal monitoring technology.

Chapter 6 presented a multi-modal monitoring system for assessing movement disorders, known as the PD-3. The system is currently specifically targeted to parkinsonism and uses the electrophysiologic features described in Chapter 5, along with motor features from wearable accelerometers and a gyroscope. In human subject testing, we analyzed which motor sensors and features provided the most statistically significant classification between activity types and parkinsonian movement. We found that multiple sensors on different body locations allowed more accurate classification of simulated parkinsonism than single sensors. We also showed that parkinsonism signs can be classified without prior knowledge of which activity is occurring, by first using the motor data to classify the activity type and then applying the appropriate classification approach for that activity type.

REFERENCES

- [1] ABOSCH, A., LANCTIN, D., ONARAN, I., EBERLY, L., SPANIOL, M., and INCE, N. F., “Long-term recordings of local field potentials from implanted deep brain stimulation electrodes,” *Neurosurgery*, vol. 71, no. 4, pp. 804–814, 2012.
- [2] ADACHI, M., HOSOYA, T., HAKU, T., YAMAGUCHI, K., and KAWANAMI, T., “Evaluation of the substantia nigra in patients with Parkinsonian syndrome accomplished using multishot diffusion-weighted MR imaging,” *American Journal of Neuroradiology*, vol. 20, no. 8, pp. 1500–1506, 1999.
- [3] ADAME, M. R., AL-JAWAD, A., ROMANOVAS, M., HOBERT, M. A., MAETZLER, W., MOLLER, K., and MANOLI, Y., “TUG test instrumentation for Parkinson’s disease patients using inertial sensors and dynamic time warping,” *Biomed Tech (Berl)*, 2012.
- [4] ALBIN, R., YOUNG, A., and PENNEY, J., “The functional anatomy of basal ganglia disorders,” *Trends in Neurosciences*, vol. 12, no. 10, pp. 366–375, 1989.
- [5] BARON, M., WICHMANN, T., MA, D., and DELONG, M., “Effects of transient focal inactivation of the basal ganglia in parkinsonian primates,” *The Journal of Neuroscience*, vol. 22, no. 2, pp. 592–599, 2002.
- [6] BARRAUD, Q., LAMBRECQ, V., FORNI, C., MCGUIRE, S., HILL, M., BILOULAC, B., BALZAMO, E., BEZARD, E., TISON, F., and GHORAYEB, I., “Sleep disorders in Parkinson’s disease: the contribution of the MPTP non-human primate model,” *Experimental Neurology*, vol. 219, no. 2, pp. 574–582, 2009.
- [7] BELLUSCIO, M. A., MIZUSEKI, K., SCHMIDT, R., KEMPTER, R., and BUZSAKI, G., “Cross-frequency phase-phase coupling between theta and gamma oscillations in the hippocampus,” *J Neurosci*, vol. 32, no. 2, pp. 423–35, 2012.
- [8] BERGMAN, H., WICHMANN, T., KARMON, B., and DELONG, M., “The primate subthalamic nucleus. II. Neuronal activity in the MPTP model of parkinsonism,” *Journal of neurophysiology*, vol. 72, no. 2, pp. 507–520, 1994.
- [9] BERGMAN, H., WICHMANN, T., KARMON, B., and DELONG, M., “The primate subthalamic nucleus. ii. neuronal activity in the mptp model of parkinsonism,” *Journal of neurophysiology*, vol. 72, no. 2, pp. 507–520, 1994.

- [10] BREIT, S., BOUALI-BENAZZOUZ, R., POPA, R., GASSER, T., BENABID, A., and BENAZZOUZ, A., “Effects of 6-hydroxydopamine-induced severe or partial lesion of the nigrostriatal pathway on the neuronal activity of pallido-subthalamic network in the rat,” *Experimental Neurology*, vol. 205, no. 1, pp. 36–47, 2007.
- [11] BREWER, B. R., PRADHAN, S., CARVELL, G., and DELITTO, A., “Application of modified regression techniques to a quantitative assessment for the motor signs of Parkinson’s disease,” *Neural Systems and Rehabilitation Engineering, IEEE Transactions on*, vol. 17, no. 6, pp. 568–575, 2009.
- [12] BRONSTEIN, J. M., TAGLIATI, M., ALTERMAN, R. L., LOZANO, A. M., VOLKMANN, J., STEFANI, A., HORAK, F. B., OKUN, M. S., FOOTE, K. D., KRACK, P., PAHWA, R., HENDERSON, J. M., HARIZ, M. I., BAKAY, R. A., REZAI, A., MARKS, W. J., J., MORO, E., VITEK, J. L., WEAVER, F. M., GROSS, R. E., and DELONG, M. R., “Deep brain stimulation for Parkinson disease: an expert consensus and review of key issues,” *Arch Neurol*, vol. 68, no. 2, p. 165, 2011.
- [13] BROWN, E., KASS, R., and MITRA, P., “Multiple neural spike train data analysis: state-of-the-art and future challenges,” *Nature Neuroscience*, vol. 7, no. 5, pp. 456–461, 2004.
- [14] BROWN, P., OLIVIERO, A., MAZZONE, P., INSOLA, A., TONALI, P., and DI LAZZARO, V., “Dopamine dependency of oscillations between subthalamic nucleus and pallidum in Parkinson’s disease,” *The Journal of Neuroscience*, vol. 21, no. 3, pp. 1033–1038, 2001.
- [15] BRUSSE, K., ZIMDARS, S., ZALEWSKI, K., and STEFFEN, T., “Testing functional performance in people with Parkinson disease,” *Physical therapy*, vol. 85, no. 2, pp. 134–141, 2005.
- [16] BURNS, R. S., CHIUEH, C. C., MARKEY, S. P., EBERT, M. H., JACOBOWITZ, D. M., and KOPIN, I. J., “A primate model of parkinsonism: selective destruction of dopaminergic neurons in the pars compacta of the substantia nigra by n-methyl-4-phenyl-1, 2, 3, 6-tetrahydropyridine,” *Proceedings of the National Academy of Sciences*, vol. 80, no. 14, pp. 4546–4550, 1983.
- [17] CANOLTY, R. T. and KNIGHT, R. T., “The functional role of cross-frequency coupling,” *Trends Cogn Sci*, vol. 14, no. 11, pp. 506–15, 2010.
- [18] CANOLTY, R., EDWARDS, E., DALAL, S., SOLTANI, M., NAGARAJAN, S., KIRSCH, H., BERGER, M., BARBARO, N., and KNIGHT, R., “High gamma power is phase-locked to theta oscillations in human neocortex,” *science*, vol. 313, no. 5793, pp. 1626–1628, 2006.

- [19] CANOLTY, R. T., CADIEU, C. F., KOEPESELL, K., GANGULY, K., KNIGHT, R. T., and CARMENA, J. M., “Detecting event-related changes of multivariate phase coupling in dynamic brain networks,” *Journal of neurophysiology*, vol. 107, no. 7, pp. 2020–2031, 2012.
- [20] CHANG, C. and LIN, C., “LibSVM: a library for support vector machines,” *ACM Transactions on Intelligent Systems and Technology (TIST)*, vol. 2, no. 3, p. 27, 2011.
- [21] CHEN, Y. and LIN, C., “Combining SVMs with various feature selection strategies,” *Feature Extraction*, pp. 315–324, 2006.
- [22] COMSTOCK, J., “Fitbit study: Uk adults find mobile health tracking, not public messaging, effective,” 2013.
- [23] CROSSMAN, A., CLARKE, C., BOYCE, S., ROBERTSON, R., and SAMBROOK, M., “MPTP-induced parkinsonism in the monkey: neurochemical pathology, complications of treatment and pathophysiological mechanisms,” *The Canadian journal of neurological sciences. Le journal canadien des sciences neurologiques*, vol. 14, no. 3 Suppl, p. 428, 1987.
- [24] CROWELL, A. L., RYAPOLOVA-WEBB, E. S., OSTREM, J. L., GALIFIANAKIS, N. B., SHIMAMOTO, S., LIM, D. A., and STARR, P. A., “Oscillations in sensorimotor cortex in movement disorders: an electrocorticography study,” *Brain*, vol. 135, no. Pt 2, pp. 615–30, 2012.
- [25] CUNNINGHAM, J. P., GILJA, V., RYU, S. I., and SHENOY, K. V., “Methods for estimating neural firing rates, and their application to brain-machine interfaces,” *Neural Networks*, vol. 22, no. 9, pp. 1235–1246, 2009.
- [26] D JOHNSON, M., L VITEK, J., and C MCINTYRE, C., “Pallidal stimulation that improves parkinsonian motor symptoms also modulates neuronal firing patterns in primary motor cortex in the MPTP-treated monkey,” *Experimental neurology*, vol. 219, no. 1, pp. 359–362, 2009.
- [27] DE HEMPTINNE, C., RYAPOLOVA-WEBB, E. S., AIR, E. L., GARCIA, P. A., MILLER, K. J., OJEMANN, J. G., OSTREM, J. L., GALIFIANAKIS, N. B., and STARR, P. A., “Exaggerated phase-amplitude coupling in the primary motor cortex in parkinson disease,” *Proceedings of the National Academy of Sciences*, 2013.
- [28] DE LAU, L. and BRETHER, M., “Epidemiology of Parkinson’s disease,” *The Lancet Neurology*, vol. 5, no. 6, pp. 525–535, 2006.
- [29] DELONG, M., “Primate models of movement disorders of basal ganglia origin,” *Trends in Neurosciences*, vol. 13, no. 7, pp. 281–285, 1990.
- [30] DELONG, M. and WICHMANN, T., “Circuits and circuit disorders of the basal ganglia,” *Archives of Neurology*, vol. 64, no. 1, p. 20, 2007.

- [31] DORVAL, A. D., “Probability distributions of the logarithm of inter-spike intervals yield accurate entropy estimates from small datasets,” *J Neurosci Methods*, vol. 173, no. 1, pp. 129–39, 2008.
- [32] DORVAL, A. D., KUNCEL, A. M., BIRDNO, M. J., TURNER, D. A., and GRILL, W. M., “Deep brain stimulation alleviates parkinsonian bradykinesia by regularizing pallidal activity,” *J Neurophysiol*, vol. 104, no. 2, pp. 911–21, 2010.
- [33] DUNN, O., “Multiple comparisons among means,” *Journal of the American Statistical Association*, vol. 56, no. 293, pp. 52–64, 1961.
- [34] ELDER CM, V. J., *The motor thalamus: Alteration of neuronal activity in the Parkinsonian state. In: Basal Ganglia and Thalamus in Health and Movement Disorders*. New York: Kluwer Academic, 2001.
- [35] ENGEL, A. and FRIES, P., “Beta-band oscillations - signalling the status quo?,” *Current opinion in neurobiology*, vol. 20, no. 2, pp. 156–165, 2010.
- [36] FENG, X., GREENWALD, B., RABITZ, H., SHEA-BROWN, E., and KOSUT, R., “Toward closed-loop optimization of deep brain stimulation for Parkinson’s disease: concepts and lessons from a computational model,” *Journal of neural engineering*, vol. 4, p. L14, 2007.
- [37] FILION, M. and TREMBLAY, L., “Abnormal spontaneous activity of globus pallidus neurons in monkeys with MPTP-induced Parkinsonism,” *Brain research*, vol. 547, no. 1, pp. 140–144, 1991.
- [38] GALE, J. T., AMIRNOVIN, R., WILLIAMS, Z. M., FLAHERTY, A. W., and ESKANDAR, E. N., “From symphony to cacophony. pathophysiology of the human basal ganglia in Parkinson disease,” *Neuroscience and Biobehavioral Reviews*, vol. 32, no. 3, pp. 378–387, 2008.
- [39] GALVAN, A. and WICHMANN, T., “Pathophysiology of parkinsonism,” *Clinical Neurophysiology*, vol. 119, no. 7, pp. 1459–1474, 2008.
- [40] GARRETT, D., PETERSON, D., ANDERSON, C., and THAUT, M., “Comparison of linear, nonlinear, and feature selection methods for EEG signal classification,” *Neural Systems and Rehabilitation Engineering, IEEE Transactions on*, vol. 11, no. 2, pp. 141–144, 2003.
- [41] GATEV, P., DARBIN, O., and WICHMANN, T., “Oscillations in the basal ganglia under normal conditions and in movement disorders,” *Movement disorders*, vol. 21, no. 10, pp. 1566–1577, 2006.
- [42] GATEV, P. and WICHMANN, T., “Interactions between cortical rhythms and spiking activity of single basal ganglia neurons in the normal and parkinsonian state,” *Cereb Cortex*, vol. 19, no. 6, pp. 1330–44, 2009.

- [43] GATEV, P. and WICHMANN, T., “Changes in arousal alter neuronal activity in primate basal ganglia,” in *Soc Neurosci Abstr*, vol. 29, 2003.
- [44] GOEDERT, M., “Alpha-synuclein and neurodegenerative diseases,” *Nature Reviews Neuroscience*, vol. 2, no. 7, pp. 492–501, 2001.
- [45] GOETZ, C. G., TILLEY, B. C., SHAFTMAN, S. R., STEBBINS, G. T., FAHN, S., MARTINEZ-MARTIN, P., POEWE, W., SAMPAIO, C., STERN, M. B., and DODEL, R., “Movement Disorder Society sponsored revision of the Unified Parkinson’s Disease Rating Scale (MDS-UPDRS). Scale presentation and clinimetric testing results,” *Movement disorders*, vol. 23, no. 15, pp. 2129–2170, 2008.
- [46] GOLDBERG, J., BORAUD, T., MARATON, S., HABER, S., VAADIA, E., and BERGMAN, H., “Enhanced synchrony among primary motor cortex neurons in the 1-methyl-4-phenyl-1, 2, 3, 6-tetrahydropyridine primate model of Parkinson’s disease,” *The Journal of Neuroscience*, vol. 22, no. 11, pp. 4639–4653, 2002.
- [47] GRIMALDI, G. and MANTO, M., “Neurological tremor: Sensors, signal processing and emerging applications,” *Sensors*, vol. 10, no. 2, pp. 1399–1422, 2010.
- [48] GUEHL, D., PESSIGLIONE, M., FRANCOIS, C., YELNIK, J., HIRSCH, E., FEGER, J., and TREMBLAY, L., “Tremor-related activity of neurons in the motor thalamus: changes in firing rate and pattern in the MPTP vervet model of Parkinsonism,” *European Journal of Neuroscience*, vol. 17, no. 11, pp. 2388–2400, 2003.
- [49] HAMMOND, C., BERGMAN, H., and BROWN, P., “Pathological synchronization in Parkinson’s disease: networks, models and treatments,” *Trends in Neurosciences*, vol. 30, no. 7, pp. 357–364, 2007.
- [50] HELMICH, R. C., HALLETT, M., DEUSCHL, G., TONI, I., and BLOEM, B. R., “Cerebral causes and consequences of parkinsonian resting tremor: a tale of two circuits?,” *Brain*, vol. 135, no. 11, pp. 3206–3226, 2012.
- [51] HIGASHI, Y., YAMAKOSHI, K., FUJIMOTO, T., SEKINE, M., and TAMURA, T., “Quantitative evaluation of movement using the timed up-and-go test,” *Engineering in Medicine and Biology Magazine, IEEE*, vol. 27, no. 4, pp. 38–46, 2008.
- [52] HIRSCHMANN, J., HARTMANN, C. J., BUTZ, M., HOOGENBOOM, N., ZKURT, T. E., ELBEN, S., VESPER, J., WOJTECKI, L., and SCHNITZLER, A., “A direct relationship between oscillatory subthalamic nucleus-cortex coupling and rest tremor in Parkinson’s disease,” *Brain*, vol. 136, no. 12, pp. 3659–3670, 2013.

- [53] HOLGADO, A., TERRY, J., and BOGACZ, R., “Conditions for the generation of beta oscillations in the subthalamic nucleus’ globus pallidus network,” *The Journal of Neuroscience*, vol. 30, no. 37, pp. 12340–12352, 2010.
- [54] HSU, C., CHANG, C., and LIN, C., “A practical guide to support vector classification,” 2003.
- [55] HUTCHISON, W., LOZANO, A., DAVIS, K., SAINT-CYR, J., LANG, A., and DOSTROVSKY, J., “Differential neuronal activity in segments of globus pallidus in Parkinson’s disease patients,” *Neuroreport*, vol. 5, no. 12, p. 1533, 1994.
- [56] HYLTON, L., SANDERS, T., and CLEMENTS, M., “Comparing tremor detection algorithms using acceleration data from an android smartphone,” *IEEE Engineering in Medicine and Biology Neural Engineering Conference*, 2013.
- [57] JALLON, P., DUPRE, B., and ANTONAKIOS, M., “A graph based method for timed up and go test qualification using inertial sensors,” in *Acoustics, Speech and Signal Processing (icaSSP), 2011 IEEE International Conference on*, pp. 689–692, IEEE.
- [58] JARVIS, M. and MITRA, P., “Sampling properties of the spectrum and coherency of sequences of action potentials,” *Neural Computation*, vol. 13, no. 4, pp. 717–749, 2001.
- [59] JOHNSON, R. and WICHERN, D., *Applied multivariate statistical analysis*, vol. 4. Prentice hall Englewood Cliffs, NJ, 1992.
- [60] JOUNDI, R. A., BRITAIN, J. S., JENKINSON, N., GREEN, A. L., and AZIZ, T., “Rapid tremor frequency assessment with the iphone accelerometer,” *Parkinsonism Relat Disord*, vol. 17, no. 4, pp. 288–90, 2011.
- [61] KALCHER, J. and PFURTSCHELLER, G., “Discrimination between phase-locked and non-phase-locked event-related EEG activity,” *Electroencephalography and Clinical Neurophysiology*, vol. 94, no. 5, pp. 381–384, 1995.
- [62] KILLIAN, N. J., JUTRAS, M. J., and BUFFALO, E. A., “A map of visual space in the primate entorhinal cortex,” *Nature*, vol. 491, no. 7426, pp. 761–4, 2012.
- [63] KLIEM, M. A., PARE, J.-F., KHAN, Z. U., WICHMANN, T., and SMITH, Y., “Ultrastructural localization and function of dopamine d1-like receptors in the substantia nigra pars reticulata and the internal segment of the globus pallidus of parkinsonian monkeys,” *European Journal of Neuroscience*, vol. 31, no. 5, pp. 836–851, 2010.
- [64] KRAVITZ, A. V., FREEZE, B. S., PARKER, P. R., KAY, K., THWIN, M. T., DEISSEROTH, K., and KREITZER, A. C., “Regulation of parkinsonian motor behaviours by optogenetic control of basal ganglia circuitry,” *Nature*, vol. 466, no. 7306, pp. 622–6, 2010.

- [65] KRINGELBACH, M. L., JENKINSON, N., OWEN, S. L., and AZIZ, T. Z., “Translational principles of deep brain stimulation,” *Nat Rev Neurosci*, vol. 8, no. 8, pp. 623–35, 2007.
- [66] KRUSIENSKI, D. J., GROSSE-WENTRUP, M., GALN, F., COYLE, D., MILLER, K. J., FORNEY, E., and ANDERSON, C. W., “Critical issues in state-of-the-art braincomputer interface signal processing,” *Journal of neural engineering*, vol. 8, no. 2, p. 025002, 2011.
- [67] KUMAR, R., LOZANO, A., MONTGOMERY, E., and LANG, A. E., “Pallidotomy and deep brain stimulation of the pallidum and subthalamic nucleus in advanced Parkinson’s disease,” *Movement disorders: official journal of the Movement Disorder Society*, vol. 13, p. 73, 1998.
- [68] KHN, A. A., KUPSCH, A., SCHNEIDER, G.-H., and BROWN, P., “Reduction in subthalamic 835 hz oscillatory activity correlates with clinical improvement in parkinson’s disease,” *European Journal of Neuroscience*, vol. 23, no. 7, pp. 1956–1960, 2006.
- [69] KHN, A. A., WILLIAMS, D., KUPSCH, A., LIMOUSIN, P., HARIZ, M., SCHNEIDER, G., YARROW, K., and BROWN, P., “Event-related beta desynchronization in human subthalamic nucleus correlates with motor performance,” *Brain*, vol. 127, no. 4, pp. 735–746, 2004.
- [70] LAITINEN, L., “Pallidotomy for Parkinson’s disease,” *Neurosurgery Clinics of North America*, vol. 6, no. 1, p. 105, 1995.
- [71] LEGENDY, C. and SALCMAN, M., “Bursts and recurrences of bursts in the spike trains of spontaneously active striate cortex neurons,” *Journal of neurophysiology*, vol. 53, no. 4, pp. 926–939, 1985.
- [72] LEMOYNE, R., MASTROIANNI, T., COZZA, M., COROIAN, C., and GRUNDFEST, W., “Implementation of an iphone for characterizing Parkinson’s disease tremor through a wireless accelerometer application,” in *Engineering in Medicine and Biology Society (EMBC), 2010 Annual International Conference of the IEEE*, pp. 4954–4958.
- [73] LEVY, R., ASHBY, P., HUTCHISON, W., LANG, A., LOZANO, A., and DOSTROVSKY, J., “Dependence of subthalamic nucleus oscillations on movement and dopamine in Parkinson’s disease,” *Brain*, vol. 125, no. 6, pp. 1196–1209, 2002.
- [74] LEVY, R., HUTCHISON, W., LOZANO, A., and DOSTROVSKY, J., “High-frequency synchronization of neuronal activity in the subthalamic nucleus of Parkinsonian patients with limb tremor,” *The Journal of Neuroscience*, vol. 20, no. 20, pp. 7766–7775, 2000.

- [75] LEVY, R., HUTCHISON, W., LOZANO, A., and DOSTROVSKY, J., “Synchronized neuronal discharge in the basal ganglia of Parkinsonian patients is limited to oscillatory activity,” *The Journal of Neuroscience*, vol. 22, no. 7, pp. 2855–2861, 2002.
- [76] LIEBERMAN, D., CORTHESEY, M., CUMMINS, A., and OLDFIELD, E., “Reversal of experimental parkinsonism by using selective chemical ablation of the medial globus pallidus,” *Journal of neurosurgery*, vol. 90, no. 5, pp. 928–934, 1999.
- [77] LITTLE, S., POGOSYAN, A., KUHN, A., and BROWN, P., “Beta band stability over time correlates with parkinsonian rigidity and bradykinesia,” *Experimental neurology*, vol. 236, no. 2, pp. 383–388, 2012.
- [78] LITTLE, S., POGOSYAN, A., NEAL, S., ZAVALA, B., ZRINZO, L., HARIZ, M., FOLTYNIE, T., LIMOUSIN, P., ASHKAN, K., and FITZGERALD, J., “Adaptive deep brain stimulation in advanced parkinson disease,” *Annals of neurology*, vol. 74, no. 3, pp. 449–457, 2013.
- [79] LOPEZ-AZCARATE, J., TAINTA, M., RODRIGUEZ-OROZ, M. C., VALENCIA, M., GONZALEZ, R., GURIDI, J., IRIARTE, J., OBESO, J. A., ARTIEDA, J., and ALEGRE, M., “Coupling between beta and high-frequency activity in the human subthalamic nucleus may be a pathophysiological mechanism in Parkinson’s disease,” *J Neurosci*, vol. 30, no. 19, pp. 6667–77, 2010.
- [80] LOW, P., CHI, Y. M., JOSHI, S., UEBELHER, C., DUBOIS, Y. A., and LIU, K., “Head harness and wireless EEG monitoring system,” 2010.
- [81] LOZANO, A., LANG, A., GALVEZ-JIMENEZ, N., MIYASAKI, J., DUFF, J., HUTCHISON, W., and DOSTROVSKY, J., “Effect of GPi pallidotomy on motor function in Parkinson’s disease,” *The Lancet*, vol. 346, no. 8987, pp. 1383–1387, 1995.
- [82] MAGILL, P., BOLAM, J., and BEVAN, M., “Dopamine regulates the impact of the cerebral cortex on the subthalamic nucleus-globus pallidus network,” *Neuroscience*, vol. 106, no. 2, pp. 313–330, 2001.
- [83] MAGILL, P., SHAROTT, A., BEVAN, M., BROWN, P., and BOLAM, J., “Synchronous unit activity and local field potentials evoked in the subthalamic nucleus by cortical stimulation,” *Journal of neurophysiology*, vol. 92, no. 2, pp. 700–714, 2004.
- [84] MAGILL, P., SHAROTT, A., BOLAM, J., and BROWN, P., “Brain state dependency of coherent oscillatory activity in the cerebral cortex and basal ganglia of the rat,” *Journal of neurophysiology*, vol. 92, no. 4, pp. 2122–2136, 2004.
- [85] MAMUN, K., VAIDYANATHAN, R., LUTMAN, M., STEIN, J., LIU, X., AZIZ, T., and WANG, S., “Decoding movement and laterality from local field potentials in the subthalamic nucleus,” pp. 128–131, IEEE.

- [86] MIAO, G. J. and CLEMENTS, M. A., *Digital signal processing and statistical classification*. Artech House Publishers, 2002.
- [87] MILLER, W. and DELONG, M., “Altered tonic activity of neurons in the globus pallidus and subthalamic nucleus in the primate MPTP model of Parkinsonism,” *The basal ganglia II*, vol. 415, p. 427, 1987.
- [88] MILLER WC, D. M., “Parkinsonian symptomatology. an anatomical and physiological analysis,” *Ann N Y Acad Sci*, no. 515, pp. 287–302, 1988.
- [89] MOLNAR, G., PILLIAR, A., LOZANO, A., and DOSTROVSKY, J., “Differences in neuronal firing rates in pallidal and cerebellar receiving areas of thalamus in patients with Parkinson’s disease, essential tremor, and pain,” *Journal of neurophysiology*, vol. 93, no. 6, pp. 3094–3101, 2005.
- [90] NI, Z., GAO, D., BENABID, A., and BENAZZOUZ, A., “Unilateral lesion of the nigrostriatal pathway induces a transient decrease of firing rate with no change in the firing pattern of neurons of the parafascicular nucleus in the rat,” *Neuroscience*, no. 101, pp. 993–999, 2000.
- [91] OLANOW, C., WATTS, R., and KOLLER, W., “An algorithm (decision tree) for the management of Parkinsons disease (2001): treatment guidelines,” *Neurology*, vol. 56, no. suppl 5, pp. S1–S88, 2001.
- [92] OZKURT, T. E., BUTZ, M., HOMBURGER, M., ELBEN, S., VESPER, J., WOJTECKI, L., and SCHNITZLER, A., “High frequency oscillations in the subthalamic nucleus: a neurophysiological marker of the motor state in Parkinson’s disease,” *Experimental neurology*, vol. 229, no. 2, pp. 324–331, 2011.
- [93] PALMERINI, L., MELLONE, S., ROCCHI, L., and CHIARI, L., “Dimensionality reduction for the quantitative evaluation of a smartphone-based timed up and go test,” in *Engineering in Medicine and Biology Society, EMBC, 2011 Annual International Conference of the IEEE*, pp. 7179–7182, IEEE.
- [94] PARENT, A. and HAZRATI, L.-N., “Functional anatomy of the basal ganglia. ii. the place of subthalamic nucleus and external pallidium in basal ganglia circuitry,” *Brain Research Reviews*, vol. 20, no. 1, pp. 128–154, 1995.
- [95] PASQUEREAU, B. and TURNER, R., “Primary motor cortex of the Parkinsonian monkey: Differential effects on the spontaneous activity of pyramidal tract-type neurons,” *Cerebral Cortex*, vol. 21, no. 6, p. 1362, 2011.
- [96] PESARAN, B., PEZARIS, J. S., SAHANI, M., MITRA, P. P., and ANDERSEN, R. A., “Temporal structure in neuronal activity during working memory in macaque parietal cortex,” *Nature neuroscience*, vol. 5, no. 8, pp. 805–811, 2002.
- [97] PESSIGLIONE, M., GUEHL, D., ROLLAND, A. S., FRANCOIS, C., HIRSCH, E. C., FEGER, J., and TREMBLAY, L., “Thalamic neuronal activity in

- dopamine-depleted primates: evidence for a loss of functional segregation within basal ganglia circuits,” *J Neurosci*, vol. 25, no. 6, pp. 1523–31, 2005.
- [98] PFURTSCHELLER, G. and LOPES DA SILVA, F., “Event-related EEG/MEG synchronization and desynchronization: basic principles,” *Clinical Neurophysiology*, vol. 110, no. 11, pp. 1842–1857, 1999.
- [99] RASCOL, O., BROOKS, D. J., KORCZYN, A. D., DE DEYN, P. P., CLARKE, C. E., and LANG, A. E., “A five-year study of the incidence of dyskinesia in patients with early Parkinson’s disease who were treated with ropinirole or levodopa,” *New England Journal of Medicine*, vol. 342, no. 20, pp. 1484–1491, 2000.
- [100] RODRIGUEZ-OROZ, M. C., LOPEZ-AZCARATE, J., GARCIA-GARCIA, D., ALEGRE, M., TOLEDO, J., VALENCIA, M., GURIDI, J., ARTIEDA, J., and OBESO, J. A., “Involvement of the subthalamic nucleus in impulse control disorders associated with Parkinson’s disease,” *Brain*, vol. 134, no. Pt 1, pp. 36–49, 2011.
- [101] ROSIN, B., SLOVIK, M., MITELMAN, R., RIVLIN-ETZION, M., HABER, S., ISRAEL, Z., VAADIA, E., and BERGMAN, H., “Closed-loop deep brain stimulation is superior in ameliorating Parkinsonism,” *Neuron*, vol. 72, no. 2, pp. 370–384, 2011.
- [102] RYAPOLOVA-WEBB, E., AFSHAR, P., STANSLASKI, S., DENISON, T., DE HEMPTINNE, C., BANKIEWICZ, K., and STARR, P. A., “Chronic cortical and electromyographic recordings from a fully implantable device: preclinical experience in a nonhuman primate,” *Journal of neural engineering*, vol. 11, no. 1, p. 016009, 2014.
- [103] SALARIAN, A., HORAK, F., ZAMPIERI, C., CARLSON-KUHTA, P., NUTT, J., and AMINIAN, K., “iTUG, a sensitive and reliable measure of mobility,” *Neural Systems and Rehabilitation Engineering, IEEE Transactions on*, vol. 18, no. 3, pp. 303–310, 2010.
- [104] SANDERS, T. H., DEVERGNAS, A., WICHMANN, T., and CLEMENTS, M. A., “Remote smartphone monitoring for management of parkinson’s disease,” in *Proceedings of the 6th International Conference on PErvasive Technologies Related to Assistive Environments*, p. 42, Copyright © 2013 ACM, Inc. Reprinted with permission. <http://doi.acm.org/10.1145/2504335.2504380>.
- [105] SANDERS, T. H., DEVERGNAS, A., WICHMANN, T., and CLEMENTS, M. A., “Canonical correlation to estimate the degree of parkinsonism from local field potential and electroencephalographic signals,” *Neural Engineering (NER), 6th International IEEE/EMBS Conference on*, pp. 158–161, Copyright © 2013 IEEE. Reprinted with permission.

- [106] SANDERS, T. H., CLEMENTS, M. A., and WICHMANN, T., “Parkinsonism-related features of neuronal discharge in primates,” *Journal of neurophysiology*, Copyright © 2013, The American Physiological Society.
- [107] SCHNITZLER, A. and GROSS, J., “Normal and pathological oscillatory communication in the brain,” *Nature Reviews Neuroscience*, vol. 6, no. 4, pp. 285–296, 2005.
- [108] SHIMAMOTO, S. A., RYAPOLOVA-WEBB, E. S., OSTREM, J. L., GALIFIANAKIS, N. B., MILLER, K. J., and STARR, P. A., “Subthalamic nucleus neurons are synchronized to primary motor cortex local field potentials in parkinson’s disease,” *The Journal of Neuroscience*, vol. 33, no. 17, pp. 7220–7233, 2013.
- [109] SMITH, Y. and VILLALBA, R., “Striatal and extrastriatal dopamine in the basal ganglia: an overview of its anatomical organization in normal and Parkinsonian brains,” *Mov Disord*, vol. 23 Suppl 3, pp. S534–47, 2008.
- [110] SOARES, J., KLIEM, M. A., BETARBET, R., GREENAMYRE, J. T., YAMAMOTO, B., and WICHMANN, T., “Role of external pallidal segment in primate parkinsonism: comparison of the effects of 1-methyl-4-phenyl-1,2,3,6-tetrahydropyridine-induced parkinsonism and lesions of the external pallidal segment,” *J Neurosci*, vol. 24, no. 29, pp. 6417–26, 2004.
- [111] SPILLANTINI, M. G., SCHMIDT, M. L., LEE, V. M.-Y., TROJANOWSKI, J. Q., JAKES, R., and GOEDERT, M., “Alpha-synuclein in Lewy bodies,” *Nature*, vol. 388, no. 6645, pp. 839–840, 1997.
- [112] SUBASI, A. and ISMAIL GURSOY, M., “EEG signal classification using PCA, ICA, LDA and support vector machines,” *Expert Systems with Applications*, vol. 37, no. 12, pp. 8659–8666, 2010.
- [113] THEODORIDIS, S. and KOUTROUMBAS, L., *Pattern recognition*. 2009.
- [114] TORT, A., KOMOROWSKI, R., EICHENBAUM, H., and KOPELL, N., “Measuring phase-amplitude coupling between neuronal oscillations of different frequencies,” *Journal of neurophysiology*, vol. 104, no. 2, pp. 1195–1210, 2010.
- [115] UHLHAAS, P. and SINGER, W., “Neural synchrony in brain disorders: relevance for cognitive dysfunctions and pathophysiology,” *Neuron*, vol. 52, no. 1, pp. 155–168, 2006.
- [116] VAN LUMMEL, R. C., AINSWORTH, E., LINDEMANN, U., ZIJLSTRA, W., CHIARI, L., VAN CAMPEN, P., and HAUSDORFF, J. M., “Automated approach for quantifying the repeated sit-to-stand using one body fixed sensor in young and older adults,” *Gait Posture*, 2012.

- [117] VAZEY, E. M. and ASTON-JONES, G., “New tricks for old dogmas: Optogenetic and designer receptor insights for Parkinson’s disease,” *Brain research*, vol. 1511, pp. 153–163, 2013.
- [118] VILA, M., PERIER, C., FEGER, J., YELNIK, J., FAUCHEUX, B., RUBERG, M., VOZARI, R., AGID, Y., and HIRSCH, E., “Evolution of changes in neuronal activity in the subthalamic nucleus of rats with unilateral lesion of the substantia nigra assessed by metabolic and electrophysiological measurements,” *European Journal of Neuroscience*, vol. 12, no. 1, pp. 337–344, 2000.
- [119] VITEK, J., BAKAY, R., FREEMAN, A., EVATT, M., GREEN, J., McDONALD, W., HABER, M., BARNHART, H., WAHLAY, N., and TRICHE, S., “Randomized trial of pallidotomy versus medical therapy for Parkinson’s disease,” *Annals of Neurology*, vol. 53, no. 5, pp. 558–569, 2003.
- [120] WICHMANN, T., BERGMAN, H., STARR, P., SUBRAMANIAN, T., WATTS, R., and DELONG, M., “Comparison of MPTP-induced changes in spontaneous neuronal discharge in the internal pallidal segment and in the substantia nigra pars reticulata in primates,” *Experimental brain research*, vol. 125, no. 4, pp. 397–409, 1999.
- [121] WICHMANN, T. and DELONG, M., “Deep brain stimulation for Neurologic and neuropsychiatric disorders,” *Neuron*, vol. 52, no. 1, pp. 197–204, 2006.
- [122] WICHMANN, T., KLIEM, M. A., and DELONG, M. R., “Antiparkinsonian and behavioral effects of inactivation of the substantia nigra pars reticulata in hemiparkinsonian primates,” *Experimental neurology*, vol. 167, no. 2, pp. 410–424, 2001.
- [123] WILLIAM LANGSTON, J., “MPTP and Parkinson’s disease,” *Trends in Neurosciences*, vol. 8, pp. 79–83, 1985.
- [124] WINESTONE, J. S., ZAIDEL, A., BERGMAN, H., and ISRAEL, Z., “The use of macroelectrodes in recording cellular spiking activity,” *J Neurosci Methods*, vol. 206, no. 1, pp. 34–9, 2012.
- [125] WINGEIER, B., TCHENG, T., KOOP, M. M., HILL, B. C., HEIT, G., and BRONTE-STEWART, H. M., “Intra-operative STN DBS attenuates the prominent beta rhythm in the STN in Parkinson’s disease,” *Experimental neurology*, vol. 197, no. 1, pp. 244–251, 2006.
- [126] WOOD, A. and CALNE, D., “Treatment of Parkinson’s disease,” *New England Journal of Medicine*, vol. 329, no. 14, pp. 1021–1027, 1993.
- [127] XU, J., YAZICIOGLU, R. F., HARPE, P., MAKINWA, K. A., and VAN HOOF, C., “A 160W 8-channel active electrode system for EEG monitoring,” in *Solid-State Circuits Conference Digest of Technical Papers (ISSCC), 2011 IEEE International*, pp. 300–302, IEEE.

- [128] YU, L. and LIU, H., “Efficient feature selection via analysis of relevance and redundancy,” *The Journal of Machine Learning Research*, vol. 5, pp. 1205–1224, 2004.
- [129] YUKSEL, Y., “Sensor and GPS monitor,” 2011.
- [130] ZIRH, T., LENZ, F., REICH, S., and DOUGHERTY, P., “Patterns of bursting occurring in thalamic cells during parkinsonian tremor,” *Neuroscience*, vol. 83, no. 1, pp. 107–121, 1998.

VITA

Teresa Hinkle Sanders was born in Lansing, Michigan, but grew up in Madison, Alabama. After receiving her undergraduate degree in Electrical and Computer Engineering, she moved to Southern California where she worked for Hughes Aircraft Company Missile Systems Group while obtaining her Master's degree in Electrical Engineering from UCLA. She moved to Atlanta, Georgia in 2000 and, after working at the Georgia Tech Research Institute for several years, returned to school for her PhD in Bioengineering at the Georgia Institute of Technology in 2008.